ANALYSIS OF SOUNDING DATA FROM PORTO SANTO ISLAND DURING ASTEX

by

Wayne H. Schubert, Stephen K. Cox, Thomas B. McKee, David A. Randall
Paul E. Ciesielski, John D. Kliest and Eric L. Stevens

Colorado State University

DEPARTMENT OF ATMOSPHERIC SCIENCE

PAPER NO. 512

ANALYSIS OF SOUNDING DATA FROM PORTO SANTO ISLAND DURING ASTEX

Wayne H. Schubert
Stephen K. Cox
Thomas B. McKee
David A. Randall
Paul E. Ciesielski
John D. Kleist
Eric L. Stevens

Department of Atmospheric Science
Colorado State University
Fort Collins, Colorado 80523

7 November 1992

Atmospheric Science Paper 512

Contents

ABSTRACT

We present an analysis of the ASTEX radiosonde data obtained on Porto Santo Island during 1–28 June 1992. The data consists of 203 soundings and is available in two forms—Level I and Level II. The Level I data is the raw data produced by the real time software of the AIR radiosonde system. This data is at irregular pressure and height levels. Level II data consists of processed thermodynamic and wind data at a uniform vertical resolution of 10m, which essentially retains the highest possible vertical resolution in the original raw data. Plots of temperature and dew point temperature are presented for each of the 203 soundings taken during ASTEX. Plots of the 28 day means and of the diurnal variations are also presented. Accessibility of this data via anonymous ftp is also discussed.

1. ASTEX

The field phase of the Atlantic Stratocumulus Transition Experiment (ASTEX) was conducted from 1 to 28 June 1992 in the region of the Azores and Madeira Islands of the north Atlantic Ocean (see Fig. 1). The primary goal of ASTEX is to gain a better physical understanding of the processes responsible for the generation, maintenance and dissipation of boundary layer clouds, and, in particular, on the transition back and forth between stratocumulus clouds and trade cumulus clouds. A detailed report on the experiment design can be found in the ASTEX Operations Plan (FIRE Project Office 1992).

The purpose of the present report is to discuss the radiosonde data taken on Porto Santo Island by a team of scientists from the Department of Atmospheric Science, Colorado State University. We describe the Porto Santo observation site in section 2, the radiosonde system in section 3, and the thermodynamic data processing and wind data processing in sections 4 and 5. Graphs of the complete set of soundings are presented in section 6. The availability of this data via anonymous ftp is discussed in section 7.

2. The Porto Santo site

Porto Santo is a small island (3 to 6 km wide and 12 km long) sixty kilometers north of Madeira. In summer, the Azores high pressure center lies to the west of Porto Santo, and the island experiences a nearly continual northerly flow. A detailed study of surface winds on Porto Santo can be found in Ballard et al. (1983). To minimize island effects the chosen site was on the north side of the island, as shown in Fig. 2. The center of the observational site (the operations center trailer) was 97m above mean sea level and was located 295m north of the end of the Porto Santo Airport runway and 200m south of the cliff edge. The coordinates of the site were 33° 5′ 2″ N latitude and 16° 20′ 49″ W longitude. Instrumentation was provided by two groups—the CSU Department of Atmospheric Science and the Wave Propagation Laboratory of NOAA/ERL. Equipment provided by CSU included a surface meteorological station, wind profiler, RASS, laser ceilometer, radiosonde system and an IR spectrometer, all of which were located near the paved road paralleling the airport runway. Equipment provided by NOAA/ERL/WPL included a millimeter wave Doppler cloud radar, a microwave radiometer, and a lidar. The operations center was in the centrally located trailer containing telephone and FAX lines to the ASTEX operations center in Santa Maria. This report discussses only the radiosonde data.

3. Radiosonde system

Soundings were taken with the Intellisonde Rawin System (Model IS-4A1-MET) manufactured by Atmospheric Instrumentation Research (AIR), Inc., Boulder, Colorado. The AIR system hardware consists of an automatically tracking radiotheodolite (Fig. 3), a PC-AT compatible computer with an AIR Metdecoder board in one of its expansion slots, and a supply of sondes (Intellisonde model IS-4A-1680) and 200 gram balloons. The system provides soundings of pressure, temperature, relative humidity, and the azimuth and elevation angles of the radiotheodolite. The AIR system software also computes real-time derived quantities (e.g., dew-point temperature, geopotential height, winds) but we have chosen to recompute these derived quantities in the post-analysis phase.

The sondes, shown in Fig. 4, are 10cm on the sides, 15cm high and have a mass of 240 grams. The upper third of the sonde consists of a shielded compartment for the humidity sensor. As the sonde rises, air enters the top of the sonde into the hygristor compartment, flows past the hygristor, and then exits through the side of the sonde. The 200 gram balloons were inflated with helium (or, early in the experiment, with hydrogen) to provide approximately 4–5 ms^{-1} rise rate, which yields adequate flow past the hygristor. The bottom of the sonde is a ground plane with a downward extending quarter wave antenna for telemetry to the surface. The oscillator frequency on the sonde is 1680 MHz. Power is provided by two 9 volt alkaline batteries. The system has an auto-launch feature which automatically begins data collection when a 0.8 mb change of pressure is detected.

Pressure is measured with an aneroid sensor whose capacitance varies with pressure. The transfer function which translates capacitance to pressure is a fifth-order polynomial whose coefficients are different for each sonde. These calibration coefficients are stored in the sonde and transmitted to the radiotheodolite in the preflight phase, while the sonde is on its prelaunch support stand.

Temperature and relative humidity are measured with resistive sensors, both manufactured by VIZ. The temperature sensor is a rod thermistor whose lock-in value is printed on the radiosonde body and is entered into the computer in the prelaunch phase. The relative humidity is measured with a VIZ Accu-Lok humidity sensor (a carbon strip hygristor). These sensors are individually calibrated at 25°C and 33% relative humidity. The relative humidity sensor is removed from its sealed foil package and its lock-in value is also entered into the computer before launch.

During ASTEX the radiosonde system was set up at an elevation of 97 m on the north side of Porto Santo Island, which provided good exposure to the prevailing northerly flow. During the period from 1 June to 28 June 1992, 203 soundings were obtained. Observation times, maximum altitudes and observer comments for these soundings are summarized in Table 1.

4. Analysis of the thermodynamic data

a. Time lag effects

Whenever radiosondes ascend through inversions there arise questions about errors due to sensor time lag. Before proceeding to the analysis of the thermodynamic data, let us briefly discuss these effects.

Let T denote the sensor temperature and T_e the environmental temperature. According to the Newtonian cooling law, T and T_e are related by the first order differential equation

$$\frac{dT}{dt} = -\frac{1}{\tau}(T - T_e)$$

where τ is the sensor response time. Let us assume that the environmental temperature changes linearly in time as the balloon ascends so that $dT_e/dt = \lambda$. The above equation can then be written

$$\frac{d(T - T_e)}{dt} + \frac{1}{\tau}(T - T_e) = -\lambda,$$

which has the solution

$$T - T_e = [(T - T_e)_0 + \lambda\tau]\exp(-t/\tau) - \lambda\tau$$

If we wait long enough for the initial condition $(T - T_e)_0$ to be forgotten, the sensor temperature T and the environmental temperature T_e will differ by $-\lambda\tau$. If the sensor rises at 5 ms^{-1} in an atmosphere with a dry adiabatic lapse rate, then $\lambda = -0.05$ Ks^{-1}. Since the temperature sensor in the AIR sonde has a 3 to 5 s lag constant, $-\lambda\tau \approx 0.2$ K, i.e. the sensor reads approximately 0.2 K too warm. On the other hand, if the sensor rises at 5 ms^{-1} through a 100 m thick temperature inversion of 5 K, then $\lambda = 0.25$ Ks^{-1} and $\lambda\tau \approx 1.0$ K, which means the sensor reads approximately 1.0 K too cold.

The lag of the humidity sensor depends on temperature. At 25°C, the lag constant is between 1 and 2 seconds, at 0°C it is between 3 and 5 seconds, and below

-20°C it is between 5 and 10 seconds. If equations similar to those for temperature lags are applied to the humidity sensor, the slow rate of increase of relative humidity in the boundary layer, coupled with a 2 s lag of the hygristor element, causes the sensor to read too dry by only a few tenths of a per cent. However, a 60% decrease in humidity in a 100 m layer above cloud top leads to a sensor reading about 6% too high.

Although these lag effects are not entirely negligible in strong inversions, we have not corrected for them in any way.

b. Derived quantities

The raw radiosonde data consists of pressure, temperature, relative humidity, and azimuth and elevation angles as a function of time. The AIR software creates files of these raw data along with several derived quantities.. An example is shown in Table 2. Each row consists of time (UTC), pressure, temperature, dew point temperature, relative humidity, geopotential height, azimuth, elevation, wind speed, wind direction, and elapsed time from launch. Several points are worth noting.

First of all, although 2.2 s time intervals are common, the data are not equally spaced in time. To obtain data equally spaced in time or equally spaced in height (determined hydrostatically), interpolation is necessary.

Secondly, although the average rate of pressure change is about -0.5 mb/s (i.e. about 5 m/s rise rate), there are irregularities in plots of pressure versus time. In fact, pressure can sometimes be nonmonotonic with time. Since downdrafts in stratocumulus are unlikely to be strong enough to force the balloon downward, the slight nonmonotonic nature of the pressure profile is probably a deficiency in the aneroid sensor. Thus, editing of obviously bad data and slight smoothing of the resulting pressure profile are apparently justified.

Finally, the 3–5s lag constants of the temperature and humidity sensors allow resolution of the sharp temperature and humidity gradients just above cloud top. To preserve these sharp gradients, smoothing of the temperature and humidity data should be avoided.

With these points in mind we have proceeded to produce Level II thermodynamic data in the following manner. After editing obviously bad data we have fit a cubic spline interpolation function to the raw data pairs (t_i, p_i), $i = 1, 2, \ldots$, to obtain the continuous function $p(t)$. Since noise in the aneroid sensor occasionally causes $p(t)$ to be nonmonotonic, we have sampled $p(t)$ at 3 sec intervals and then applied an eleven point filter with the weights $(-1, -5, -5, 20, 70, 98, 70, 20, -5, -5, -1)/256$.

This filter has the monotone spectral response shown in Fig. 5. It effectively removes oscillations with periods shorter than 18 seconds. More detail on this filter can be found in Hamming (1983, pages 143–144). We next perform a cubic spline fit to the filtered pressure data, thus obtaining the monotonic continuous function $\bar{p}(t)$, which is then evaluated at the original t_i to produce $\bar{p}_i$. We then convert filtered pressure data into height data using the discrete hydrostatic relation

$$z_i = z_{i-1} + \frac{R}{2g}\left(T(t_i) + T(t_{i-1})\right) \ln\left(\frac{\bar{p}(t_{i-1})}{\bar{p}(t_i)}\right). \tag{4.1}$$

This upward integration commences at the 97m launch elevation. A cubic spline is then fit to the (z_i, t_i) data to obtain the continuous function $t(z)$. From the continuous function $t(z)$, we then find t_j corresponding to equally spaced 10m intervals in z_j. We then linearly interpolate temperature and relative humidity from the nearest two times to obtain data at equally spaced intervals of height.

From the pressure $\bar{p}$, temperature T and relative humidity U we could now compute derived quantities such as dew point temperature T_d, water vapor mixing ratio q, saturation water vapor mixing ratio q_s, potential temperature θ, equivalent potential temperature θ_e and saturation equivalent potential temperature θ_{es}. To guarantee a manageable size of the Level II data set, we have included only T_d. A sample from the Level II data set is shown in Table 2. The computation of T_d and the other derived fields (which the user must compute) are described below.

By first computing the saturation vapor pressure $e_s(T)$ from

$$e_s(T) = 6.112 \exp\left(\frac{17.67(T - 273.15)}{T - 29.65}\right) \tag{4.2}$$

(where $e_s(T)$ is in millibars and T in Kelvin) and the actual vapor pressure e from

$$e = U e_s(T), \tag{4.3}$$

we can compute the water vapor mixing ratio q and the saturation water vapor mixing ratio q_s from

$$q = \frac{\epsilon e}{p - e} \tag{4.4}$$

and

$$q_s = \frac{\epsilon e_s(T)}{p - e_s(T)}, \tag{4.5}$$

where $\epsilon = 0.622$ is the ratio of the molecular weight of water vapor to the molecular weight of dry air. Equation (4.2) is Bolton's (1980) fit to the highly accurate

(0.005%) formula of Wexler (1976). The accuracy of (4.2) is 0.1%. Since the dew point temperature T_d is defined by $e_s(T_d) = e$, we can rearrange (4.2) to obtain

$$T_d = 273.15 + \frac{243.5 \ln(e/6.112)}{17.67 - \ln(e/6.112)}, \tag{4.6}$$

which allows explicit determination of T_d from the vapor pressure e.

We can next compute the potential temperature, equivalent potential temperature and the saturation equivalent potential temperature from

$$\theta = T(p_0/p)^{\kappa}, \tag{4.7}$$

$$\theta_e = \theta \exp(2.67q/T_s), \tag{4.8}$$

and

$$\theta_{es} = \theta \exp(2.67q_s/T), \tag{4.9}$$

where the saturation level temperature T_s is given by

$$T_s = \frac{1}{\frac{1}{T-55} - \frac{\ln(U/100)}{2840}} + 55. \tag{4.10}$$

The constants in (4.8) and (4.9) were suggested by Betts (1982) and those in (4.10) by Bolton (1980).

5. Analysis of the wind data

The underlying principle in obtaining winds from balloon tracking is that the horizontal wind velocity is equal to the velocity of the vertical projection of the balloon onto the spherical surface through which the balloon is rising. It is obvious that this principle is not exact, since the balloon is rising through a vertically sheared wind field and requires some time to accelerate or decelerate and thus match its velocity with that of the surrounding air. In this sense, wind measurements by balloon tracking have lags just as the temperature and humidity measurements discussed in section 4. When attempting to obtain high vertical resolution in wind observations, a second topic of concern is self-induced balloon motions, i.e., a tendency for balloons to snake their way through still air rather than rising straight up. These two issues, which can be lumped under the general question of how well balloons follow the flow, are discussed in the following two subsections. In the third subsection we discuss the advantages and disadvantages of radiotheodolite systems. When computing winds from radiotheodolite measurements, the issue of the effects of the earth's curvature is also important. This subject is discussed in the fourth subsection.

a. Inertial lag of the balloon

Consider a spherical balloon filled with hydrogen or helium so that it has lift $L = \rho V g$, where ρ is the air density and V the balloon volume. Suspended below the balloon is a radiosonde, with the whole structure (balloon, gas, suspension line, radiosonde) having mass m and associated downward gravitational force mg. In still air the balloon tends to rise straight up with an associated downward drag force (neglecting the drag on the sonde) equal to $\frac{1}{2} c_D \rho A w^2$, where c_D is the drag coefficient (typically about 0.4), A is the cross-sectional area of the balloon, and w is the balloon rise rate (typically about 5ms^{-1}). The force balance for steady vertical ascent is then

$$\tfrac{1}{2} c_D \rho A w^2 + mg = \rho V g. \tag{5.1}$$

Typical values of the drag force, weight and lift are 8, 5 and 13 Newtons respectively.

If the balloon rises through a sheared flow, the drag force is not exactly vertical but is in a direction opposite to the motion of the balloon relative to the moving air. The horizontal component of this drag force will accelerate or decelerate the balloon so that its velocity becomes closer to that of the air. The formal solution of this problem has been given by Perkins (1952), who concludes that the measured wind is a weighted average of the actual wind over a layer of thickness

$$d = \frac{6m}{c_D \rho A}. \tag{5.2}$$

Retaining (5.1) as the approximate force balance in the vertical, we can eliminate $c_D \rho A$ between (5.1) and (5.2) to obtain

$$d = \frac{3w^2}{g(\gamma - 1)}, \tag{5.3}$$

where $\gamma = L/(mg)$ is the lift ratio. Note that $\gamma > 1$ is a necessary condition for the balloon to rise. For rise rates $3 < w < 6\text{ms}^{-1}$ and lift ratios $2 < \gamma < 3$, (5.3) yields $1 < d < 11\text{m}$. Since the sampling interval is approximately 10m, we can assume that there are negligible lag effects in the wind data. In other words, it can be safely assumed that the balloon is moving with the wind, with the qualifications discussed in the next subsection.

b. Self-induced balloon motions

McVehil et al. (1965) tracked one-meter and two-meter diameter metalized spherical balloons with a pulsed Doppler radar, which yielded high vertical resolution soundings of the radial (i.e., along the radar beam) velocity component of the

balloon. For a two-meter diameter balloon rising at 8 ms^{-1}, regular oscillations with a vertical wavelength of 30 to 80 m were found. Such oscillations may be associated with turbulence in the boundary layer flow about the balloon. Experiments with one-meter diameter balloons yielded qualitatively similar oscillations with a vertical wavelenth of approximately 15 m. McVehil et al. concluded that one-meter and two-meter diameter balloons do not move entirely with the wind but have spurious oscillatory components that are aerodynamically induced. The wind speed errors associated with these spurious oscillations are expected to be approximately 1 to 2.5 ms^{-1}.

Self-induced motions of flexible rubber balloons and rigid mylar balloons were also observed by Murrow and Henry (1965) in a large dirigible hangar at Lakehurst, NJ. The balloons were released in the still air of the hangar and the deviations from perfectly vertical ascent measured with phototheodolites. The root-mean-square horizontal velocity was proportional to the vertical terminal velocity. For smooth rigid spheres of two-meter diameter the rms horizontal velocity was approximately one-half the vertical terminal velocity. Scoggins (1965) found that the use of roughened spheres (i.e., spheres with 90 or 270 cup-like structures protruding from the surface) reduced the amplitude of the aerodynamically induced motion.

Two brands of flexible rubber balloons were used in ASTEX. We believe these balloons produce self-induced motions, although the radiosonde train below the balloon probably reduces the effect somewhat. Thus, we suggest that it may be misleading to examine the wind data at vertical resolutions higher than approximately 100m.

c. Advantages and disadvantages of radiotheodolite systems

The measurements used in making upper air wind computations through balloon tracking by radiotheodolite or radar include the azimuth angle (α), the elevation angle (ϵ), the balloon height (z), and the slant range (r), all as functions of time. Given α, only two of the remaining three variables (ϵ, z, r) are required for wind computation. Thus, de Jong (1958) has arranged wind observations into three classes—those using (ϵ, z), those using (ϵ, r), and those using (z, r). Radiotheodolite systems fall into the (ϵ, z) class, while radar systems measuring elevation and slant range fall into any class and radar systems measuring slant range but not elevation fall into either or both of the (ϵ, r) and (z, r) classes. By performing an error analysis, de Jong has concluded that no one class is always superior and that each class has its advantages in certain ranges of the variables. The (ϵ, z) class is best when

balloon distances are not too large and elevation angles are not too small. When the balloon is a large distance away, the (z, r) class is most suitable and the (ϵ, z) class least suitable. In addition, when the balloon instantly moves in the direction of observation, the wind speed errors maximize, while when the balloon instantly moves perpendicular to the direction of observation these same errors minimize.

In summary, the use of a radiotheodolite system for boundary layer wind measurements as required by ASTEX is a good choice. In cases of strong unidirectional flow, when the balloon drifts directly away at low elevation angles, the upper level winds are less reliable. However, it should be noted that tropospheric winds are also available from a 400 MHz wind profiler on Porto Santo.

d. Effects of the earth's curvature on wind computations

When pibal observations are used to compute winds, the distances from the theodolite are not large and it is acceptable to neglect the curvature of the earth. Since the advent of the AN/GMD-1 system in the early 1950's it has become common to track balloons to heights above 30km and out to ranges exceeding 200km, with elevation angles as low as 6 degrees. For such cases it is important to include the effects of the earth's curvature (Gustafson 1954, Clem et al. 1954, Kessler 1954).

Consider a cross section which contains the center of the earth (C), the radiotheodolite observation site (O) and the balloon position (B), as shown in Fig. 6 (after Clem et al. 1954). In this figure $z - z_s$ is the height of the balloon above the observation site (which is at height z_s above sea level), ε the elevation angle, ϕ the angle subtended at the center of the earth, a the radius of the earth (assumed spherical), D the great circle distance along AB (which is concentric with OS), d the horizontal distance to the position of the balloon projected onto the tangent plane OP.

Since OPB and CGB are right triangles, we have $h/d = \tan\varepsilon$, $d/(a+z-z_s) = \sin\phi$ and $d/(a+h) = \tan\phi$. Using the first of these to eliminate h from the third, and then using the second to eliminate d, we obtain

$$\cos\phi\cos\varepsilon - \sin\phi\sin\varepsilon = \frac{a\cos\varepsilon}{a+z-z_s}. \tag{5.4}$$

Since the left hand side of (5.4) can be written as $\cos(\phi+\varepsilon)$, we can solve for ϕ to obtain

$$\phi = \cos^{-1}\left(\frac{a\cos\varepsilon}{a+z-z_s}\right) - \varepsilon. \tag{5.5}$$

The great circle distance D is then given by

$$D = (a + z - z_s)\phi. \tag{5.6}$$

The velocity components v_r and v_α are given by

$$v_r = \dot{D}, \tag{5.7}$$

$$v_\alpha = \dot{\alpha}(a + z - z_s)\sin\phi, \tag{5.8}$$

where the dot denotes a time derivative. The eastward component u and the northward component v are then obtained from v_r and v_α by

$$u = v_r \sin\alpha + v_\alpha \cos\alpha, \tag{5.9}$$

$$v = v_r \cos\alpha - v_\alpha \sin\alpha. \tag{5.10}$$

Wind speed and wind direction are easily obtained from either v_r, v_α or u, v.

We can now summarize our Level II wind calculations as follows. We first fit spline interpolation functions to the raw azimuth and elevation angles. We then evaluate the spline functions at equally spaced 3 second intervals. This data is then filtered with the same eleven-point filter described in the previous section, which produces $\bar{\alpha}(t)$ and $\bar{\varepsilon}(t)$. From the time series $\bar{\varepsilon}(t)$ and $z(t)$ we compute the new time series $\phi(t)$ and $D(t)$ using (5.5) and (5.6). We then perform a spline fit to $D(t)$, which gives, as a by-product, $\dot{D}(t)$. The quantities $\dot{D}(t)$ and $\dot{\alpha}(t)$ are then used in (5.7) and (5.8) to compute v_r and v_α, after which wind speed and direction are computed.

Due to problems in measuring the wind discussed earlier in this section, some undesirable oscillations are present in the wind data. To remove these oscillations the AIR software filters the wind data by taking layer averages of the vector wind components u and v. The length of this layer average is a function of the balloon height as follows:

30	sec	up to	2500m AGL
45	sec	up to	5000m AGL
60	sec	up to	7500m AGL
75	sec	up to	10km AGL
90	sec	up to	15km AGL
105	sec	up to	20km AGL
120	sec	above	20km AGL

This filtering is present in the Level I analysis. In the Level II analysis no filtering of u and v is done so that considerable noise is still present in the Level II wind data. Thus, depending on their purposes, users of this data must decide what type of additional smoothing should be applied.

6. Atmospheric sounding data

Each of the soundings was processed by the techniques described in sections 4 and 5. Thus, a table similar to Table 2 is available for each sounding. Here we have chosen to present the data in graphical rather than tabular form. The average temperature and dew point temperature in the lowest 300 mb for the whole experiment period is shown in Fig. 7. The variable inversion height leads to a highly smoothed trade wind inversion structure in this mean sounding. Interesting diurnal variations can be seen in the two-day section of record shown in Fig. 8. This figure illustrates the tendency of the boundary layer to become deeper during the night and morning and to become shallower during the afternoon and early evening. The vertical profiles of T and T_d for each sounding are shown in Fig. 9.

7. Concluding remarks

The Level I and Level II data described in this report are available via anonymous ftp from the machine *rossby.atmos.colostate.edu* (IP address 129.82.107.97). The Level I data totals 39.1 megabytes and the Level II data 23.8 megabytes. Detailed instructions on how to obtain either the Level I or Level II data are contained in the file /dist/astex/sonde/README. Any problems with the data or difficulties in accessing it should be reported to Paul Ciesielski at the following email address: paulc@einstein.atmos.colostate.edu.

Acknowledgments Our participation in ASTEX has been supported by the Marine Meteorology Program of the Office of Naval Research under contract N000014-88-K-0214. For the success of the Porto Santo observational program we are indebted to Dr. William R. Cotton, Dr. Steven K. Krueger, Dr. John M. Davis, Mr. Chris R. Cornwall,

REFERENCES

Ballard, L. J., R. H. Swansborough and R. Johnson, 1983: Detailed specification for a pilot wind power scheme on Porto Santo. ERA Report No. 83-0187. ERA Technology Ltd, Cleeve Road, Leatherhead, Surrey KT22 7SA, England.

Betts, A. K., 1982: Saturation point analysis of moist convective overturning. *J. Atmos. Sci.*, **39**, 1484–1505.

Bolton, D., 1980: The computation of equivalent potential temperature. *Mon. Wea. Rev.*, **108**, 1046–1053.

Clem, L. H., D. Colson and L. P. Harrison, 1954: Corrections of upper-level wind computations for effect of earth's curvature. *Bull. Amer. Meteor. Soc.*, **35**, 357–362.

de Jong, H. M., 1958: Errors in upper-level wind computations. *J. Meteor.*, **15**, 131–137.

FIRE Project Office, 1992: ASTEX Operations Plan. Available from David S. McDougal, FIRE Project Manager, Mail Stop 483, NASA Langley Research Center, Hampton, VA 23665-5225.

Gustafson, A. F., 1954: The error in rawin computations due to neglecting the earth's curvature. *Bull. Amer. Meteor. Soc.*, **35**, 295–300.

Hamming, R. W., 1983: *Digital Filters*, Second Edition. Prentice-Hall, Englewood Cliffs, New Jersey, 257 pp.

Kessler, E., 1954: Curvature corrections for radiowind reports. *Bull. Amer. Meteor. Soc.*, **35**, 328–330.

McVehil, G. E., R. J. Pilié and G. A. Zigrossi, 1965: Some measurements of balloon motions with Doppler radar. *J. Appl. Meteor.*, **4**, 146–148.

Murrow, H. N., and R. M. Henry, 1965: Self-induced balloon motions. *J. Appl. Meteor.*, **4**, 131–138.

Perkins, D. T., 1952: The response of balloons to the wind. *Bull. Amer. Meteor. Soc.*, **33**, 135–139.

Scoggins, J. R., 1965: Spherical balloon wind sensor behavior. *J. Appl. Meteor.*, **4**, 139–145.

Wexler, A., 1976: Vapor pressure formulation for water in range 0 to 100°C. A revision. *J. Res. Nat. Bur. Stand.*, **80A**, 775–785.

TABLE 1

Sounding Number	Date	Start Time (UTC)	End Time (UTC)	Maximum Altitude (km)	Observer's Comments
1	June 01	02:03	03:05	18.5	
2	June 01	04:56	05:35	12.0	
3	June 01	08:04	09:16	22.0	
4	June 01	10:55	12:04	23.9	
5	June 01	14:00	14:56	17.8	
6	June 01	16:56	18:19	26.0	
7	June 01	23:01	23:46	13.5	
8	June 02	05:02	05:28	9.9	Tracking problems below 800mb
9	June 02	07:58	09:20	24.3	
10	June 02	10:57	12:19	23.9	
11	June 02	16:57	18:18	22.6	
12	June 02	20:08	21:12	19.5	
13	June 02	23:28	00:16	14.1	
14	June 03	01:52	02:36	12.7	
15	June 03	04:57	05:20	6.1	Tracking problems below 700mb
16	June 03	07:57	09:09	22.1	
17	June 03	11:02	12:14	20.9	
18	June 03	16:57	17:27	7.8	
19	June 03	23:05	00:15	20.7	
20	June 04	05:00	06:13	21.3	Tracking problems below 600mb
21	June 04	07:57	09:09	23.8	
22	June 04	11:01	12:14	25.0	
23	June 04	14:01	15:16	24.3	
24	June 04	16:50	18:15	25.5	
25	June 04	22:51	00:10	24.9	
26	June 05	05:05	06:16	21.5	
27	June 05	07:55	09:06	23.7	
28	June 05	10:51	12:15	24.7	
29	June 05	13:50	15:15	25.3	
30	June 05	16:47	18:02	24.8	
31	June 05	22:55	00:12	24.8	Tracking problems below 700mb
32	June 06	05:02	06:17	21.5	
33	June 06	07:58	09:15	20.7	
34	June 06	10:51	12:06	24.5	
35	June 06	13:46	15:03	25.3	
36	June 06	16:54	18:14	22.2	
37	June 06	23:03	23:30	7.7	Tracking problems throughout
38	June 07	04:59	06:44	25.2	
39	June 07	08:06	09:28	26.5	
40	June 07	10:56	12:17	24.5	
41	June 07	16:49	17:48	19.1	
42	June 07	22:51	00:19	22.0	
43	June 08	04:56	06:42	15.0	
44	June 08	08:30	09:50	26.0	
45	June 08	10:57	12:14	24.1	
46	June 08	13:59	15:44	25.3	
47	June 08	16:50	18:12	20.0	Noisy wind signal above 70mb
48	June 08	22:48	00:19	19.5	Noisy wind signal above 200mb
49	June 09	01:44	04:04	24.9	Noisy wind signal above 100mb
50	June 09	04:53	05:21	5.8	Missing data from 950-800mb / noisy winds below 700mb
51	June 09	08:05	09:17	19.3	
52	June 09	11:07	12:13	18.6	
53	June 09	14:07	15:18	22.5	
54	June 09	17:03	18:08	20.8	
55	June 09	22:52	23:31	11.7	
56	June 10	01:52	03:21	24.0	
57	June 10	04:55	05:47	14.5	
58	June 10	07:54	09:14	25.1	
59	June 10	13:03	14:28	23.5	
60	June 10	16:55	18:16	26.2	
61	June 10	19:42	21:28	25.5	
62	June 10	22:47	00:15	24.2	
63	June 11	02:01	03:57	28.9	Noisy wind signal above 150 mb
64	June 11	04:49	06:13	21.3	
65	June 11	08:09	09:18	17.5	

66	June 11	11:03	12:19	22.7	
67	June 11	14:03	15:19	18.9	
68	June 11	16:53	18:17	21.7	
69	June 11	20:05	21:17	9.9	Missing and bad data throughtout
70	June 11	22:46	00:05	20.8	
71	June 12	01:50	03:36	24.5	
72	June 12	04:45	06:17	23.0	
73	June 12	08:07	09:18	18.2	
74	June 12	10:51	12:19	26.3	
75	June 12	13:51	15:19	26.1	
76	June 12	16:52	18:17	20.8	
77	June 12	20:06	21:23	17.3	
78	June 12	22:49	00:15	21.0	Noisy wind signal above 700mb
79	June 13	01:53	03:14	11.4	Bad wind data throughtout
80	June 13	05:38	06:39	17.0	
81	June 13	07:50	09:28	25.3	
82	June 13	10:47	12:19	23.4	
83	June 13	14:01	15:32	24.7	
84	June 13	16:52	18:20	22.0	
85	June 13	19:58	21:29	23.5	
86	June 13	22:59	00:17	21.0	
87	June 14	01:52	03:25	27.7	
88	June 14	05:42	06:17	7.9	
89	June 14	07:54	09:25	26.4	Bad wind data between 100-70mb
90	June 14	10:52	12:10	16.4	Bad wind data above 400mb
91	June 14	13:53	15:37	25.3	
92	June 14	16:47	18:20	22.4	
93	June 14	20:09	22:00	25.3	
94	June 14	23:00	23:59	16.6	
95	June 15	07:57	09:13	15.3	Bad winds above 200 mb
96	June 15	10:50	12:19	25.4	Noisy wind signal above 90mb
97	June 15	16:56	18:19	15.8	
98	June 15	19:49	21:41	25.3	
99	June 15	23:32	00:19	17.6	
100	June 16	01:58	03:18	21.7	
101	June 16	04:54	06:24	21.9	
102	June 16	07:58	09:34	25.4	
103	June 16	10:55	12:19	17.2	
104	June 16	13:47	15:49	30.0	
105	June 16	16:56	18:14	15.4	
106	June 16	20:17	21:29	20.9	
107	June 16	22:52	00:18	23.2	
108	June 17	01:56	03:08	21.0	
109	June 17	04:52	06:18	24.1	
110	June 17	08:04	09:25	18.1	
111	June 17	10:53	12:14	18.7	
112	June 17	13:54	15:29	23.7	
113	June 17	16:59	18:18	13.0	
114	June 17	19:59	21:11	20.7	Tracking problems near 600, 400 and 200mb
115	June 17	22:51	00:15	21.2	
116	June 18	01:49	03:13	22.7	
117	June 18	04:53	06:11	22.9	
118	June 18	07:53	09:46	28.0	
119	June 18	10:55	12:41	27.9	
120	June 18	13:54	15:28	22.1	
121	June 18	16:51	18:17	17.4	
122	June 18	20:01	21:18	21.0	Tracking problems above 100mb
123	June 18	22:49	00:15	23.4	
124	June 19	01:54	03:15	23.6	
125	June 19	04:53	05:54	16.3	
126	June 19	07:53	10:00	25.9	
127	June 19	10:54	12:21	14.8	
128	June 19	13:57	15:49	25.3	
129	June 19	17:07	18:20	16.6	
130	June 19	20:48	22:12	22.9	
131	June 19	22:53	00:11	21.9	
132	June 20	01:57	03:03	17.2	
133	June 20	04:54	05:55	17.4	
134	June 20	07:41	09:54	31.4	
135	June 20	10:44	12:17	22.7	
136	June 20	13:45	15:44	27.0	
137	June 20	16:46	18:19	22.6	
138	June 20	19:59	21:21	18.6	
139	June 20	22:57	23:52	12.5	
140	June 21	02:03	04:14	25.4	

141	June 21	04:58	06:18	20.8	
142	June 21	07:51	09:10	22.7	
143	June 21	10:48	12:16	13.4	Bad wind data above 400mb
144	June 21	13:52	14:51	13.4	
145	June 21	16:56	18:20	14.9	Bad wind data above 300mb
146	June 21	19:45	21:16	21.8	
147	June 21	22:54	00:14	22.3	
148	June 22	01:54	03:42	22.6	
149	June 22	04:58	06:18	20.8	
150	June 22	07:39	09:24	25.2	
151	June 22	10:45	12:14	25.4	
152	June 22	13:44	15:20	23.9	
153	June 22	16:41	18:32	23.6	
154	June 22	20:01	21:56	23.8	
155	June 22	22:53	00:16	19.2	
156	June 23	01:51	03:21	22.0	
157	June 23	04:52	06:02	21.1	
158	June 23	07:49	08:55	20.1	
159	June 23	10:47	12:00	21.9	
160	June 23	13:47	15:38	24.5	
161	June 23	16:51	18:08	22.4	
162	June 23	19:56	21:03	19.8	
163	June 23	22:50	00:01	21.2	
164	June 24	01:50	02:38	13.8	
165	June 24	05:04	06:16	22.2	
166	June 24	07:51	09:04	23.0	Missing or bad data between 400 and 100mb
167	June 24	10:44	11:48	21.7	
168	June 24	13:54	15:16	22.5	Tracking problems below 800mb
169	June 24	16:46	18:08	23.2	Tracking problems below 800mb
170	June 24	19:57	21:16	15.2	
171	June 24	22:58	00:15	18.8	
172	June 25	01:44	03:23	22.0	
173	June 25	04:58	06:15	22.2	
174	June 25	07:50	09:07	21.7	
175	June 25	10:51	12:03	22.6	
176	June 25	13:47	14:53	21.5	
177	June 25	16:47	18:15	24.1	
178	June 25	19:44	21:32	25.1	
179	June 25	22:46	00:20	22.5	
180	June 26	01:48	03:32	24.6	
181	June 26	04:37	06:07	23.4	Bad winds between 200-150mb
182	June 26	07:49	09:04	22.3	Tracking problems below 850mb
183	June 26	10:55	12:07	22.2	
184	June 26	13:51	15:08	23.6	
185	June 26	16:48	17:49	21.6	
186	June 26	19:51	20:59	22.5	
187	June 26	22:51	00:48	25.9	
188	June 27	01:59	03:17	22.8	Tracking problems below 850mb and near 400mb
189	June 27	04:49	06:04	22.0	Tracking problems below 900mb
190	June 27	07:50	09:02	21.1	
191	June 27	10:49	11:54	21.1	
192	June 27	13:51	14:45	17.6	
193	June 27	16:40	17:21	11.4	
194	June 27	20:08	21:28	21.5	
195	June 27	22:59	00:19	17.8	
196	June 28	01:48	03:20	22.5	
197	June 28	04:50	06:13	21.4	
198	June 28	07:46	09:12	23.3	
199	June 28	10:45	12:04	21.2	
200	June 28	13:48	15:18	23.3	
201	June 28	16:47	18:05	22.0	
202	June 28	20:14	21:54	22.6	
203	June 28	22:53	00:25	21.0	Tracking problems below 700mb

TABLE 2

Sample of Level I data for 2 June 0848 UTC

TIME	PMB	TEMP	TDEW	RH%	GEOPM	AZDEG	ELDEG	SPEED	DIR	E.TIME
07:58:42.35	1008.10	17.10	12.42	74.00	97	134.70	8.05	2.6	10	0.00
07:58:43.42	1007.96	16.88	12.55	75.72	98	148.45	9.38	2.6	10	1.07
07:58:46.52	1006.22	16.70	12.43	75.98	113	152.77	17.02	6.1	353	6.31
07:58:48.66	1005.23	16.63	12.41	76.21	121	154.68	19.08	6.4	352	8.45
07:58:50.81	1004.10	16.55	12.35	76.29	131	156.68	22.10	6.8	352	10.60
07:58:52.95	1002.81	16.45	12.27	76.41	142	157.32	24.55	7.2	351	12.74
07:58:55.15	1001.45	16.36	12.29	76.93	153	157.60	26.98	7.8	351	14.94
07:58:57.29	1000.12	16.27	12.27	77.26	165	161.25	29.30	7.6	351	17.08
07:58:59.43	999.05	16.17	12.25	77.68	174	161.93	29.92	7.4	352	19.22
07:59:01.57	998.18	16.03	11.99	77.03	181	162.38	31.52	7.2	353	21.36
07:59:03.71	997.26	15.92	11.88	77.01	189	164.95	31.52	7.0	353	23.50
07:59:05.91	996.12	15.83	11.82	77.11	199	166.50	30.65	6.8	357	25.70
07:59:08.05	994.91	15.63	11.75	77.75	209	168.15	31.67	6.7	358	27.84
07:59:10.20	993.82	15.53	11.76	78.33	219	167.48	31.10	6.8	358	29.99
07:59:12.39	992.90	15.46	11.79	78.84	226	167.73	30.95	6.8	359	32.18
07:59:14.53	992.19	15.38	11.80	79.31	233	169.43	30.45	6.4	360	34.32
07:59:16.73	991.08	15.29	11.87	80.11	242	168.40	29.92	6.2	2	36.52
07:59:18.87	990.28	15.22	11.92	80.79	249	168.55	29.92	6.2	2	38.66

Sample of Level II data for 2 June 0848 UTC

	z(m)	P(mb)	T(c)	Td(c)	SPEED (m/s)	DIRECTION (degrees)
1	97.	1008.10	17.10	12.42	2.60	10.00
2	100.	1007.89	16.87	12.57	11.04	328.63
3	110.	1006.70	16.75	12.48	8.79	309.83
4	120.	1005.51	16.65	12.43	6.82	327.35
5	130.	1004.33	16.57	12.38	5.83	326.02
6	140.	1003.14	16.48	12.31	6.19	329.96
7	150.	1001.96	16.39	12.30	5.36	340.61
8	160.	1000.78	16.31	12.30	4.72	355.98
9	170.	999.59	16.21	12.28	5.07	2.23
10	180.	998.42	16.07	12.08	5.17	3.82
11	190.	997.24	15.93	11.91	5.64	7.98
12	200.	996.06	15.83	11.83	7.22	2.53
13	210.	994.88	15.62	11.76	7.47	357.82
14	220.	993.70	15.51	11.78	7.37	353.39
15	230.	992.53	15.42	11.81	7.39	348.93
16	240.	991.35	15.31	11.87	7.34	348.47
17	250.	990.18	15.22	11.94	6.99	1.89

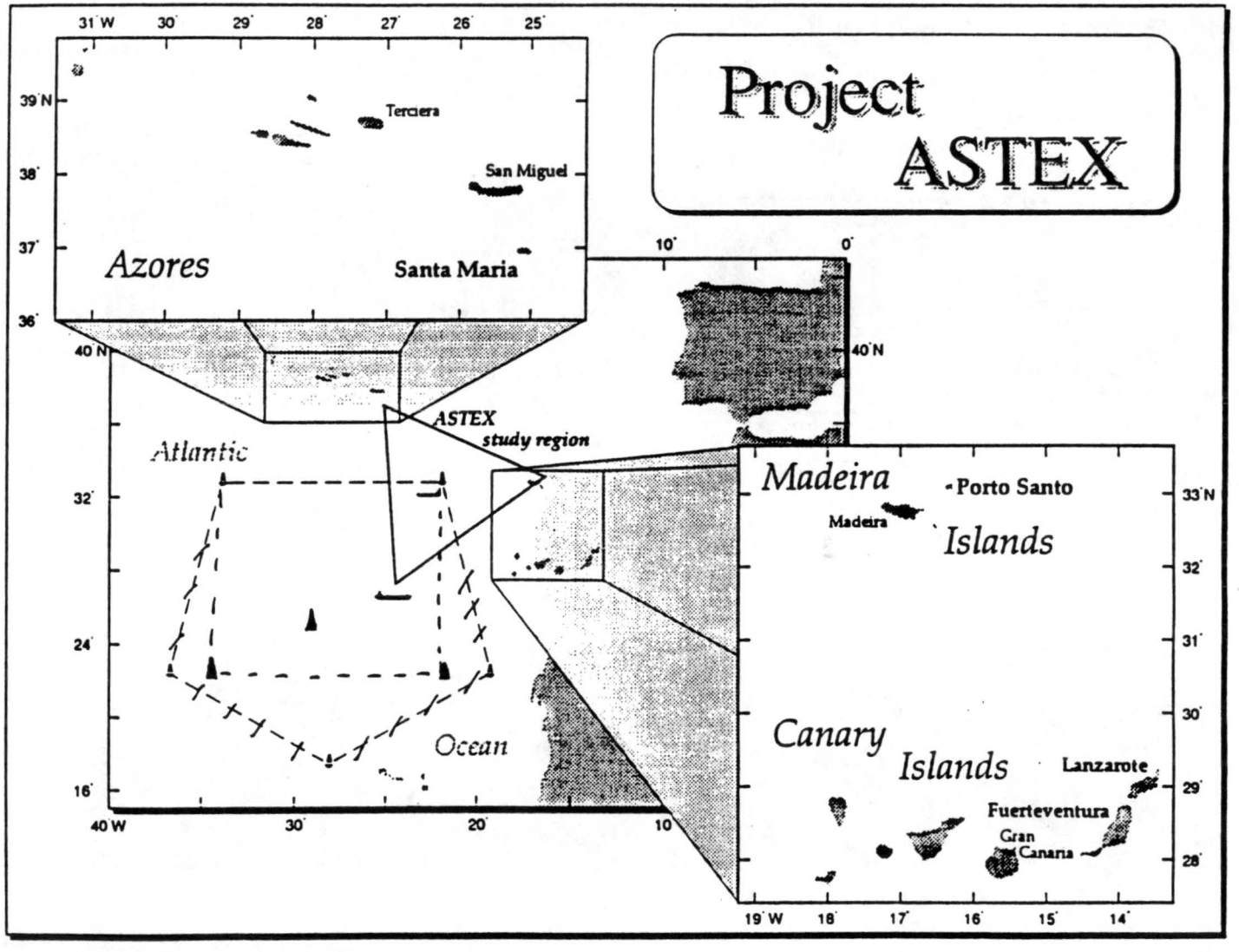

Figure 1. Map of the ASTEX region showing the triangular array of wind profiler/upper air measurements and the array of buoys associated with the oceanographic subduction experiment (from ASTEX Operations Plan, page 24).

Figure 2. Porto Santo Island. The experimental site was 97m above sea level, 295m north of the end of the airport runway, and 200m south of the cliff edge.

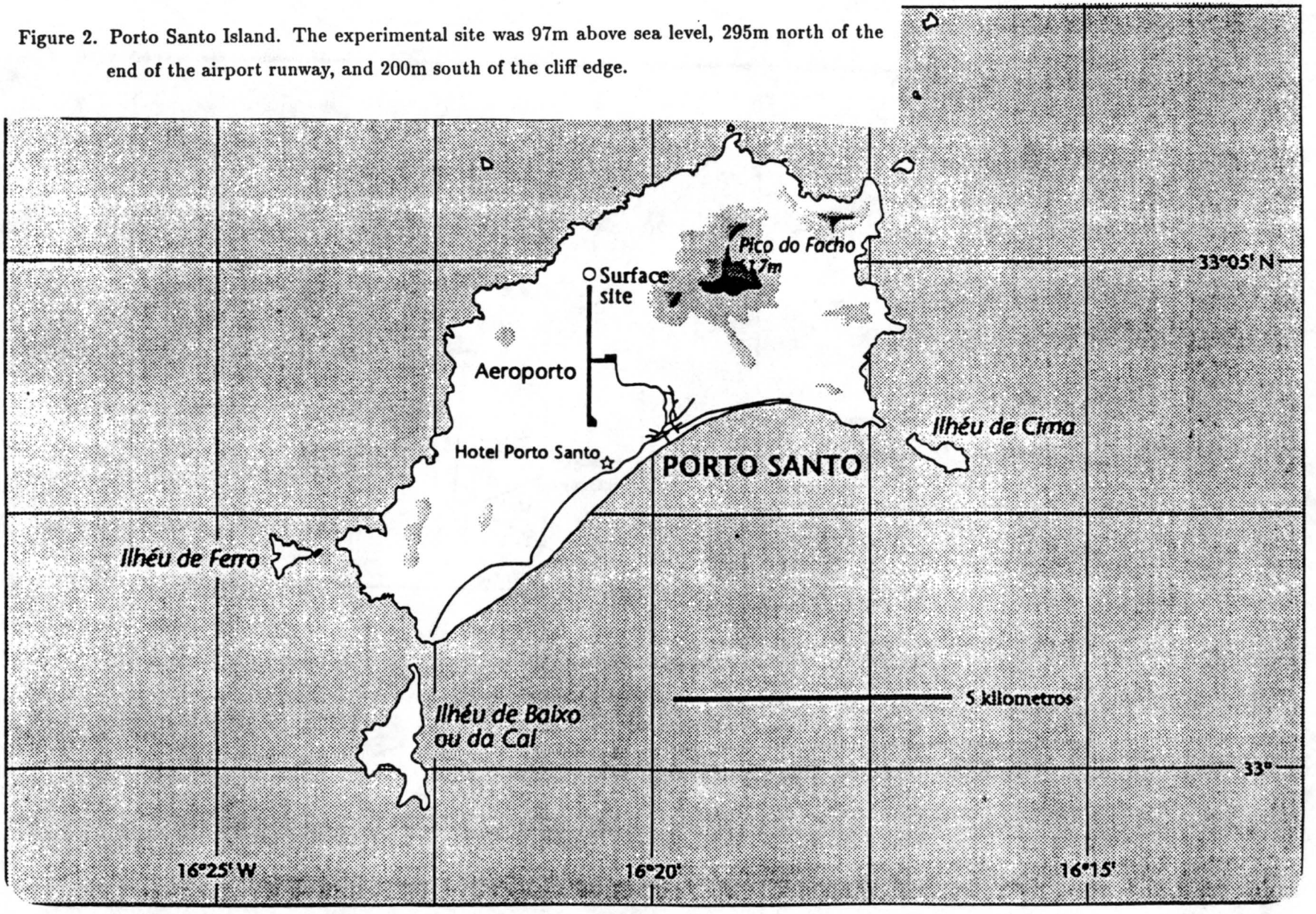

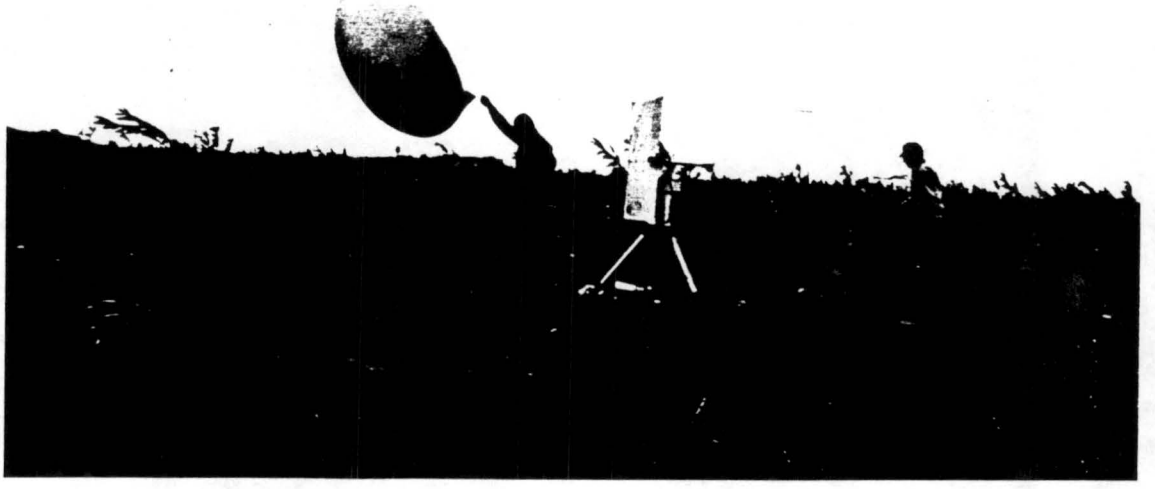

Figure 3. John Kleist (left) and William Cotton prepare for launch under windy, stratocumulus conditions on Porto Santo. Between them is the automatically tracking radiotheodolite, which measures azimuth and elevation angles of the balloon.

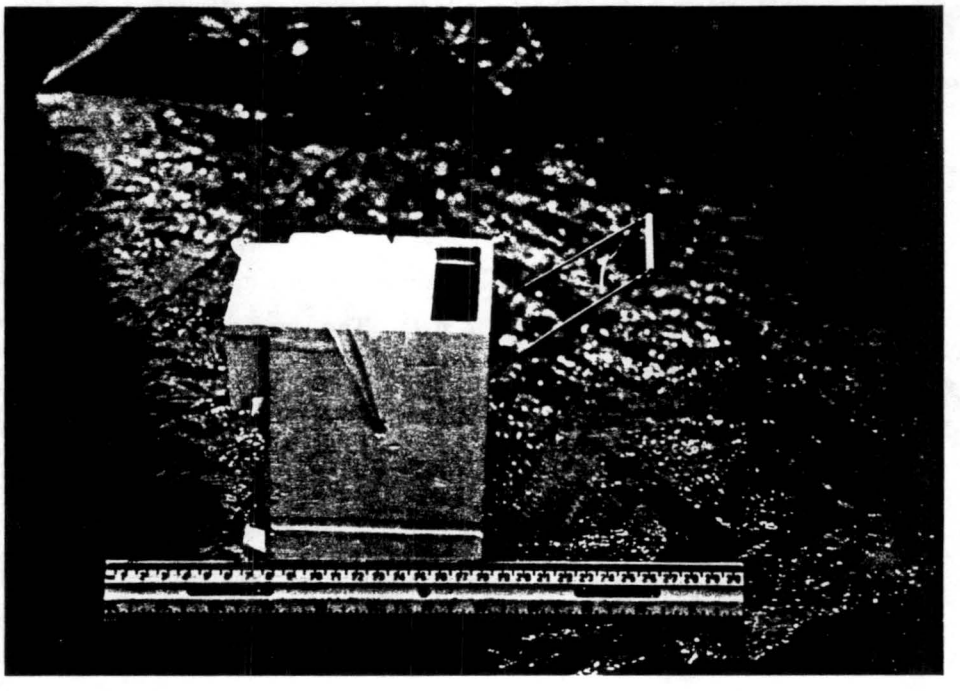

Figure 4. AIR Intellisonde, which is 10cm on the sides, 15cm high, and has a mass of 240g. The rod thermistor is on the right. The hygristor is in the radiation shielded compartment at the top of the sonde. As the sonde rises, air enters the inlet at the top, flows horizontally across the hygristor, and then exits downward at the left of the sonde. The sonde transmits at 1680 MHz via a quarter wave antenna which extends from the bottom (not visible).

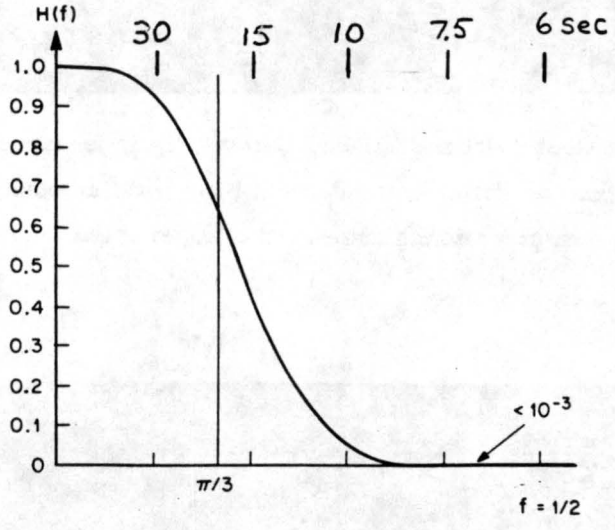

Figure 5. Monotone spectral response of the filter used in sections 4 and 5 for the processing of the thermodynamic and wind data. The lower abscissa is labeled in frequency (where $f = 1/2$ corresponds to one-half oscillation per data point) and the upper abscissa in period (seconds) assuming a 3 second interval between data points. The filter effectively removes oscillations with periods shorter than 18 seconds.

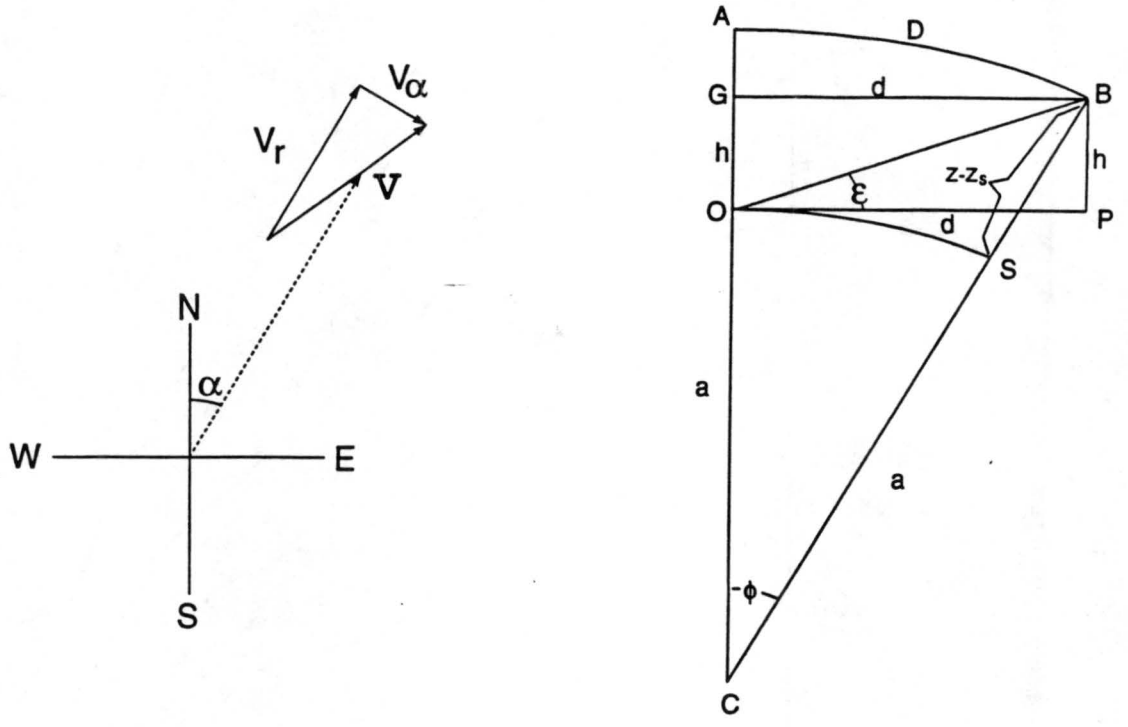

Figure 6. The left diagram shows the balloon position (dashed vector) at azimuth α. The wind at this balloon position is $\mathbf{v}$, which has horizontal components v_r in the radial direction and v_α in the tangential direction. The right diagram is a vertical plane through the center of the earth (C), the radiotheodolite observation site (O) and the balloon position (B) (after Clem et al. 1954). Here $z - z_s$ is height of the balloon above the observation site, ε the elevation angle, ϕ the angle subtended at the center of the earth, a the radius of the earth (assumed spherical), D the great circle distance along AB (which is concentric with OS), d the horizontal distance to the position of the balloon projected onto the tangent plane OP.

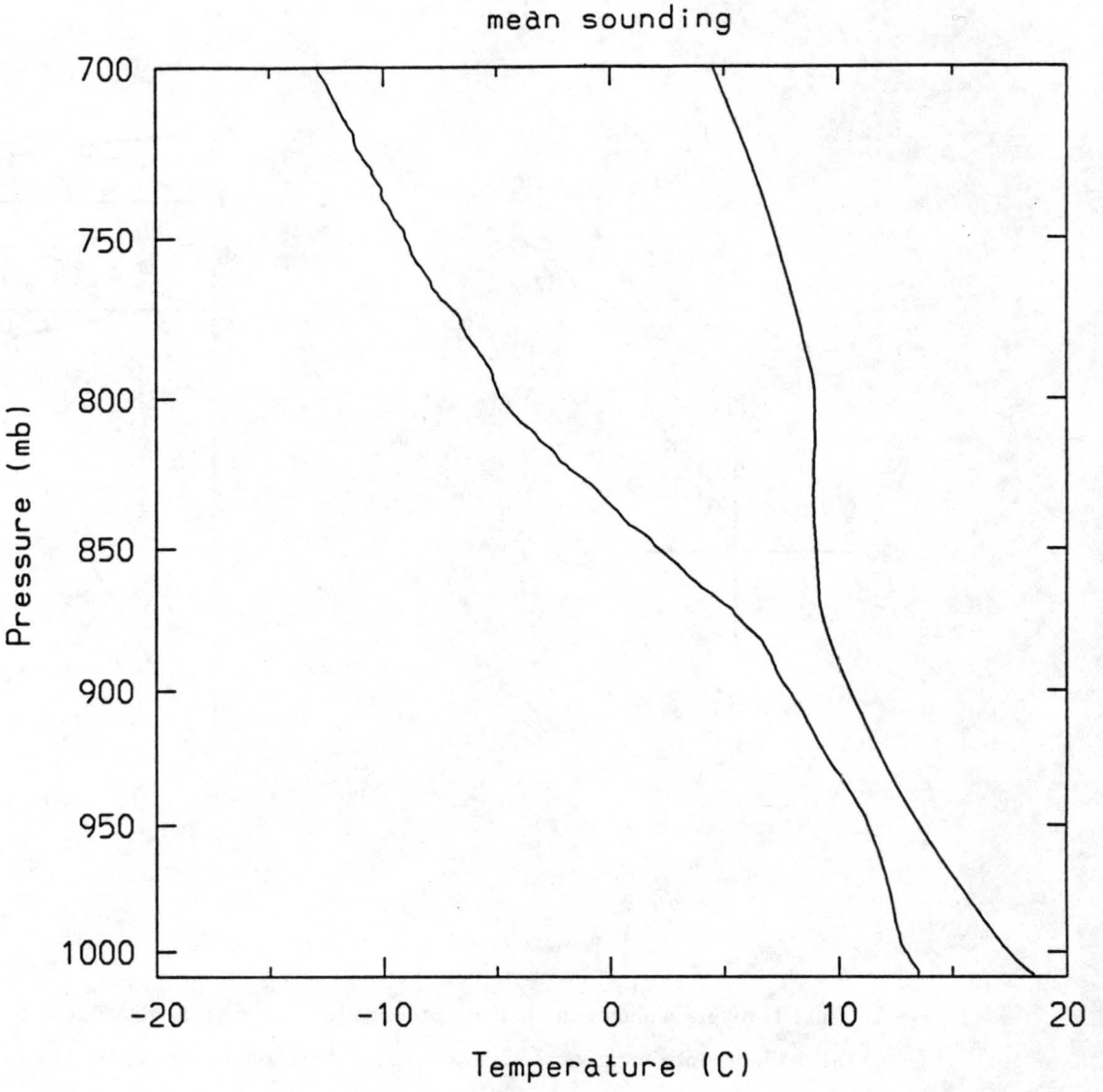

Figure 7. Average temperature and dew point temperature for the entire 1–2 June 1992 period.

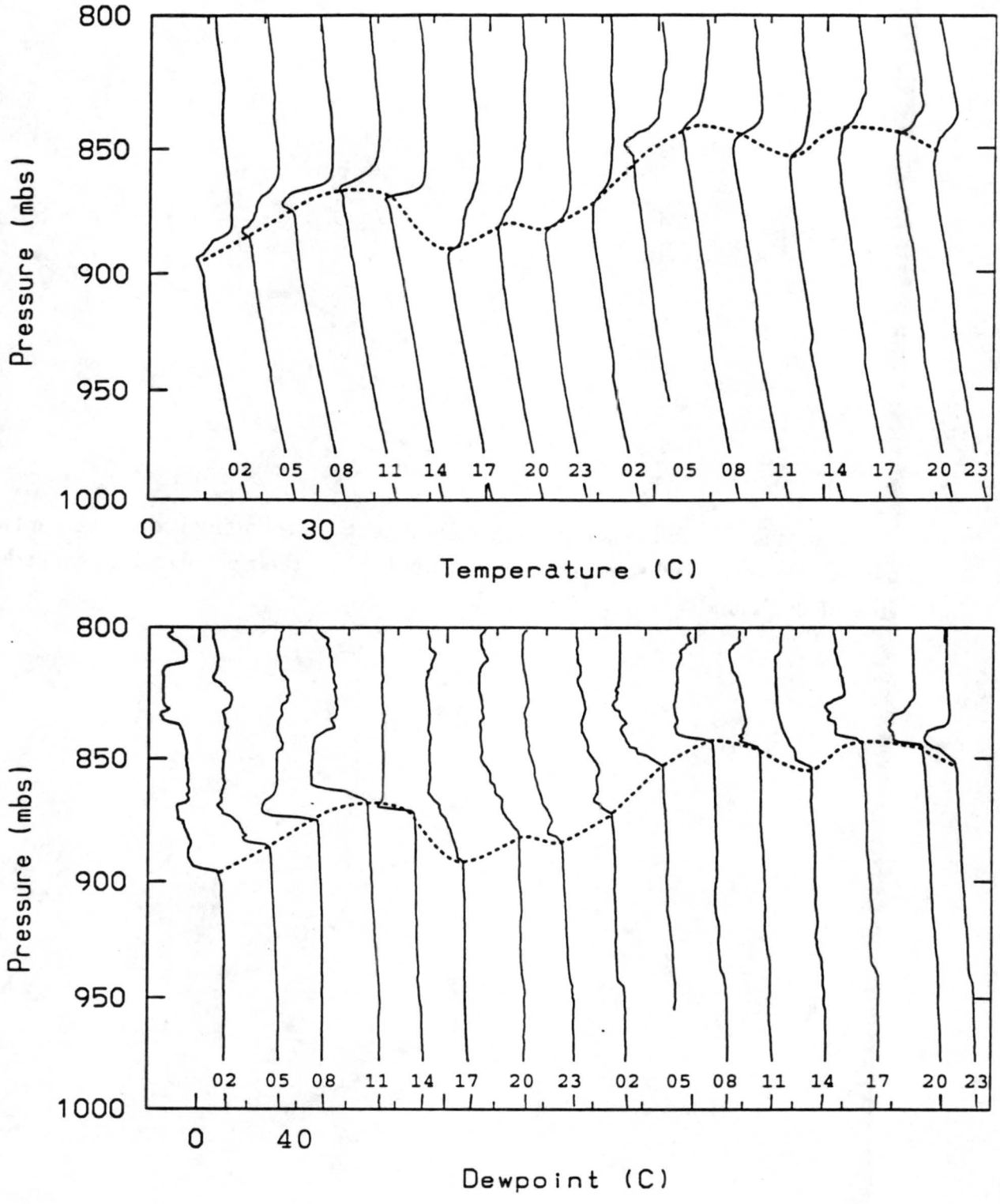

Figure 8. A two day record of temperature (top) and dew point temperature (bottom) from 18–19 June 1992. Each successive profile is shifted to the right to avoid overlap. Times labeled near the bottom of each curve are the UTC hour near launch time (e.g., the curves labeled 02 are soundings launched near 02 UTC and completed near 03 : 30 UTC, the 02 label corresponding better to the time the balloon was in the boundary layer).

Figure 9. The full set of ASTEX soundings. Each sounding is displayed in two panels—the left panel showing the full sounding and the right panal an expanded view of the boundary layer structure.

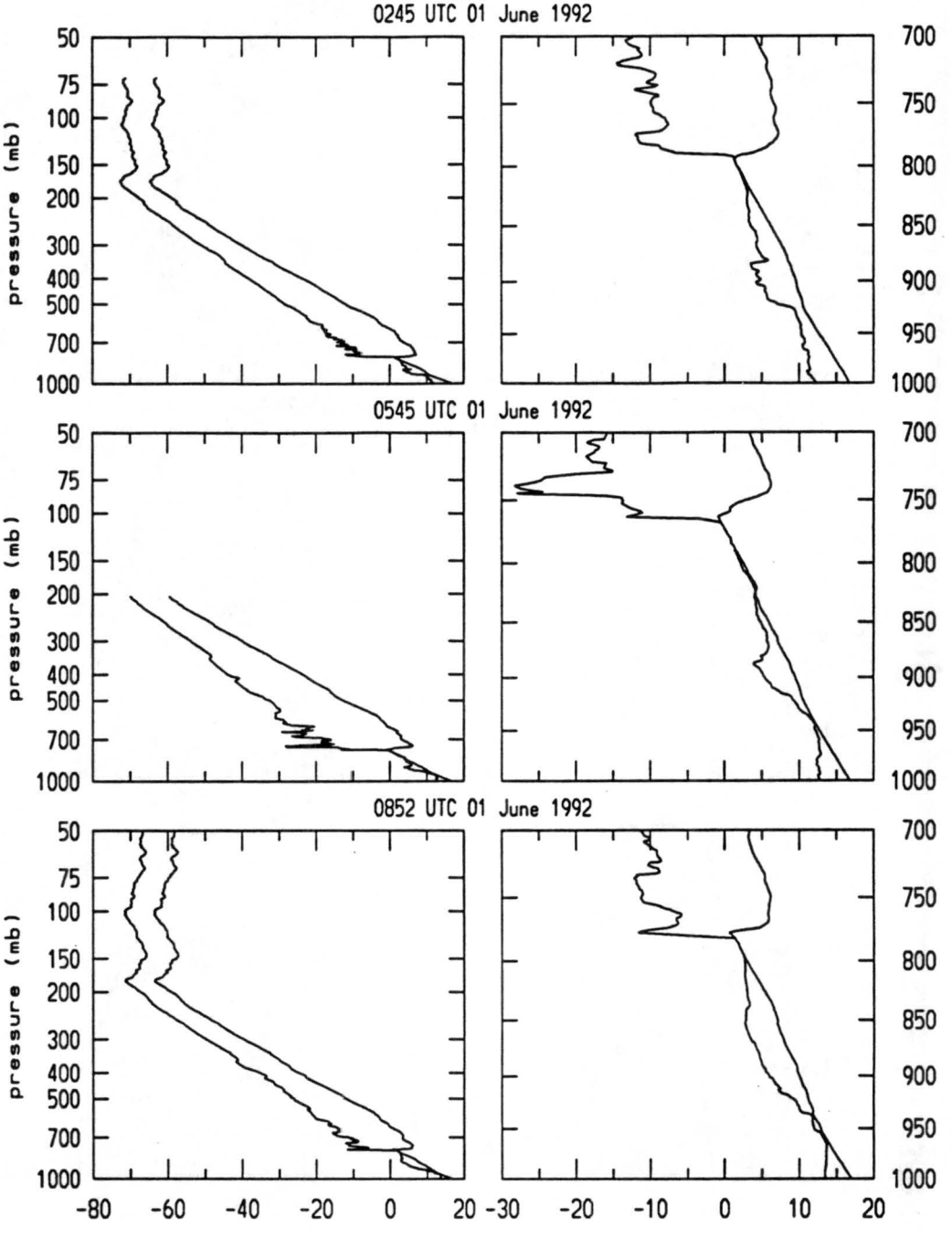
0245 UTC 01 June 1992
0545 UTC 01 June 1992
0852 UTC 01 June 1992
pressure (mb)
50
75
100
150
200
300
400
500
700
1000
700
750
800
850
900
950
1000
-80
-60
-40
-20
0
20
-30
-20
-10
0
10
20

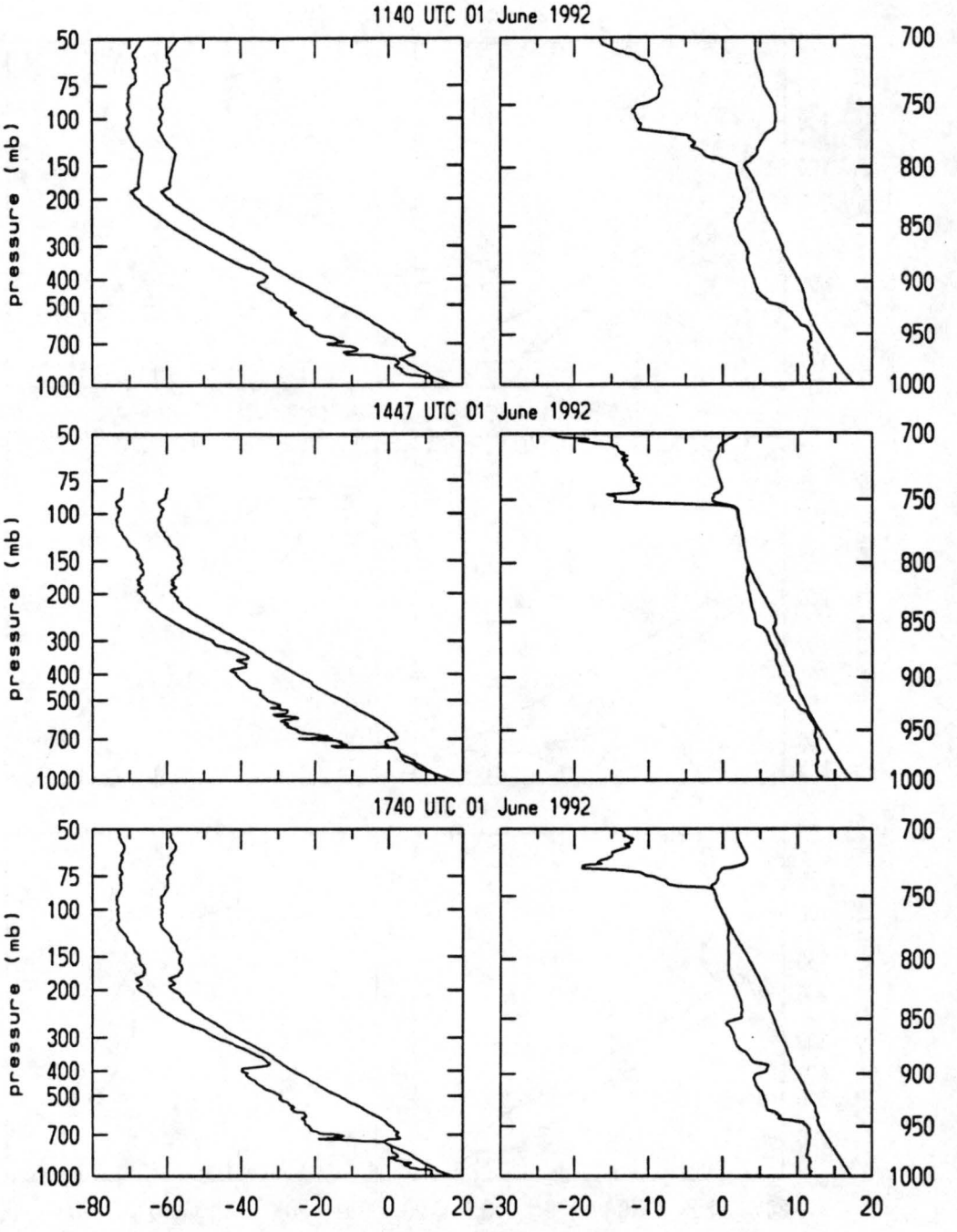
1140 UTC 01 June 1992
1447 UTC 01 June 1992
1740 UTC 01 June 1992
pressure (mb)
50
75
100
150
200
300
400
500
700
1000
700
750
800
850
900
950
1000
-80
-60
-40
-20
0
20
-30
-20
-10
0
10
20

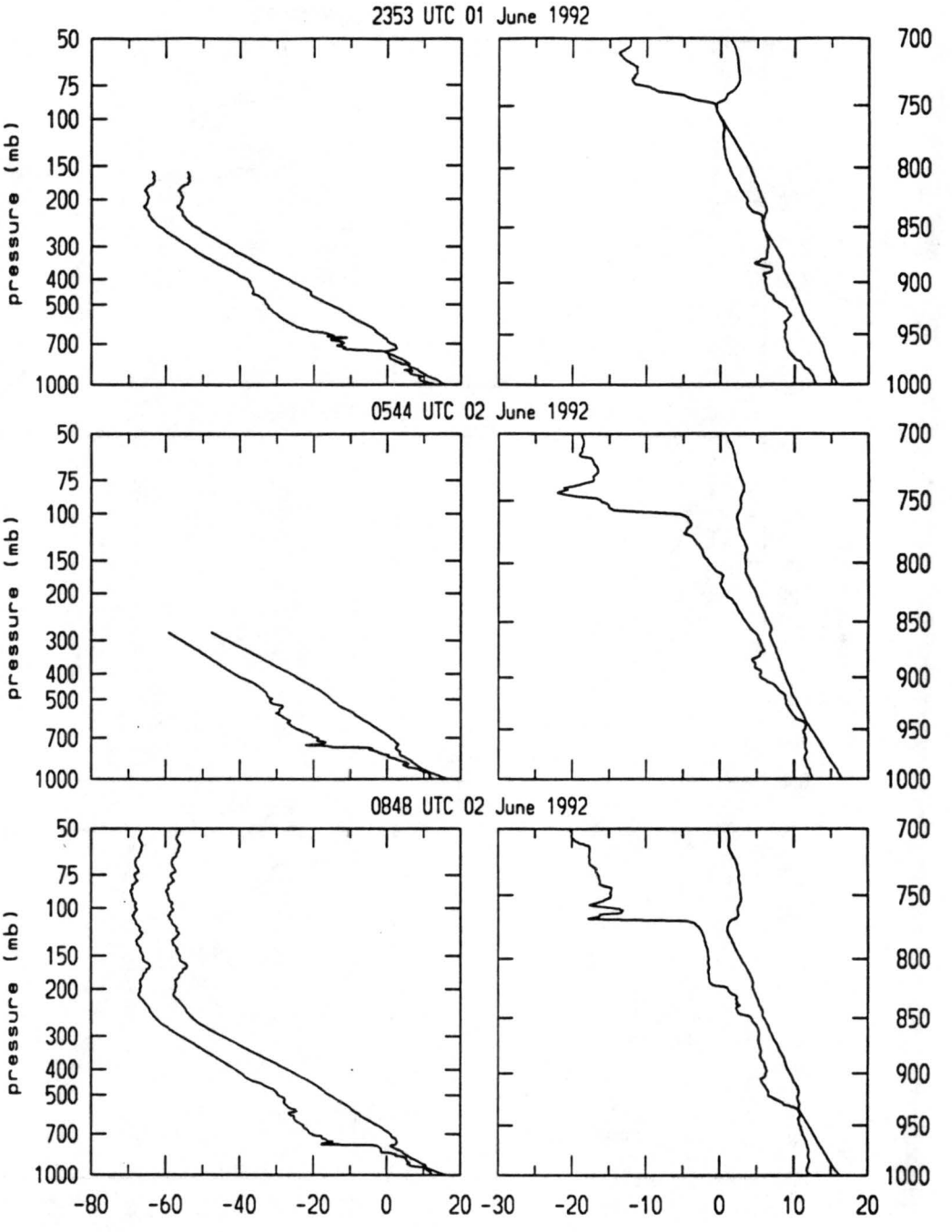
2353 UTC 01 June 1992
0544 UTC 02 June 1992
0848 UTC 02 June 1992
pressure (mb)
50
75
100
150
200
300
400
500
700
1000
700
750
800
850
900
950
1000
-80
-60
-40
-20
0
20
-30
-20
-10
0
10
20

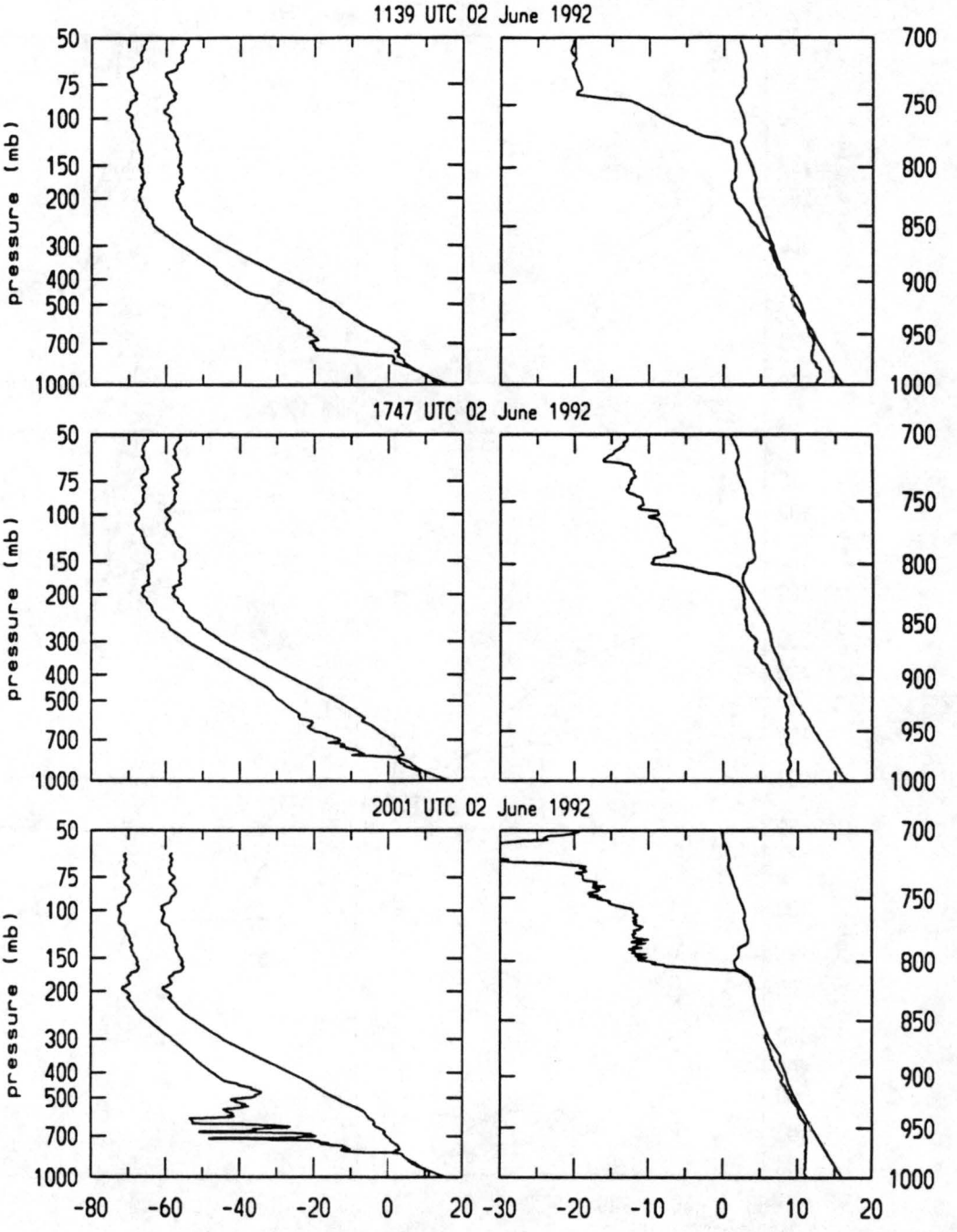
1139 UTC 02 June 1992
1747 UTC 02 June 1992
2001 UTC 02 June 1992
pressure (mb)
50
75
100
150
200
300
400
500
700
1000
700
750
800
850
900
950
1000
-80
-60
-40
-20
0
20
-30
-20
-10
0
10
20

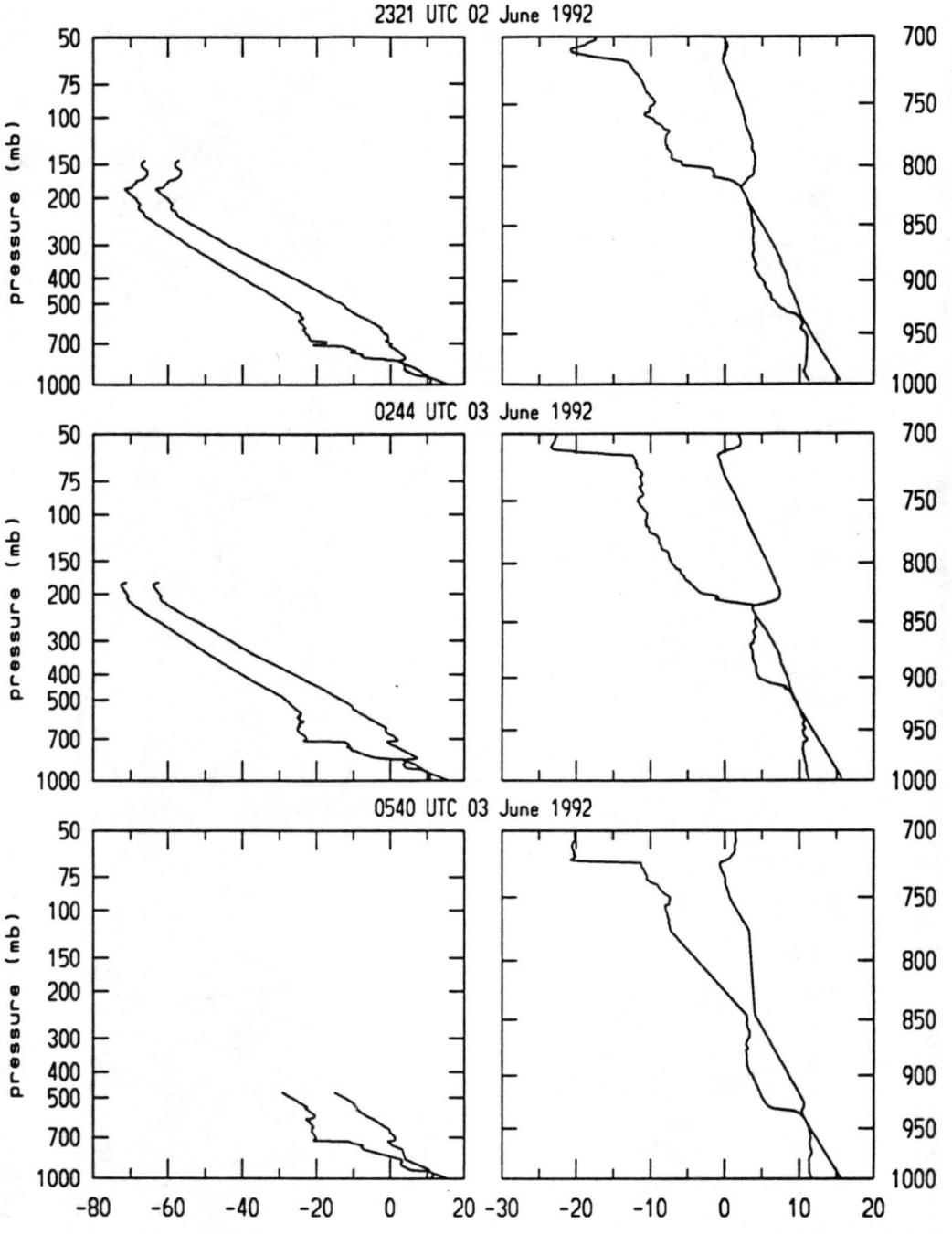
2321 UTC 02 June 1992
0244 UTC 03 June 1992
0540 UTC 03 June 1992
pressure (mb)
50
75
100
150
200
300
400
500
700
1000
700
750
800
850
900
950
1000
-80
-60
-40
-20
0
20
-30
-20
-10
0
10
20

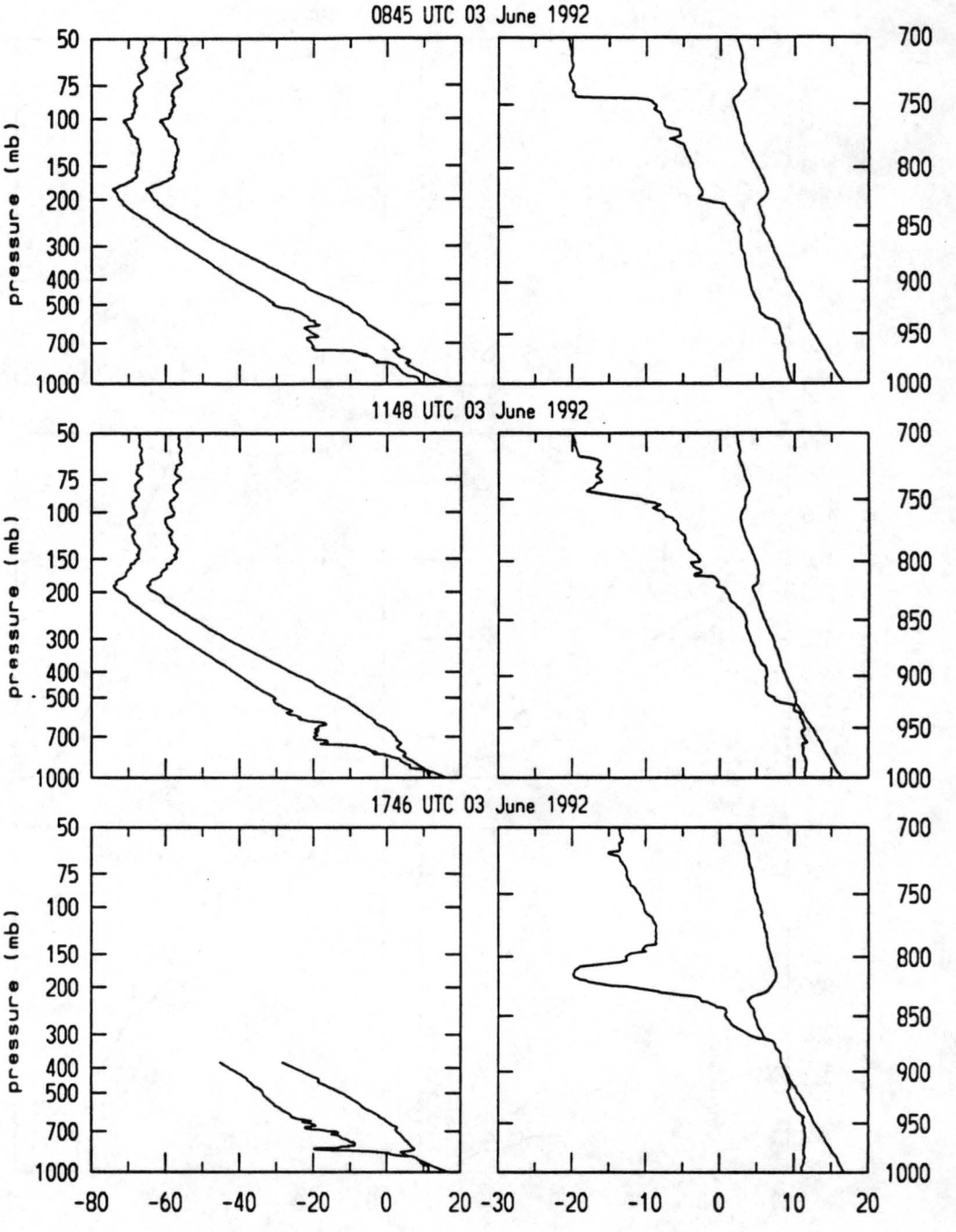
0845 UTC 03 June 1992
1148 UTC 03 June 1992
1746 UTC 03 June 1992
pressure (mb)
50
75
100
150
200
300
400
500
700
1000
700
750
800
850
900
950
1000
-80
-60
-40
-20
0
20
-30
-20
-10
0
10
20

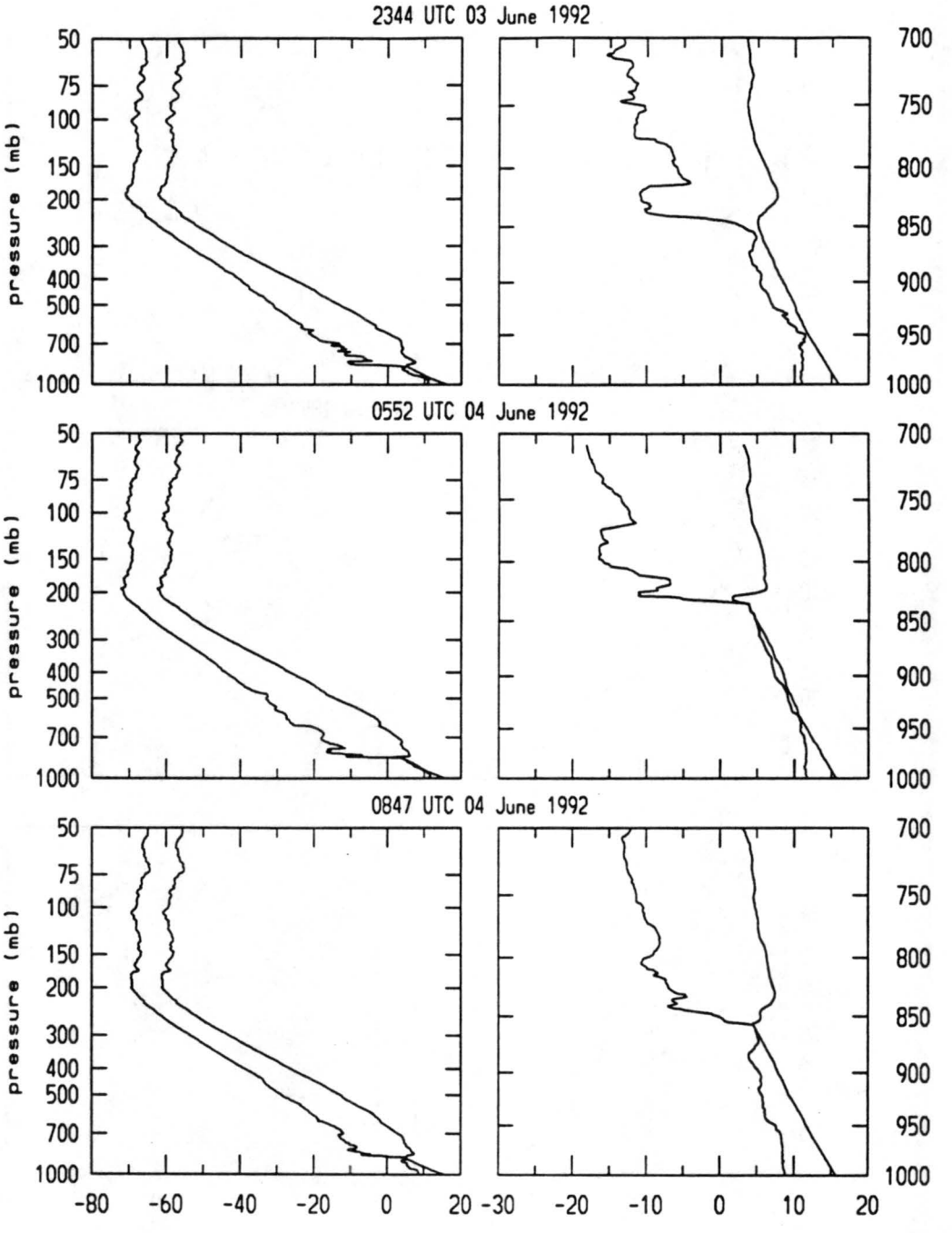
2344 UTC 03 June 1992
0552 UTC 04 June 1992
0847 UTC 04 June 1992
pressure (mb)
50
75
100
150
200
300
400
500
700
1000
700
750
800
850
900
950
1000
-80
-60
-40
-20
0
20
-30
-20
-10
0
10
20

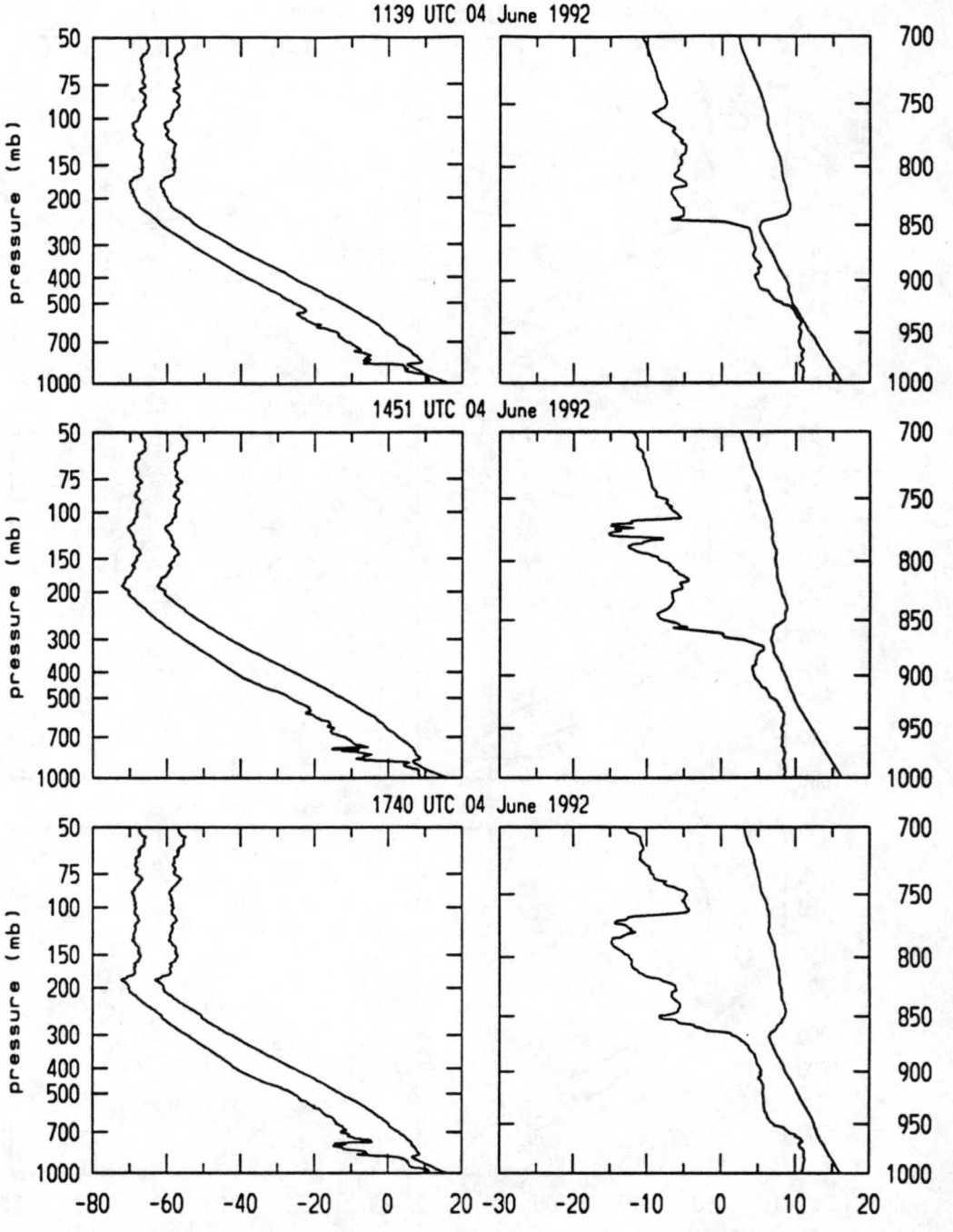
1139 UTC 04 June 1992
1451 UTC 04 June 1992
1740 UTC 04 June 1992
pressure (mb)
50
75
100
150
200
300
400
500
700
1000
700
750
800
850
900
950
1000
-80
-60
-40
-20
0
20
-30
-20
-10
0
10
20

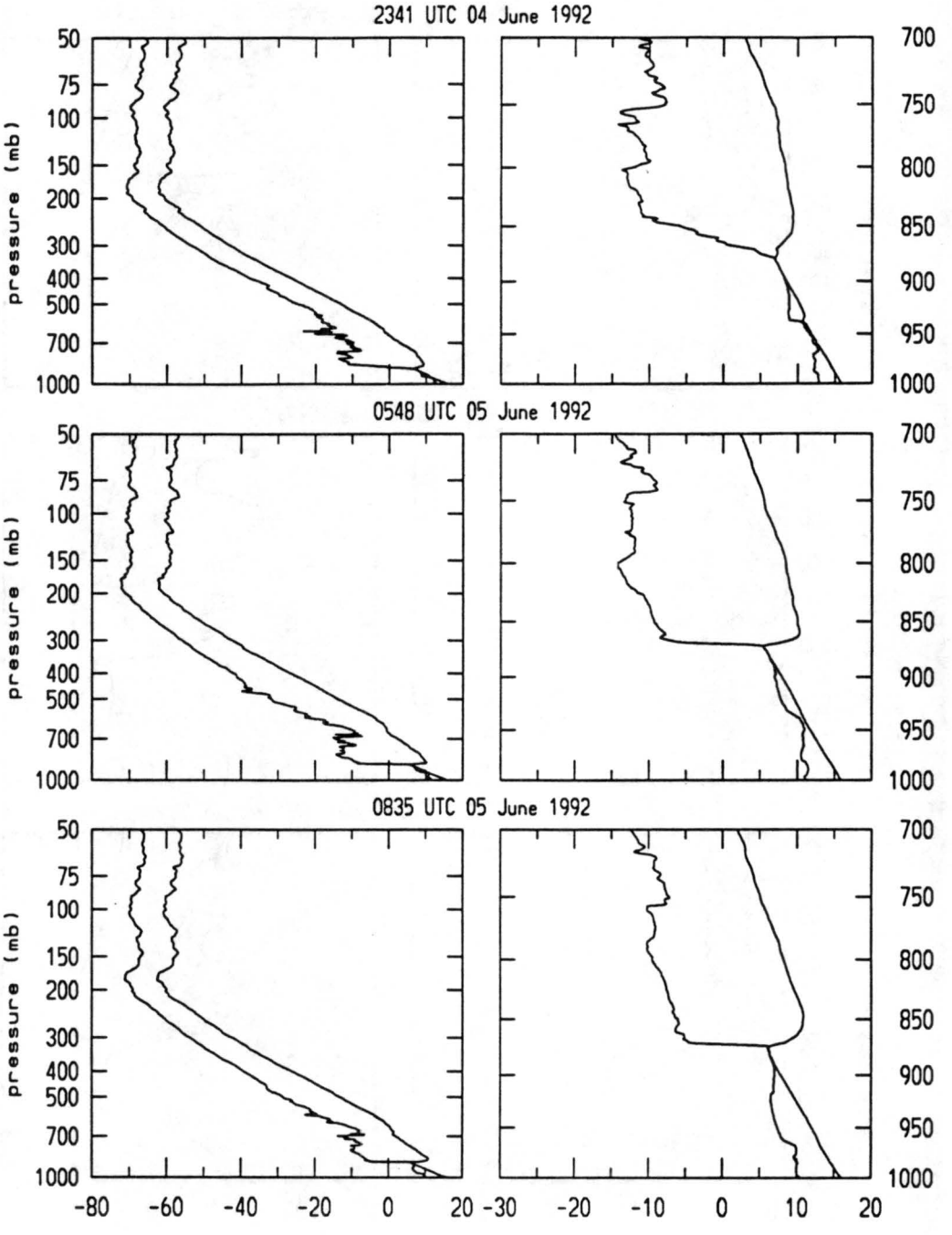
2341 UTC 04 June 1992
0548 UTC 05 June 1992
0835 UTC 05 June 1992
pressure (mb)
50
75
100
150
200
300
400
500
700
1000
700
750
800
850
900
950
1000
-80
-60
-40
-20
0
20
-30
-20
-10
0
10
20

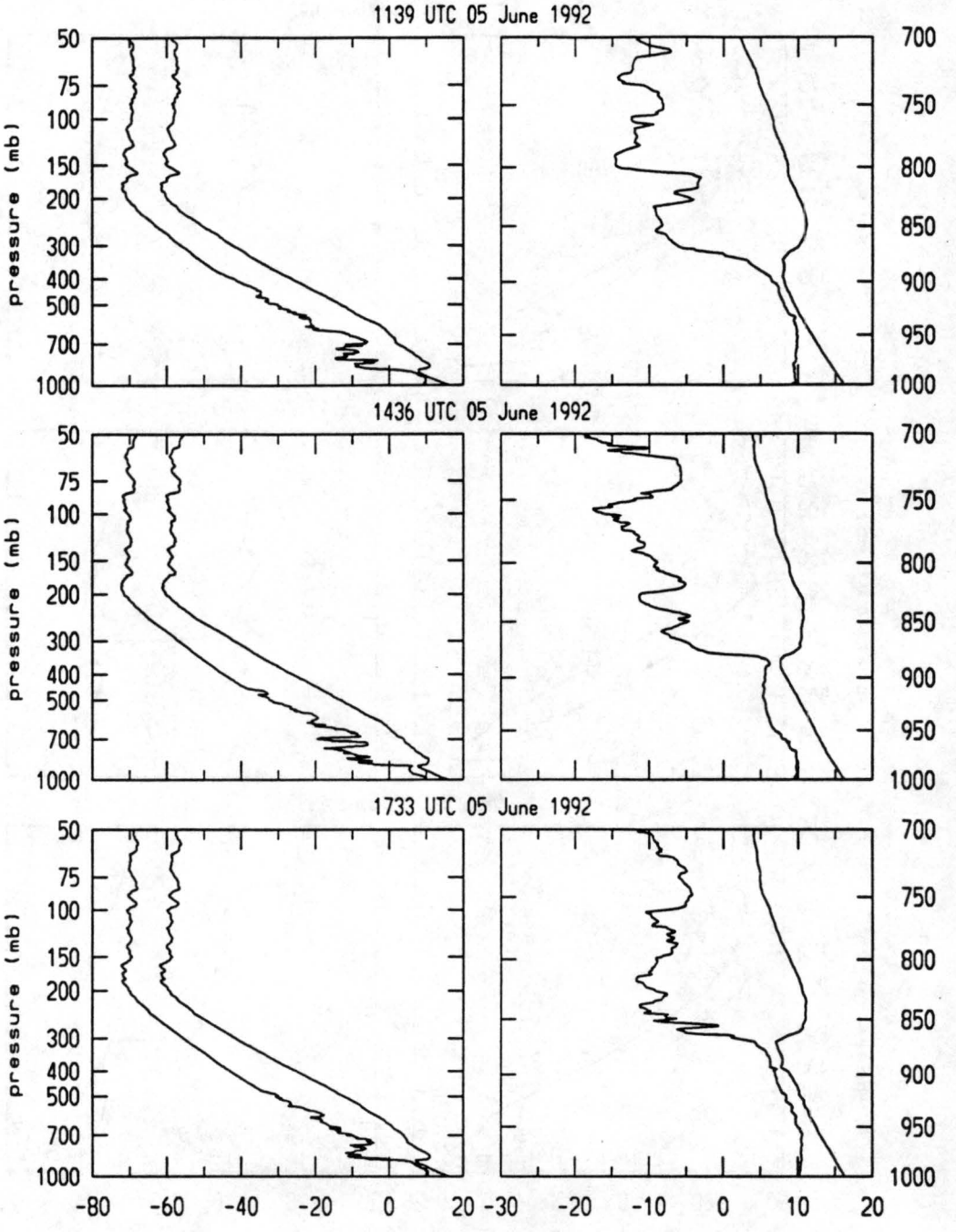
1139 UTC 05 June 1992
1436 UTC 05 June 1992
1733 UTC 05 June 1992
pressure (mb)
50
75
100
150
200
300
400
500
700
1000
700
750
800
850
900
950
1000
-80
-60
-40
-20
0
20
-30
-20
-10
0
10
20

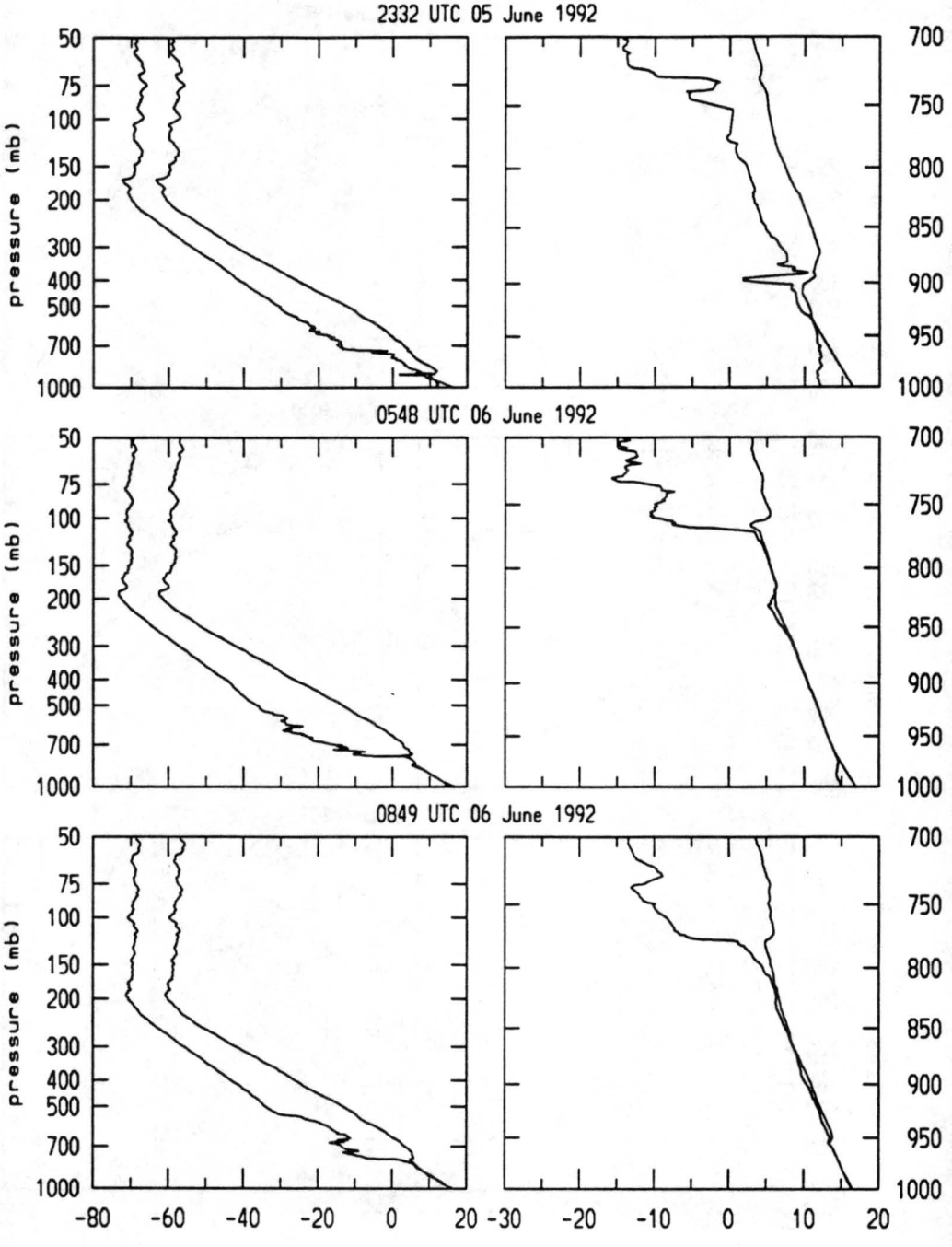
2332 UTC 05 June 1992
0548 UTC 06 June 1992
0849 UTC 06 June 1992
pressure (mb)
50
75
100
150
200
300
400
500
700
1000
700
750
800
850
900
950
1000
-80
-60
-40
-20
0
20
-30
-20
-10
0
10
20

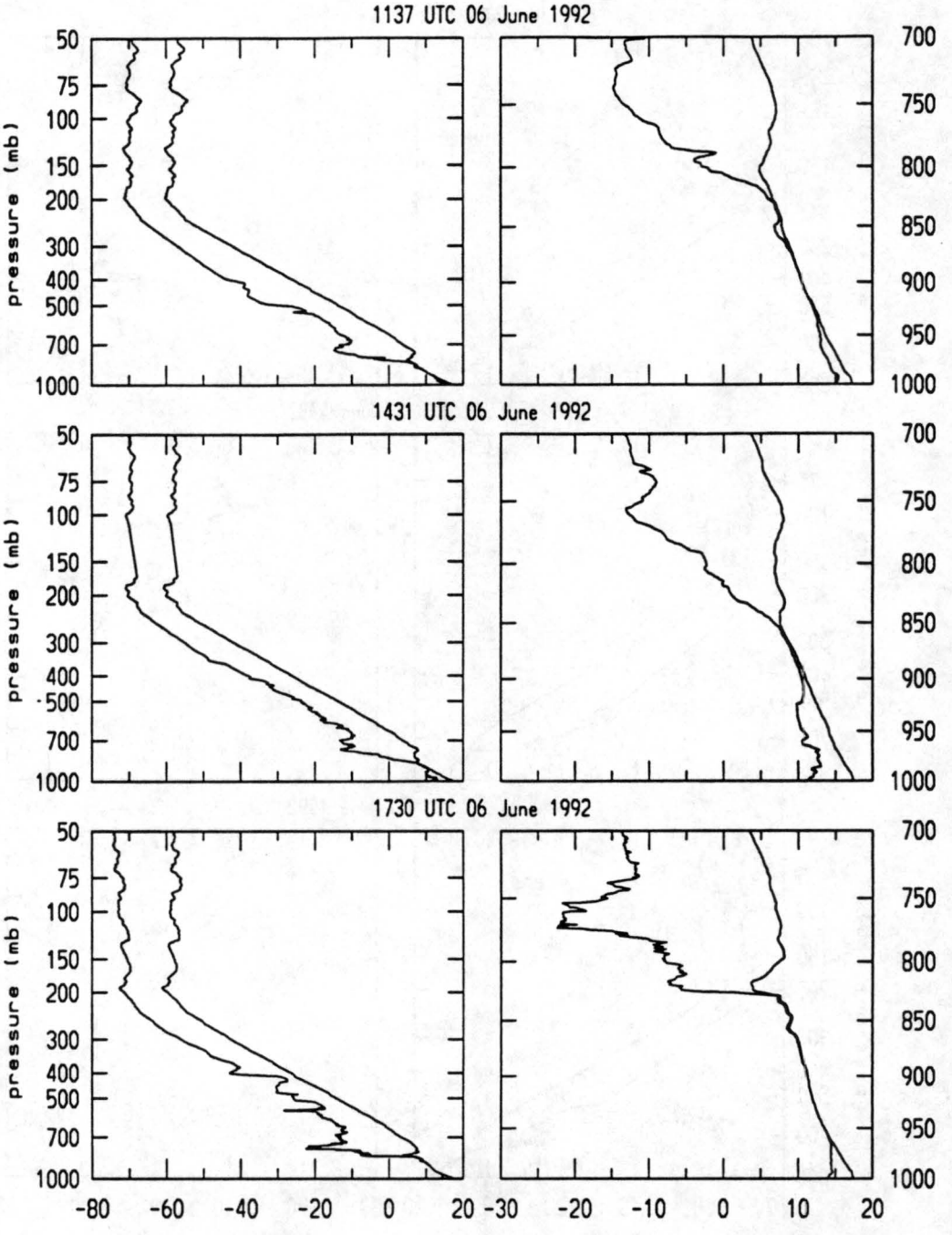
1137 UTC 06 June 1992
1431 UTC 06 June 1992
1730 UTC 06 June 1992
pressure (mb)
50
75
100
150
200
300
400
500
700
1000
700
750
800
850
900
950
1000
-80
-60
-40
-20
0
20
-30
-20
-10
0
10
20

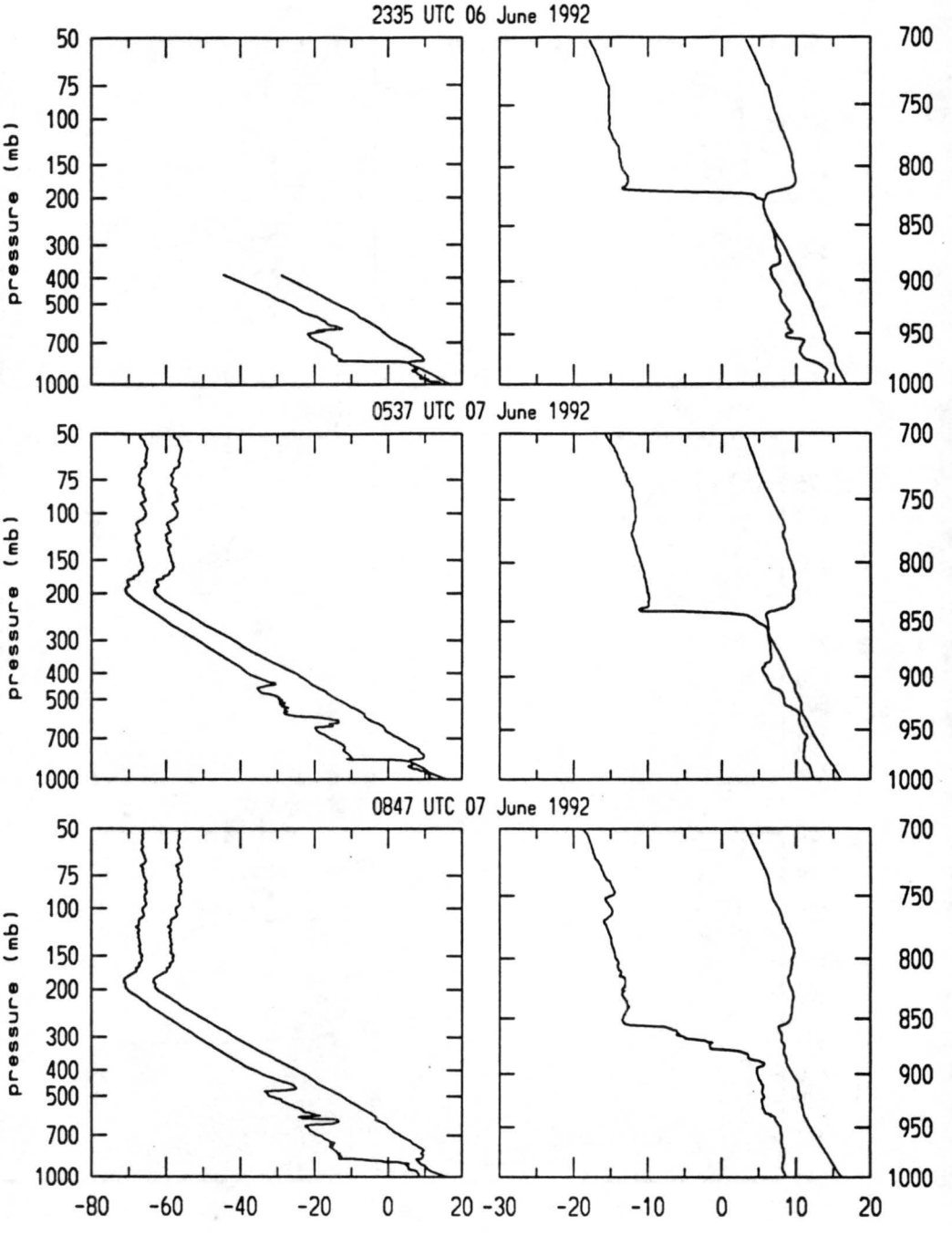
2335 UTC 06 June 1992
0537 UTC 07 June 1992
0847 UTC 07 June 1992
pressure (mb)
50
75
100
150
200
300
400
500
700
1000
700
750
800
850
900
950
1000
-80
-60
-40
-20
0
20
-30
-20
-10
0
10
20

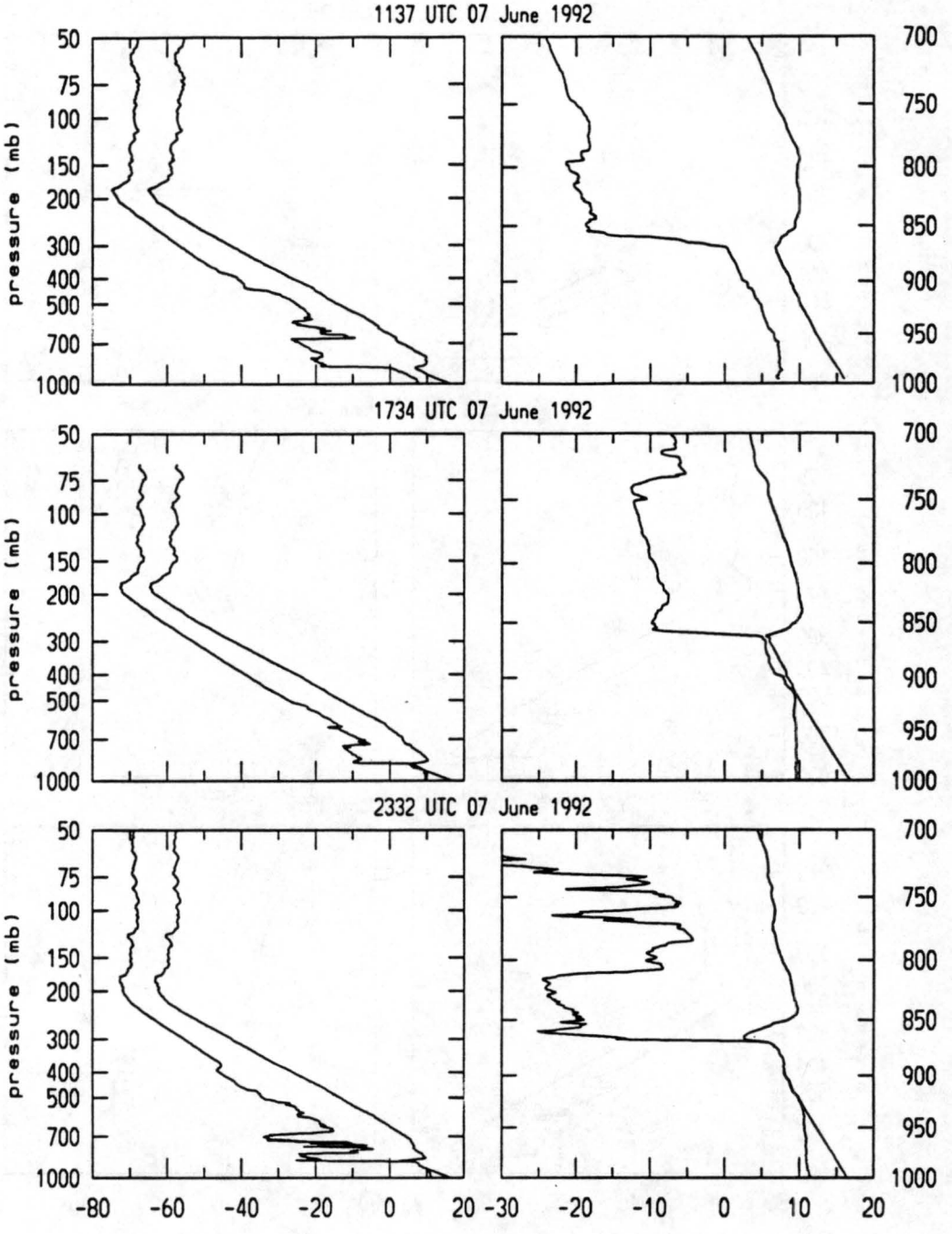
1137 UTC 07 June 1992
1734 UTC 07 June 1992
2332 UTC 07 June 1992
pressure (mb)
50
75
100
150
200
300
400
500
700
1000
700
750
800
850
900
950
1000
-80
-60
-40
-20
0
20
-30
-20
-10
0
10
20

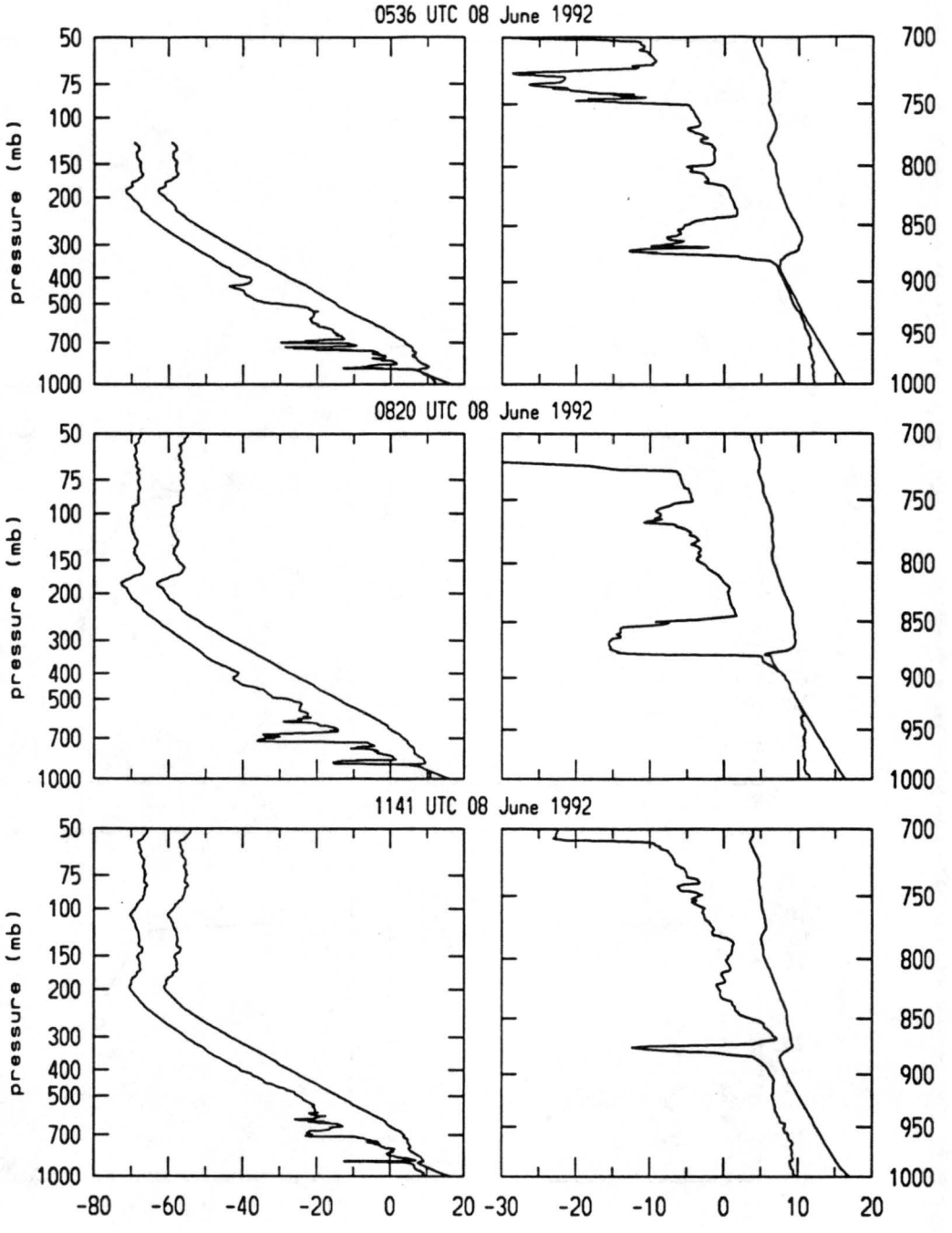
0536 UTC 08 June 1992
0820 UTC 08 June 1992
1141 UTC 08 June 1992
pressure (mb)
50
75
100
150
200
300
400
500
700
1000
700
750
800
850
900
950
1000
-80
-60
-40
-20
0
20
-30
-20
-10
0
10
20

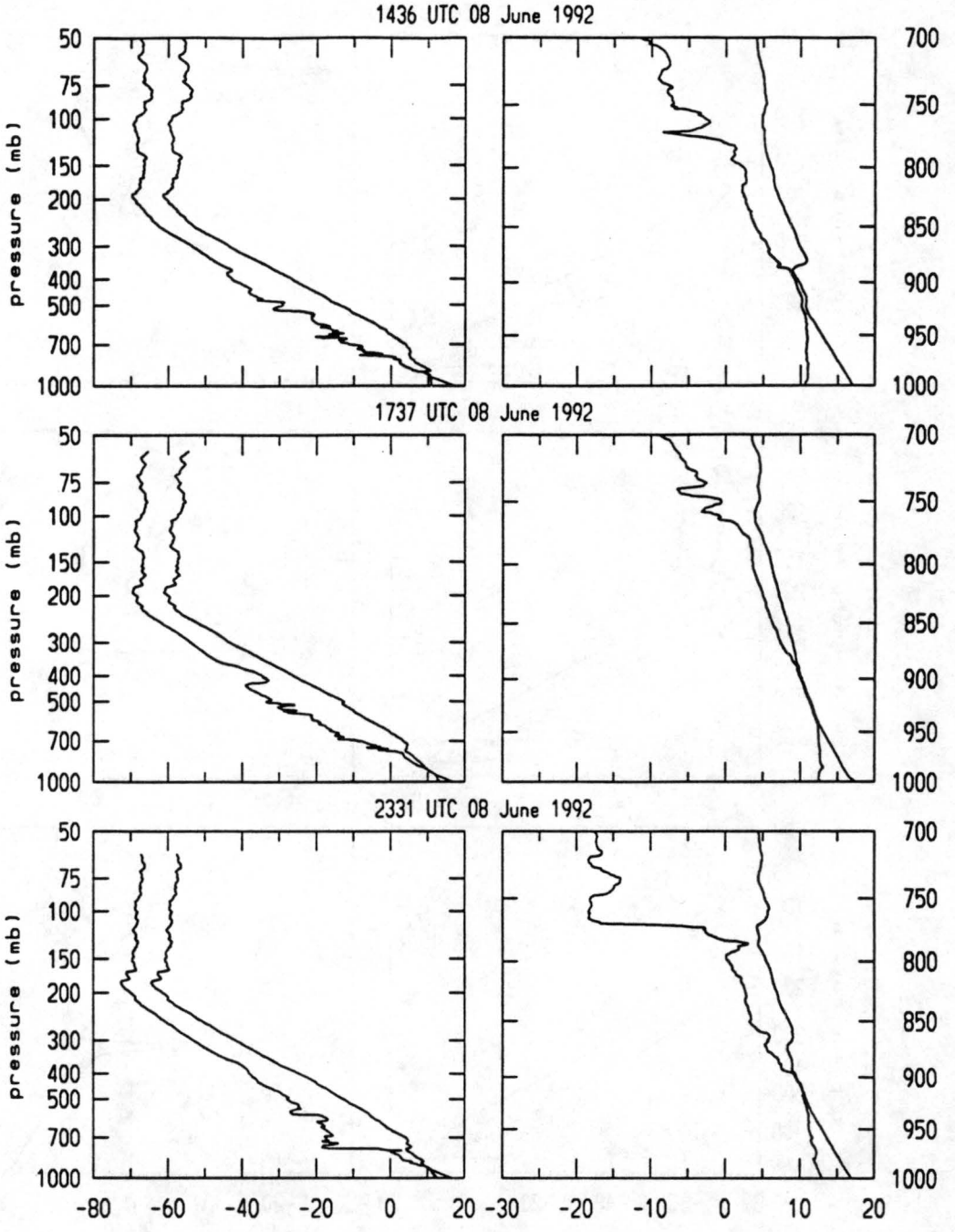
1436 UTC 08 June 1992
1737 UTC 08 June 1992
2331 UTC 08 June 1992
pressure (mb)
50
75
100
150
200
300
400
500
700
1000
700
750
800
850
900
950
1000
-80
-60
-40
-20
0
20
-30
-20
-10
0
10
20

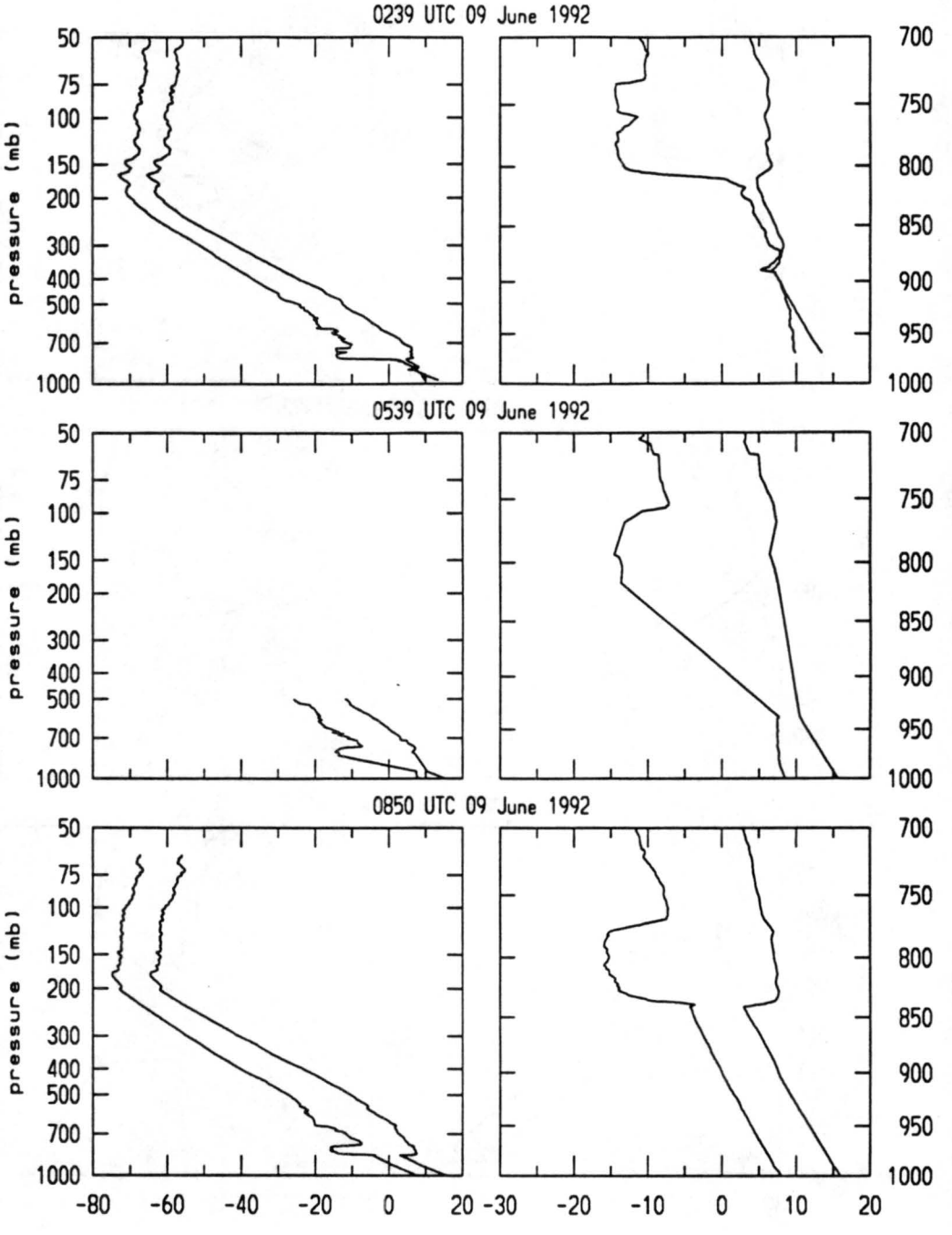
0239 UTC 09 June 1992
0539 UTC 09 June 1992
0850 UTC 09 June 1992
pressure (mb)
50
75
100
150
200
300
400
500
700
1000
700
750
800
850
900
950
1000
-80
-60
-40
-20
0
20
-30
-20
-10
0
10
20

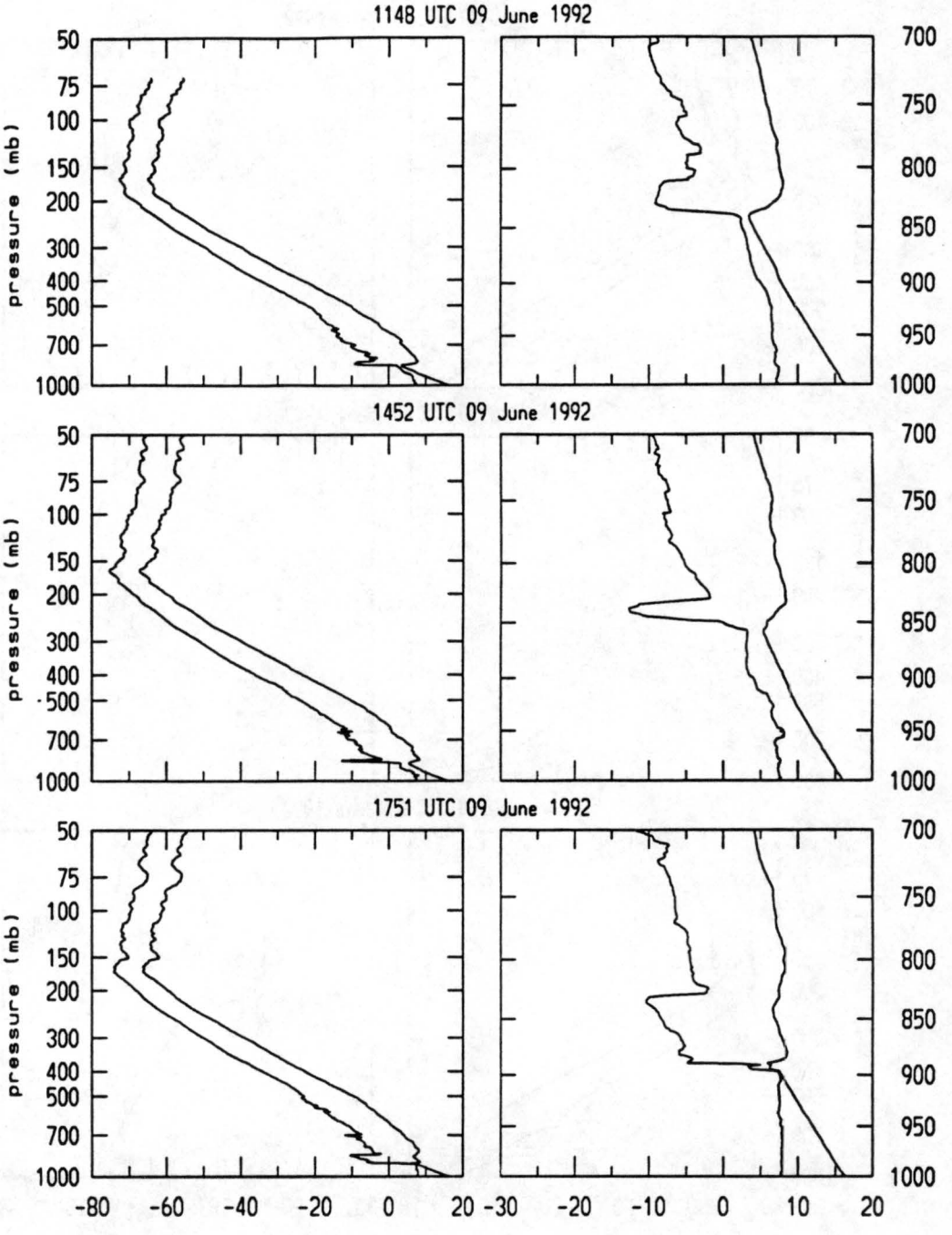
1148 UTC 09 June 1992
1452 UTC 09 June 1992
1751 UTC 09 June 1992
pressure (mb)
50
75
100
150
200
300
400
500
700
1000
700
750
800
850
900
950
1000
-80
-60
-40
-20
0
20
-30
-20
-10
0
10
20

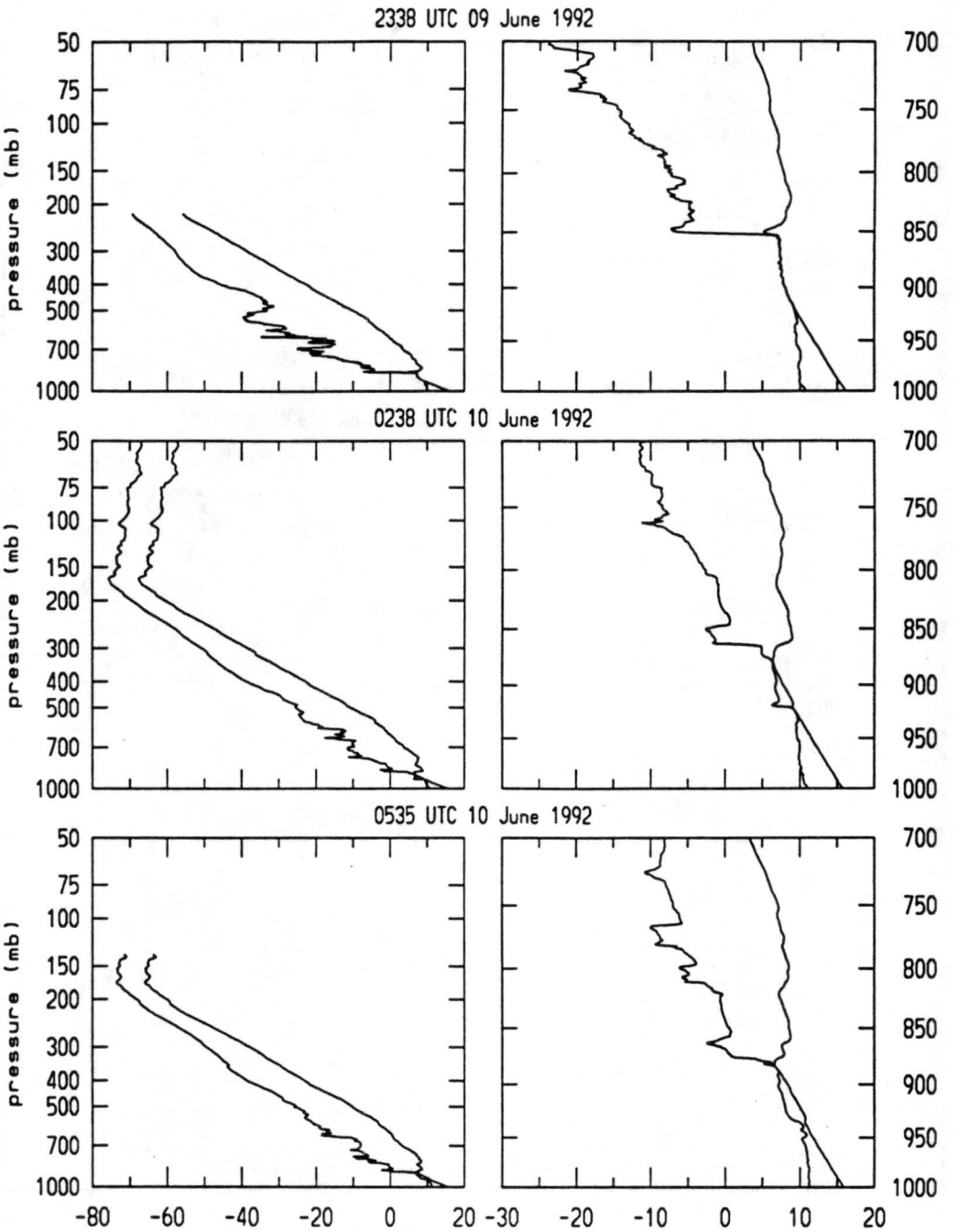
2338 UTC 09 June 1992
0238 UTC 10 June 1992
0535 UTC 10 June 1992
pressure (mb)
50
75
100
150
200
300
400
500
700
1000
700
750
800
850
900
950
1000
-80
-60
-40
-20
0
20
-30
-20
-10
0
10
20

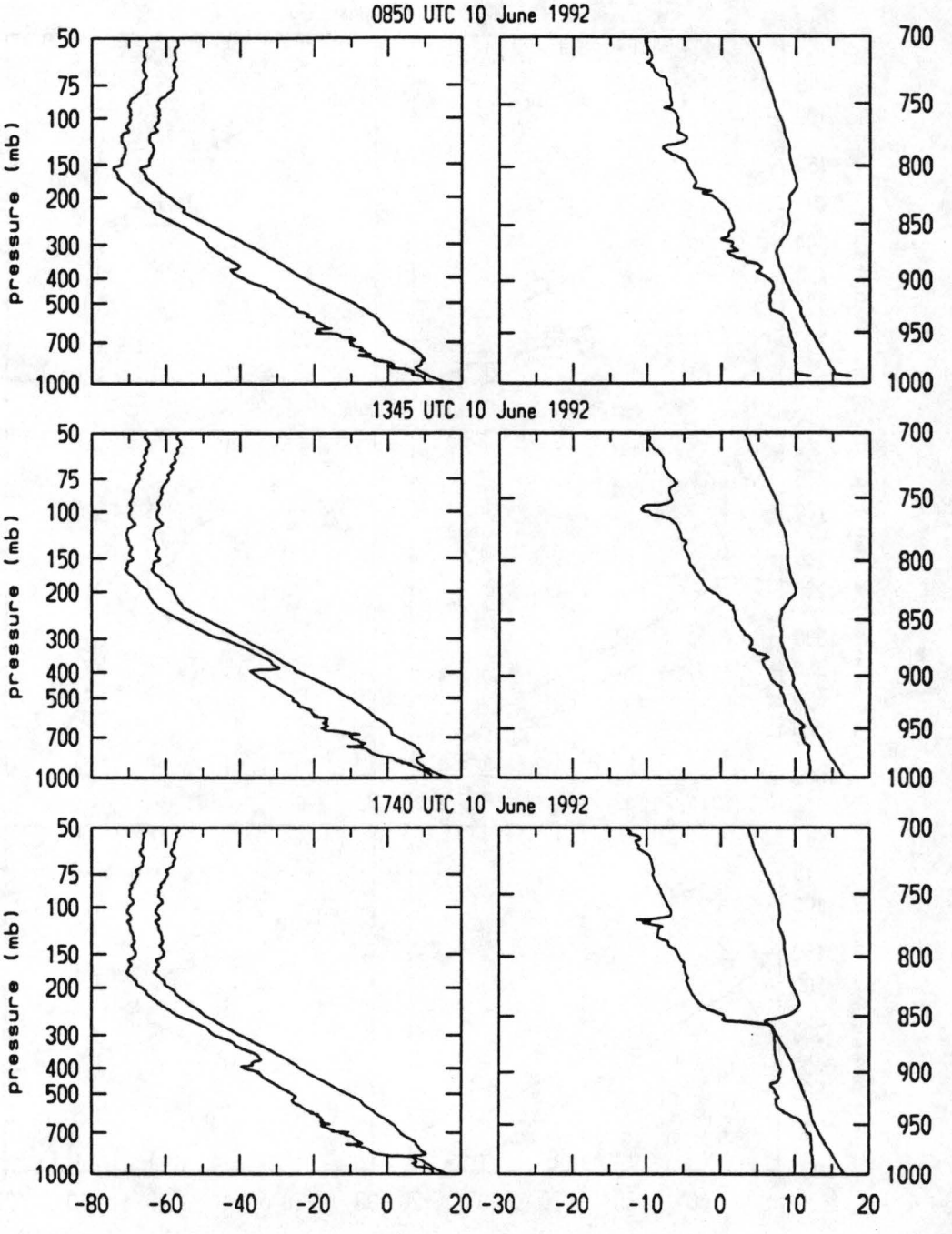
0850 UTC 10 June 1992
1345 UTC 10 June 1992
1740 UTC 10 June 1992
pressure (mb)
50
75
100
150
200
300
400
500
700
1000
700
750
800
850
900
950
1000
-80
-60
-40
-20
0
20
-30
-20
-10
0
10
20

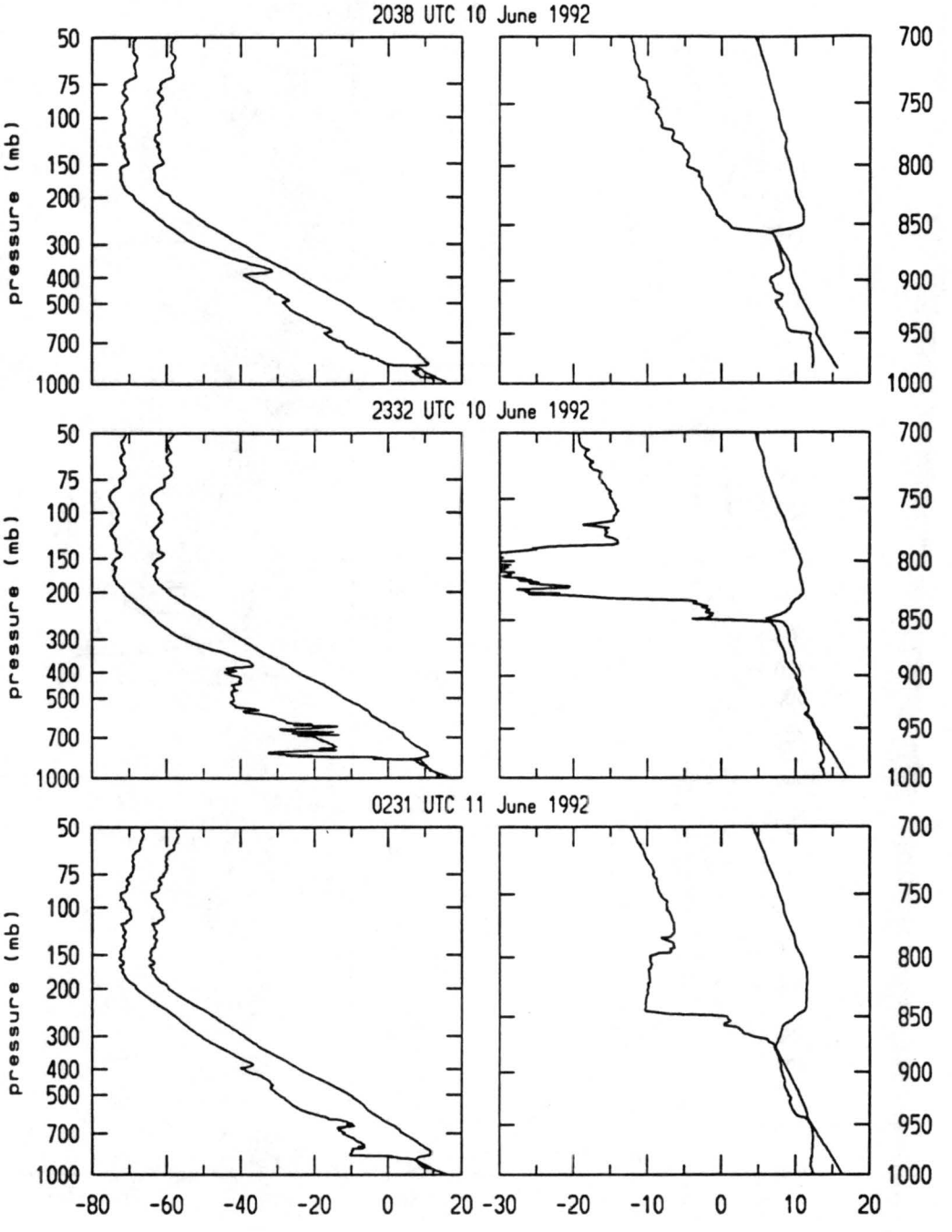
2038 UTC 10 June 1992
2332 UTC 10 June 1992
0231 UTC 11 June 1992
pressure (mb)
50
75
100
150
200
300
400
500
700
1000
700
750
800
850
900
950
1000
-80
-60
-40
-20
0
20
-30
-20
-10
0
10
20

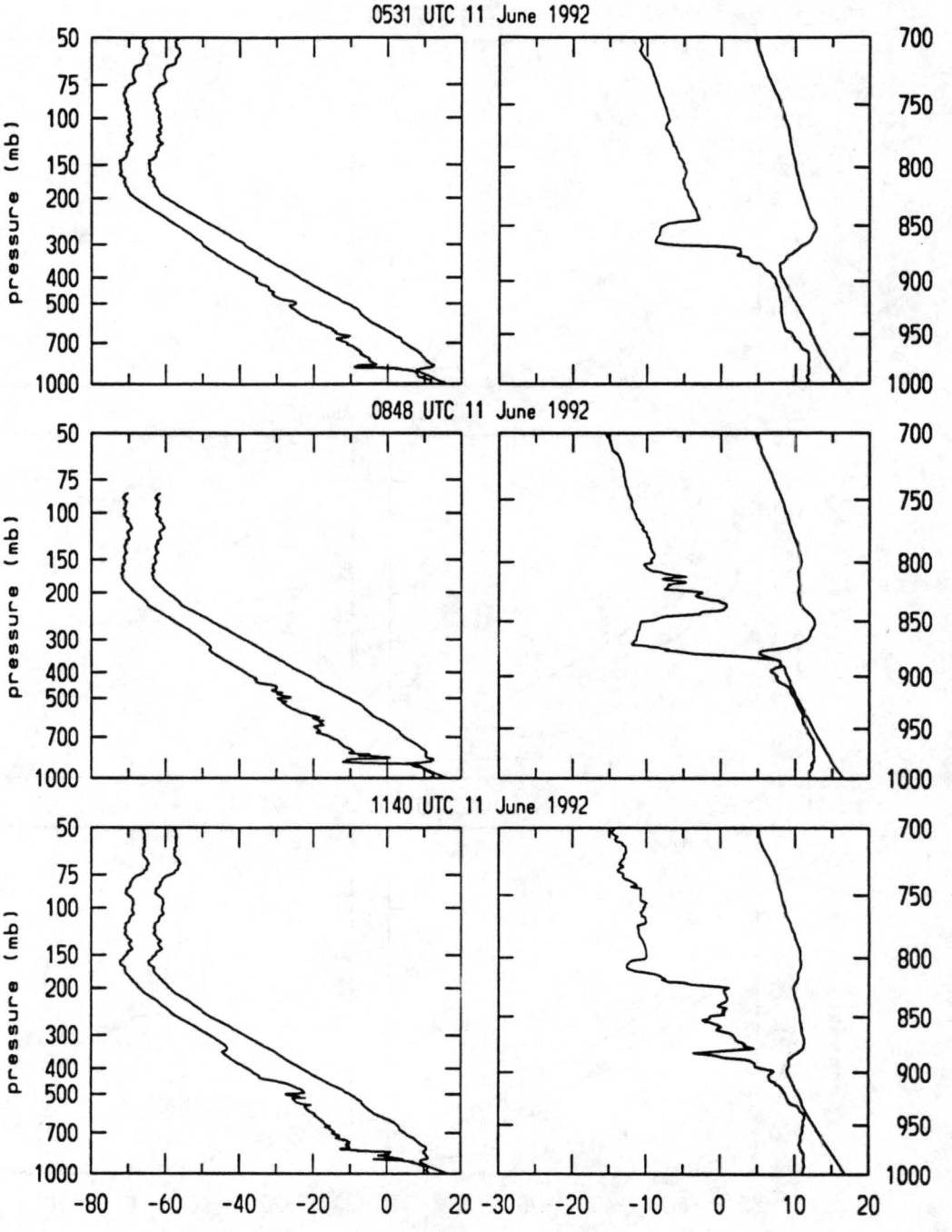
0531 UTC 11 June 1992
0848 UTC 11 June 1992
1140 UTC 11 June 1992
pressure (mb)
50
75
100
150
200
300
400
500
700
1000
700
750
800
850
900
950
1000
-80
-60
-40
-20
0
20
-30
-20
-10
0
10
20

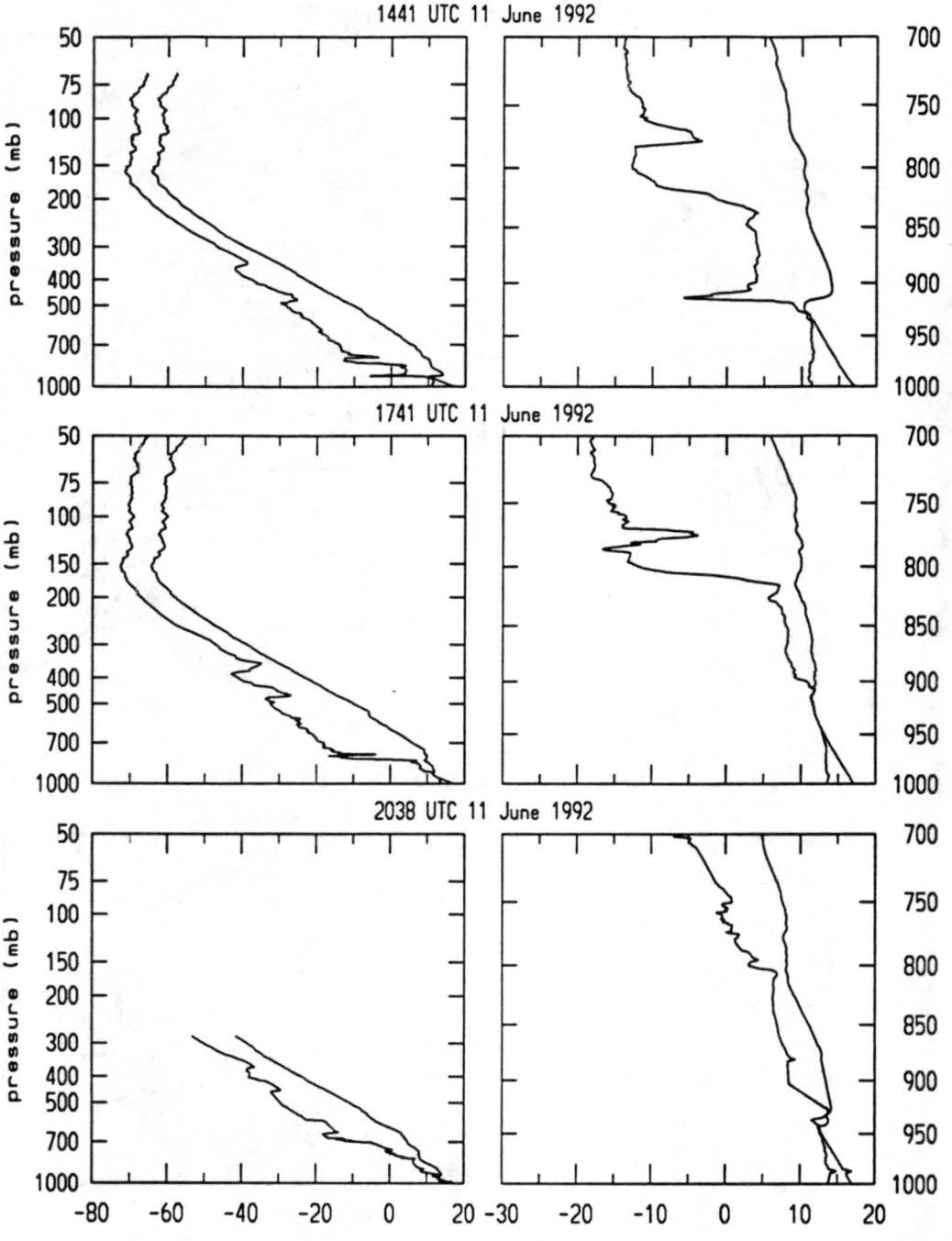
1441 UTC 11 June 1992
1741 UTC 11 June 1992
2038 UTC 11 June 1992
pressure (mb)
50
75
100
150
200
300
400
500
700
1000
700
750
800
850
900
950
1000
-80
-60
-40
-20
0
20
-30
-20
-10
0
10
20

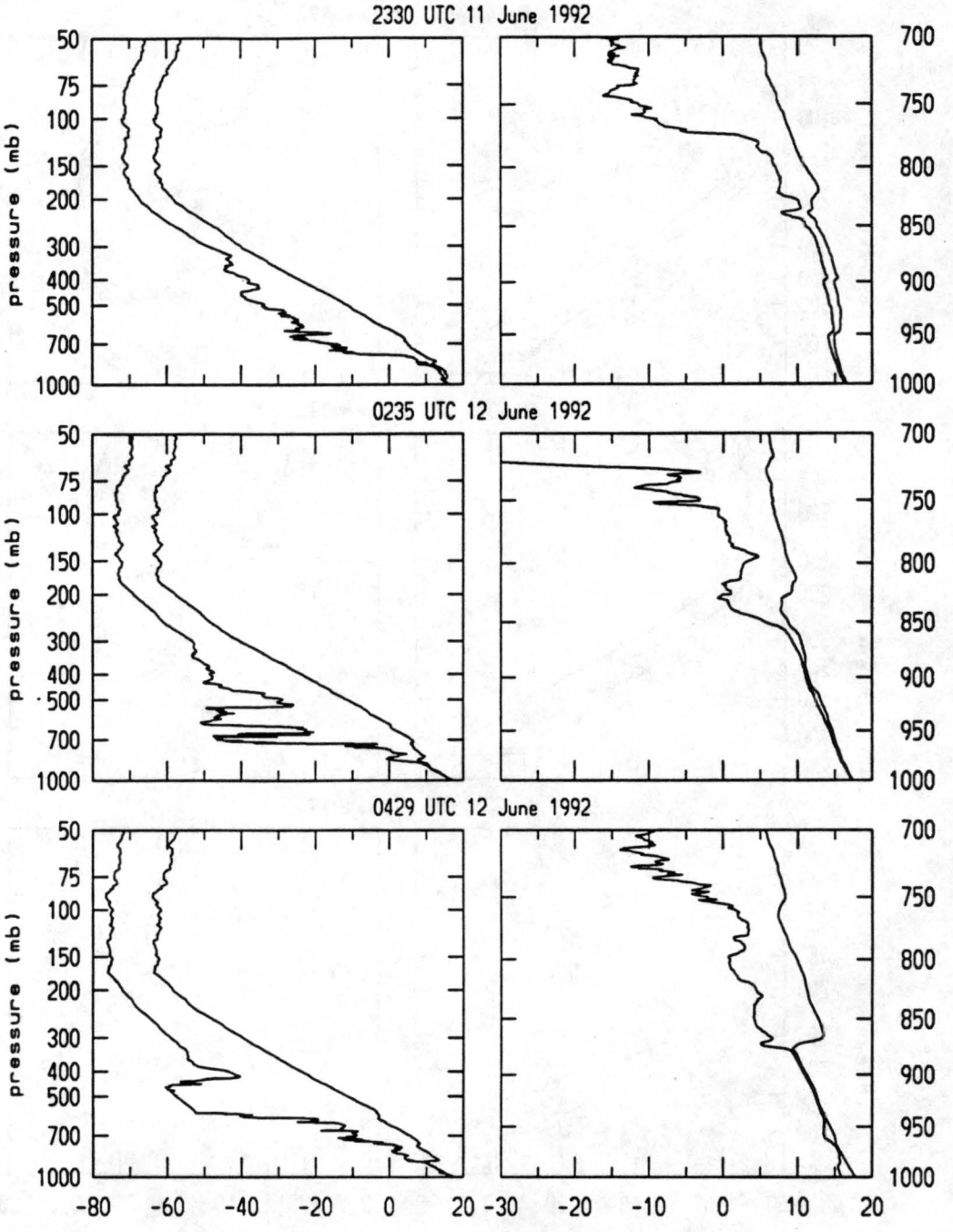
2330 UTC 11 June 1992
0235 UTC 12 June 1992
0429 UTC 12 June 1992
pressure (mb)
50
75
100
150
200
300
400
500
700
1000
700
750
800
850
900
950
1000
-80
-60
-40
-20
0
20
-30
-20
-10
0
10
20

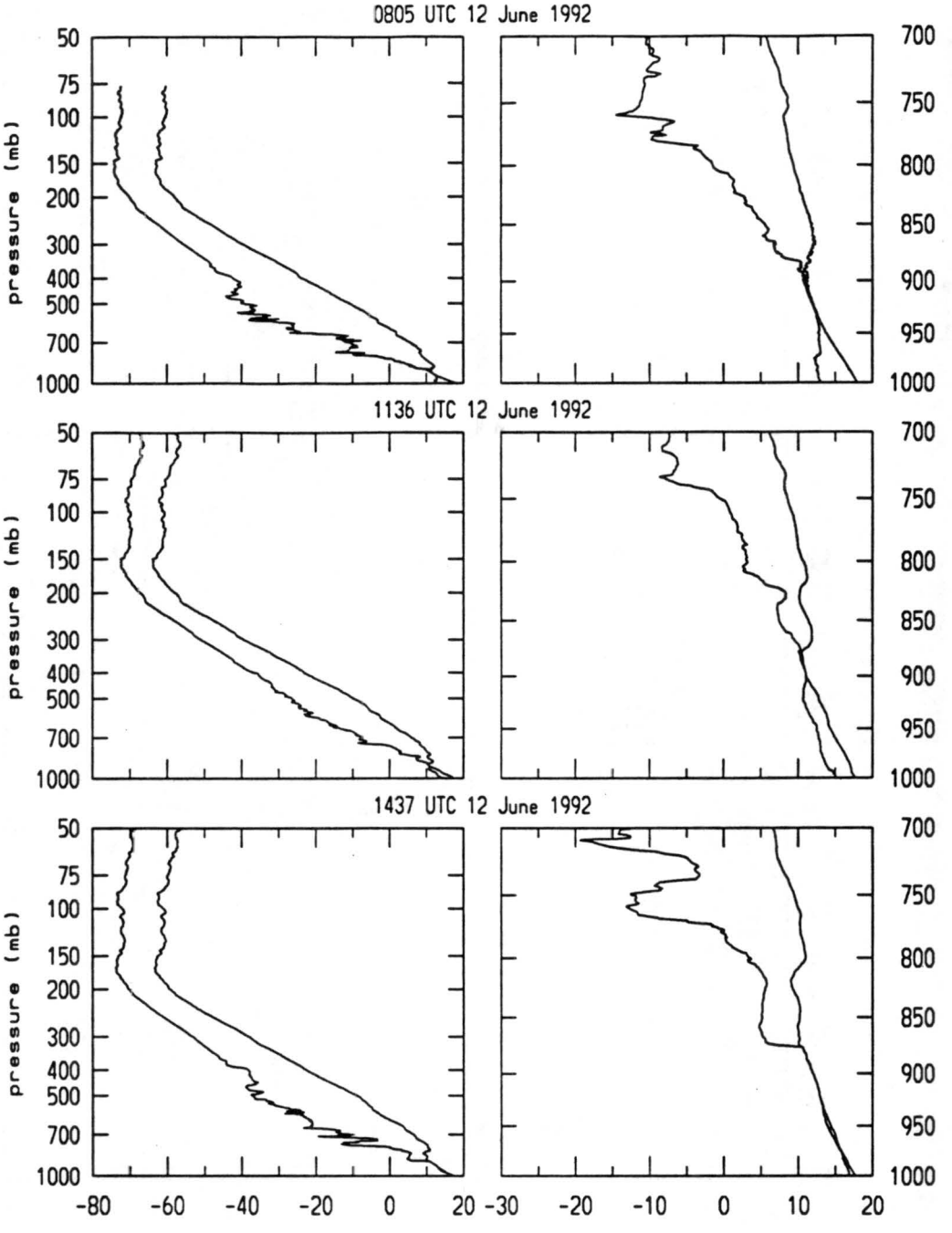
0805 UTC 12 June 1992
1136 UTC 12 June 1992
1437 UTC 12 June 1992
pressure (mb)
50
75
100
150
200
300
400
500
700
1000
700
750
800
850
900
950
1000
-80
-60
-40
-20
0
20
-30
-20
-10
0
10
20

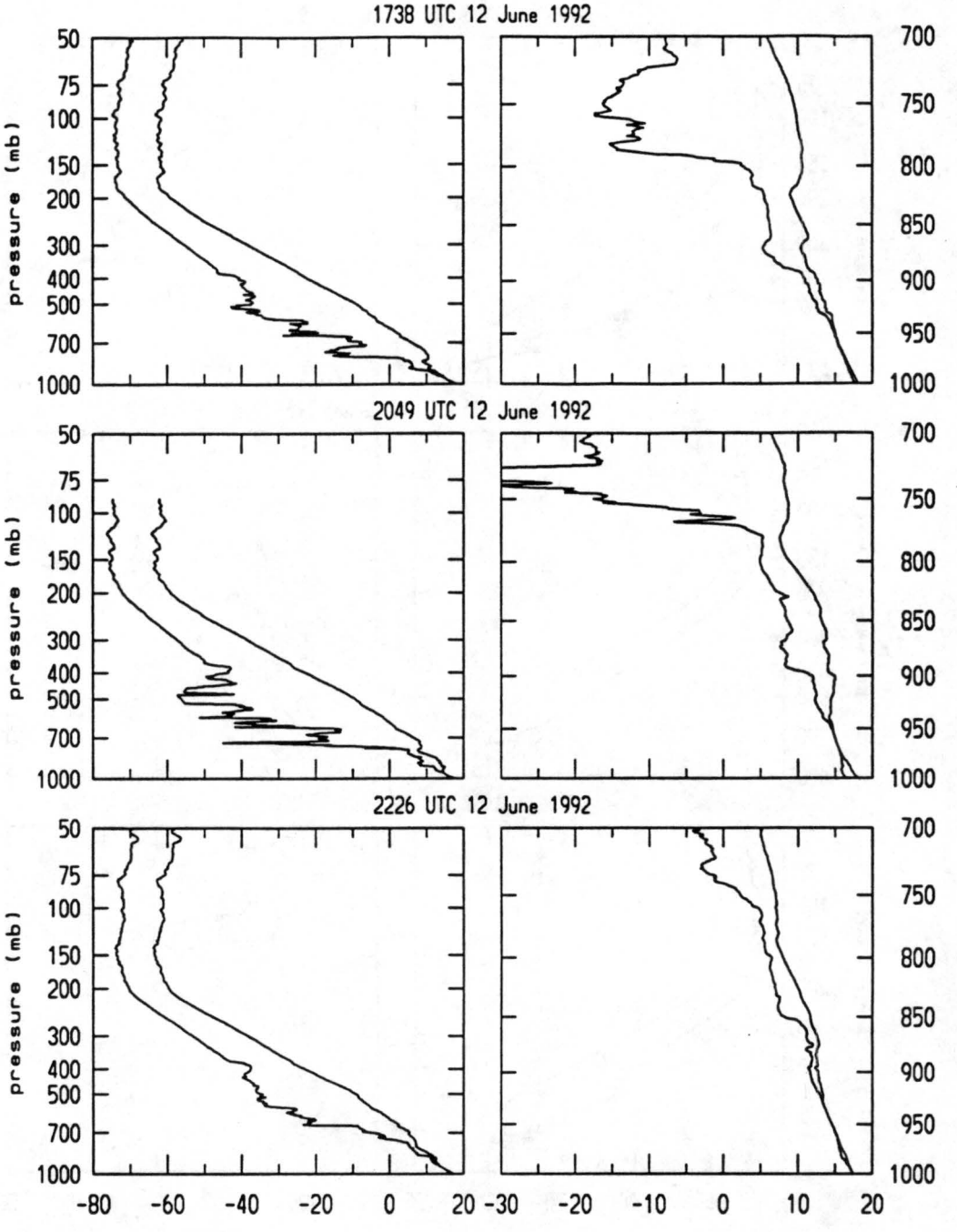
1738 UTC 12 June 1992
2049 UTC 12 June 1992
2226 UTC 12 June 1992
pressure (mb)
50
75
100
150
200
300
400
500
700
1000
700
750
800
850
900
950
1000
-80
-60
-40
-20
0
20
-30
-20
-10
0
10
20

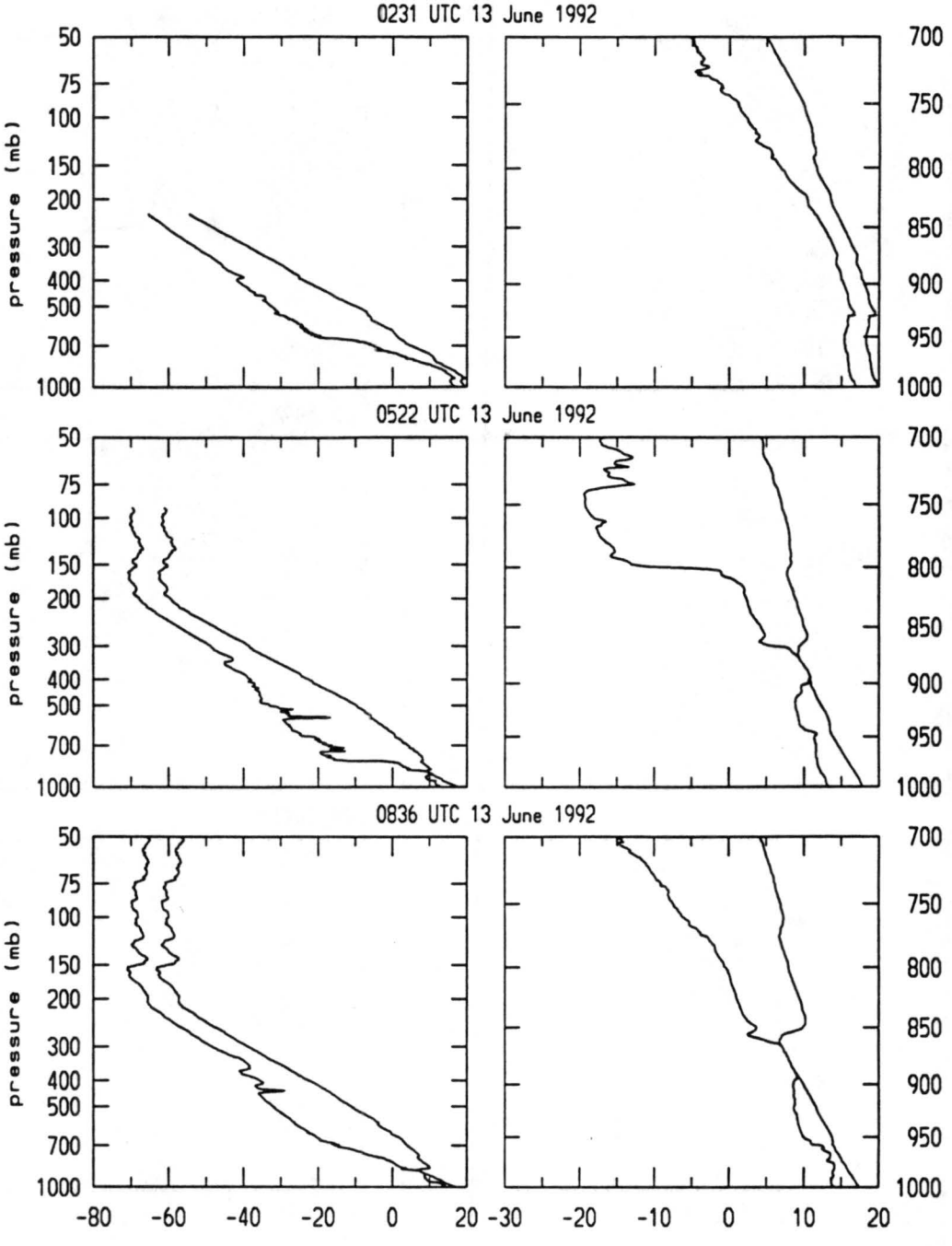
0231 UTC 13 June 1992
0522 UTC 13 June 1992
0836 UTC 13 June 1992
pressure (mb)
50
75
100
150
200
300
400
500
700
1000
700
750
800
850
900
950
1000
-80
-60
-40
-20
0
20
-30
-20
-10
0
10
20

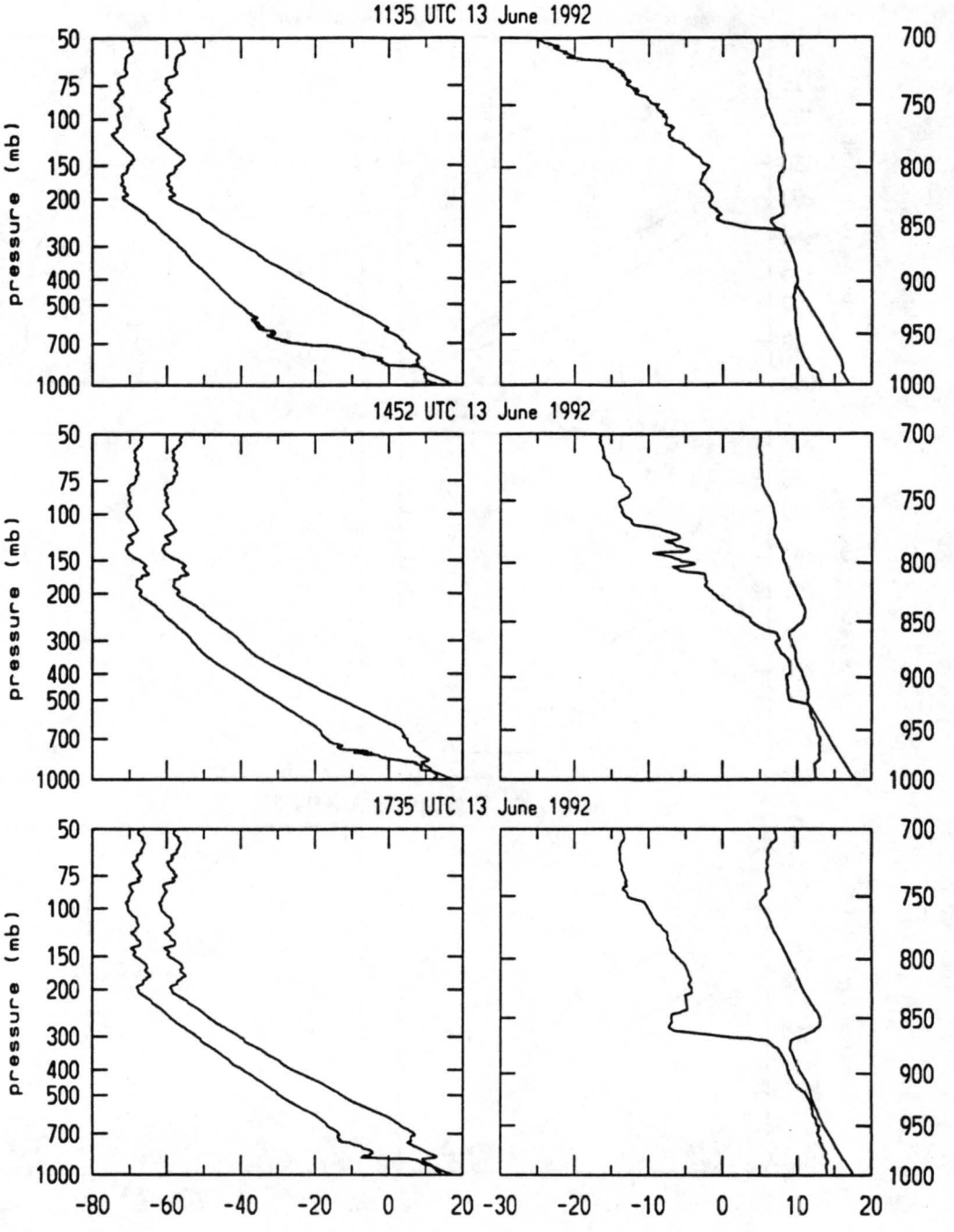
1135 UTC 13 June 1992
1452 UTC 13 June 1992
1735 UTC 13 June 1992
pressure (mb)
50
75
100
150
200
300
400
500
700
1000
700
750
800
850
900
950
1000
-80
-60
-40
-20
0
20
-30
-20
-10
0
10
20

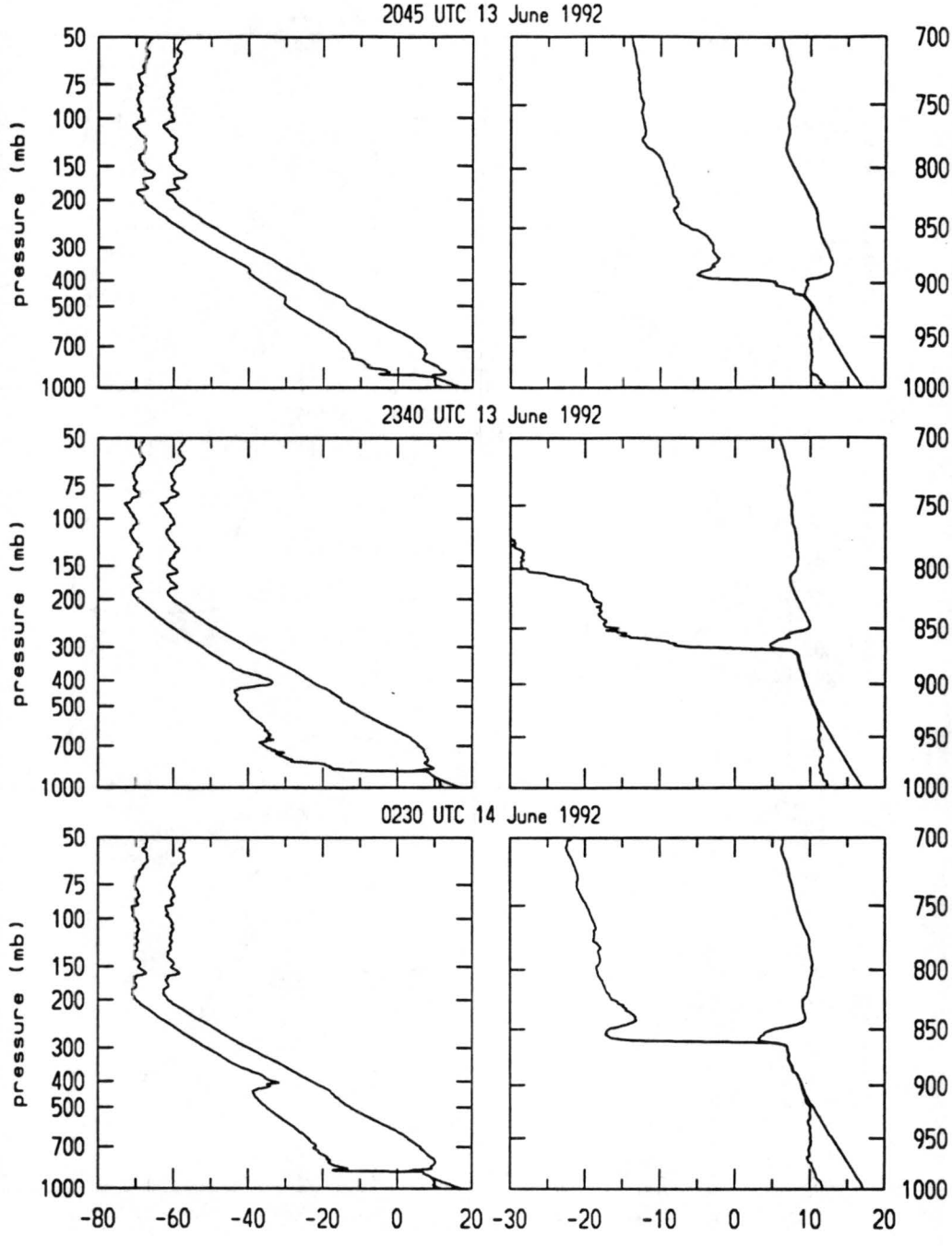
2045 UTC 13 June 1992
2340 UTC 13 June 1992
0230 UTC 14 June 1992
pressure (mb)
50
75
100
150
200
300
400
500
700
1000
700
750
800
850
900
950
1000
-80
-60
-40
-20
0
20
-30
-20
-10
0
10
20

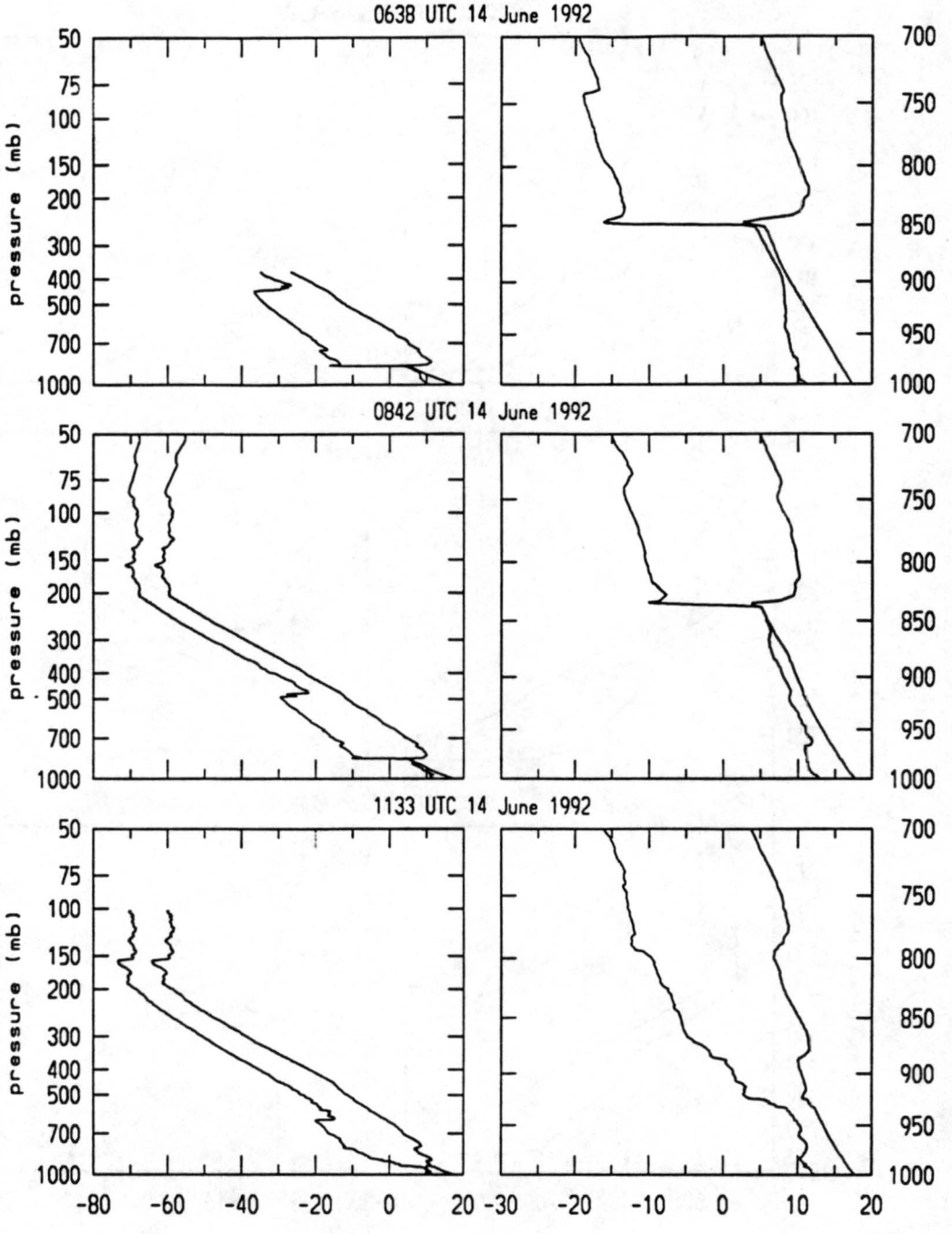
0638 UTC 14 June 1992
0842 UTC 14 June 1992
1133 UTC 14 June 1992
pressure (mb)
50
75
100
150
200
300
400
500
700
1000
700
750
800
850
900
950
1000
-80
-60
-40
-20
0
20
-30
-20
-10
0
10
20

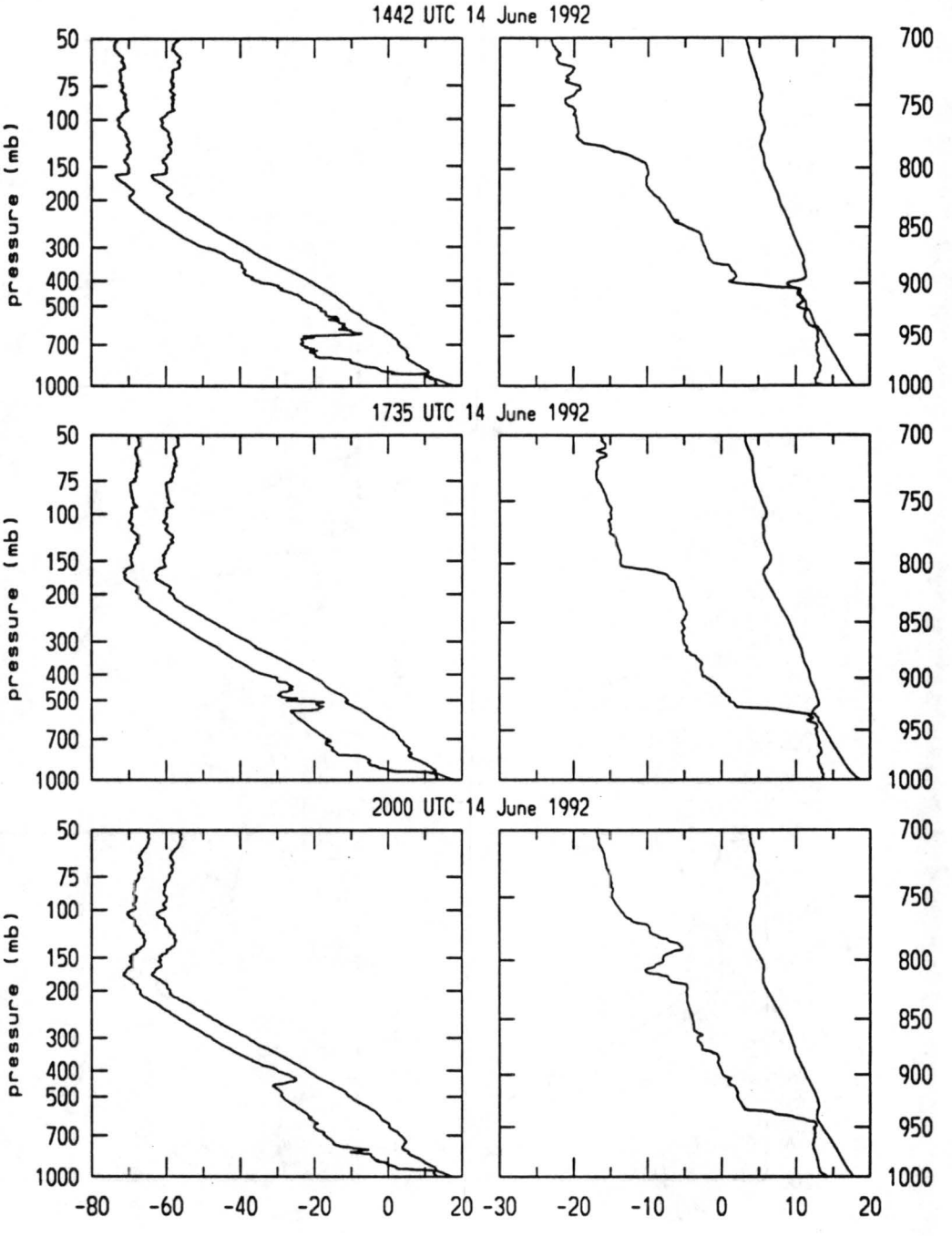
1442 UTC 14 June 1992
1735 UTC 14 June 1992
2000 UTC 14 June 1992
pressure (mb)
50
75
100
150
200
300
400
500
700
1000
700
750
800
850
900
950
1000
-80
-60
-40
-20
0
20
-30
-20
-10
0
10
20

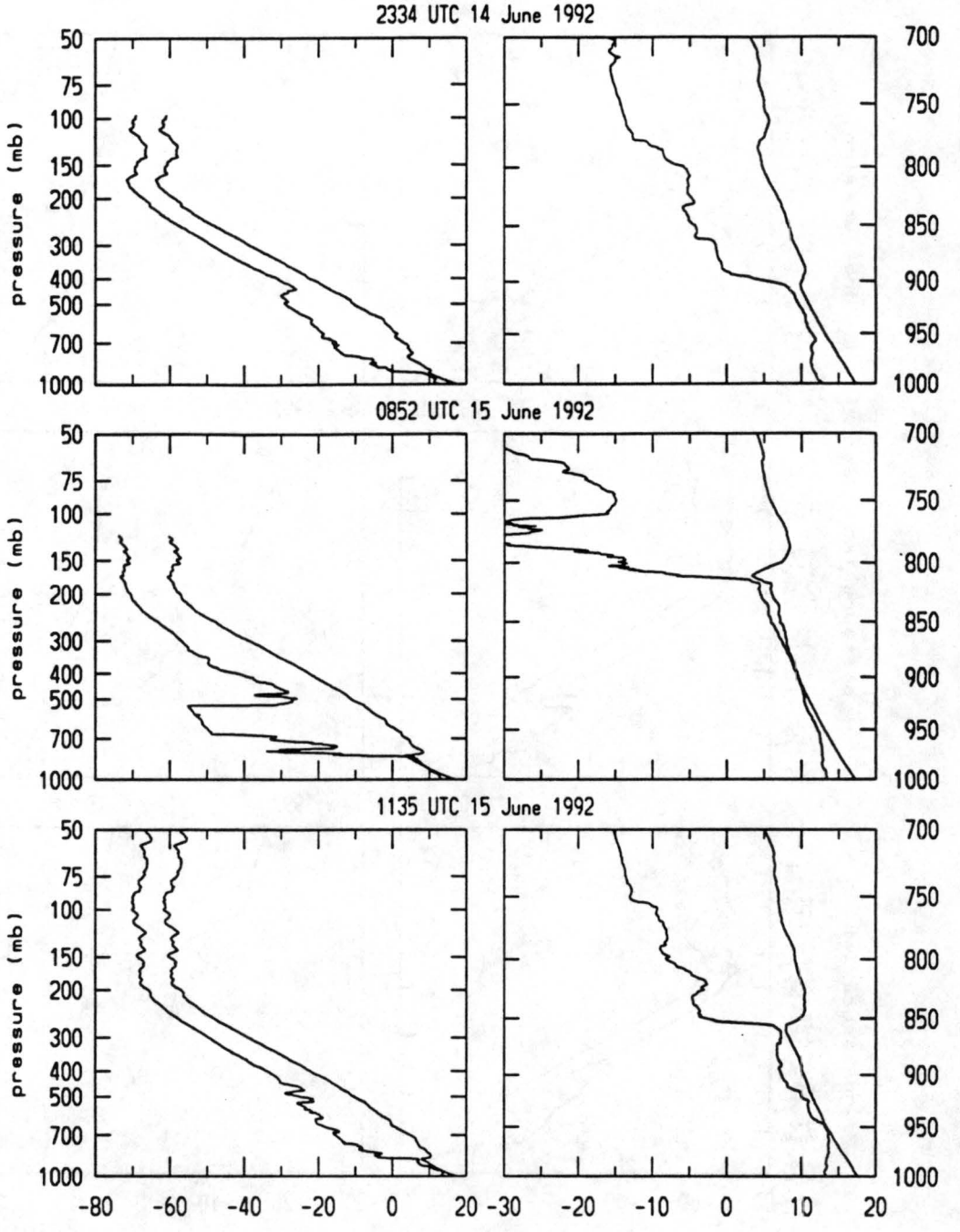
2334 UTC 14 June 1992
0852 UTC 15 June 1992
1135 UTC 15 June 1992
pressure (mb)
50
75
100
150
200
300
400
500
700
1000
700
750
800
850
900
950
1000
-80
-60
-40
-20
0
20
-30
-20
-10
0
10
20

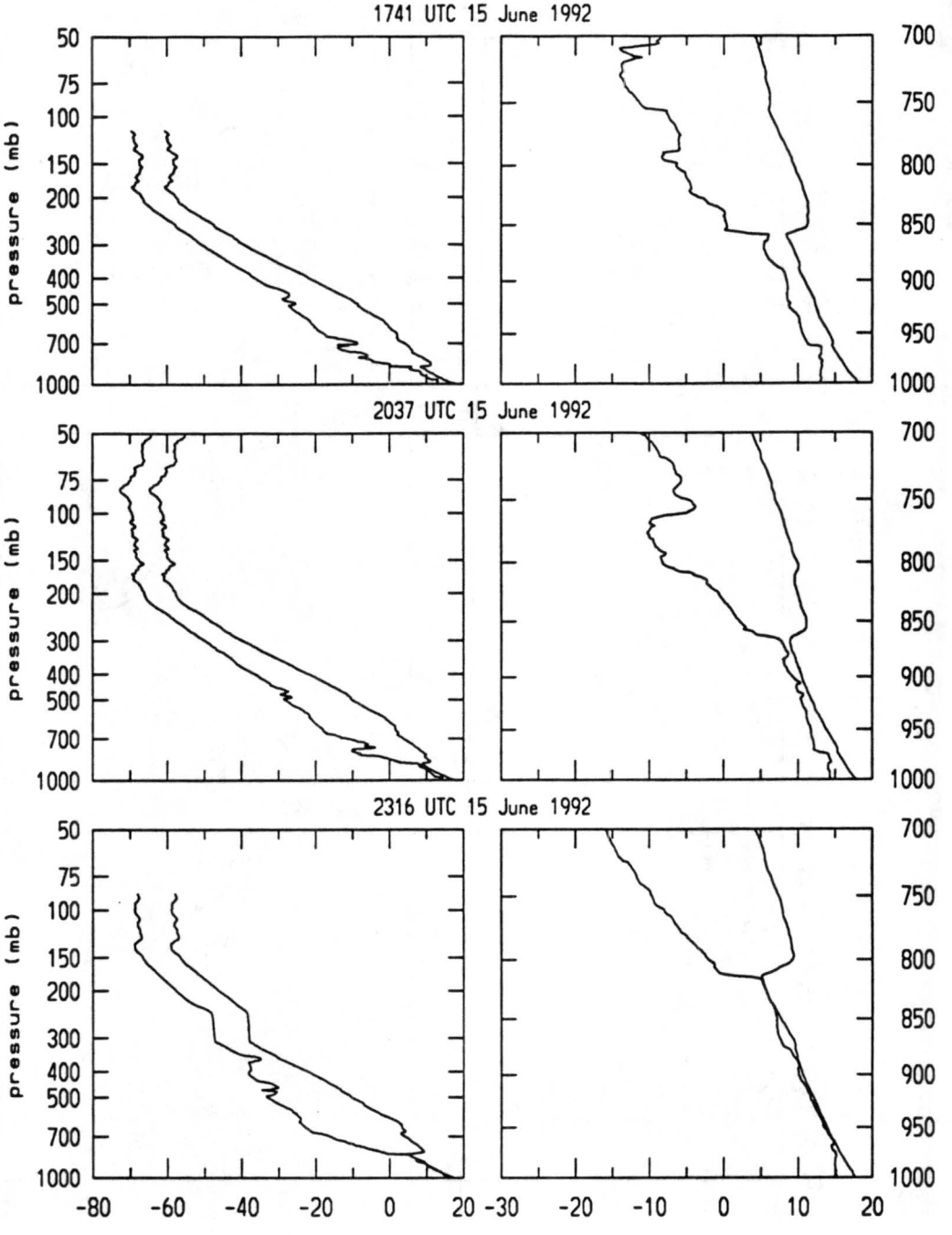
1741 UTC 15 June 1992
2037 UTC 15 June 1992
2316 UTC 15 June 1992
pressure (mb)
50
75
100
150
200
300
400
500
700
1000
700
750
800
850
900
950
1000
-80
-60
-40
-20
0
20
-30
-20
-10
0
10
20

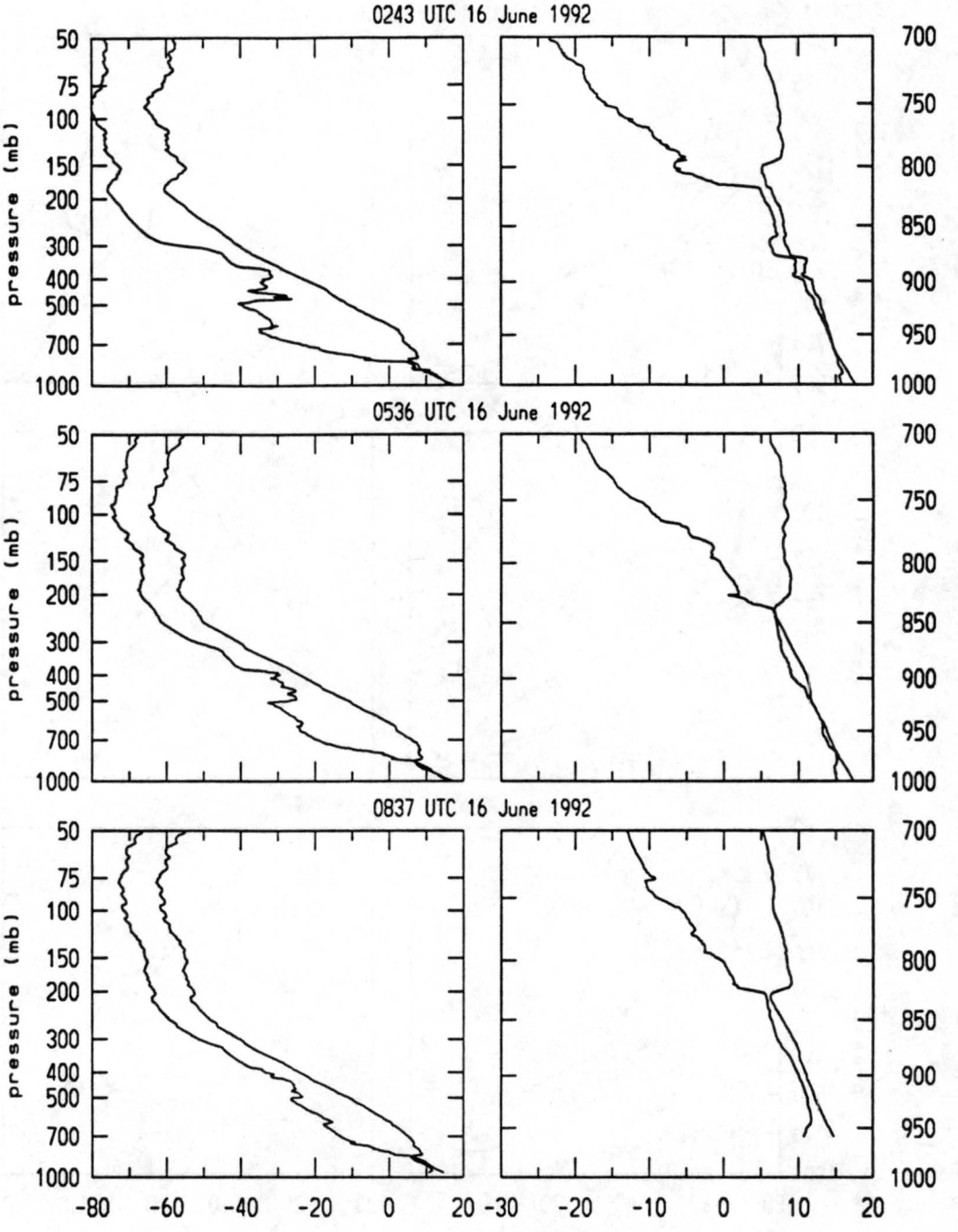
0243 UTC 16 June 1992
0536 UTC 16 June 1992
0837 UTC 16 June 1992
pressure (mb)
50
75
100
150
200
300
400
500
700
1000
700
750
800
850
900
950
1000
-80
-60
-40
-20
0
20
-30
-20
-10
0
10
20

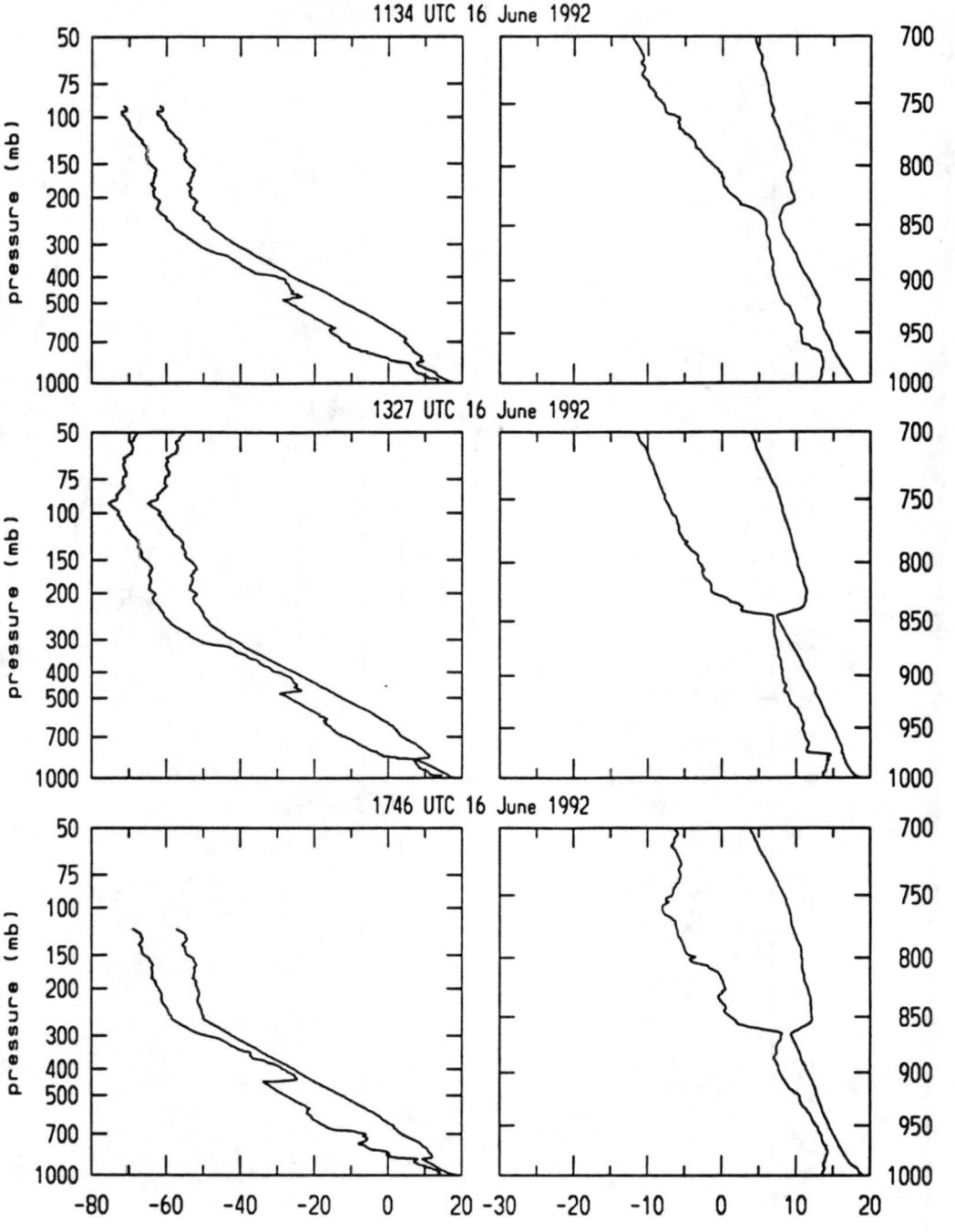
1134 UTC 16 June 1992
1327 UTC 16 June 1992
1746 UTC 16 June 1992
pressure (mb)
50
75
100
150
200
300
400
500
700
1000
700
750
800
850
900
950
1000
-80
-60
-40
-20
0
20
-30
-20
-10
0
10
20

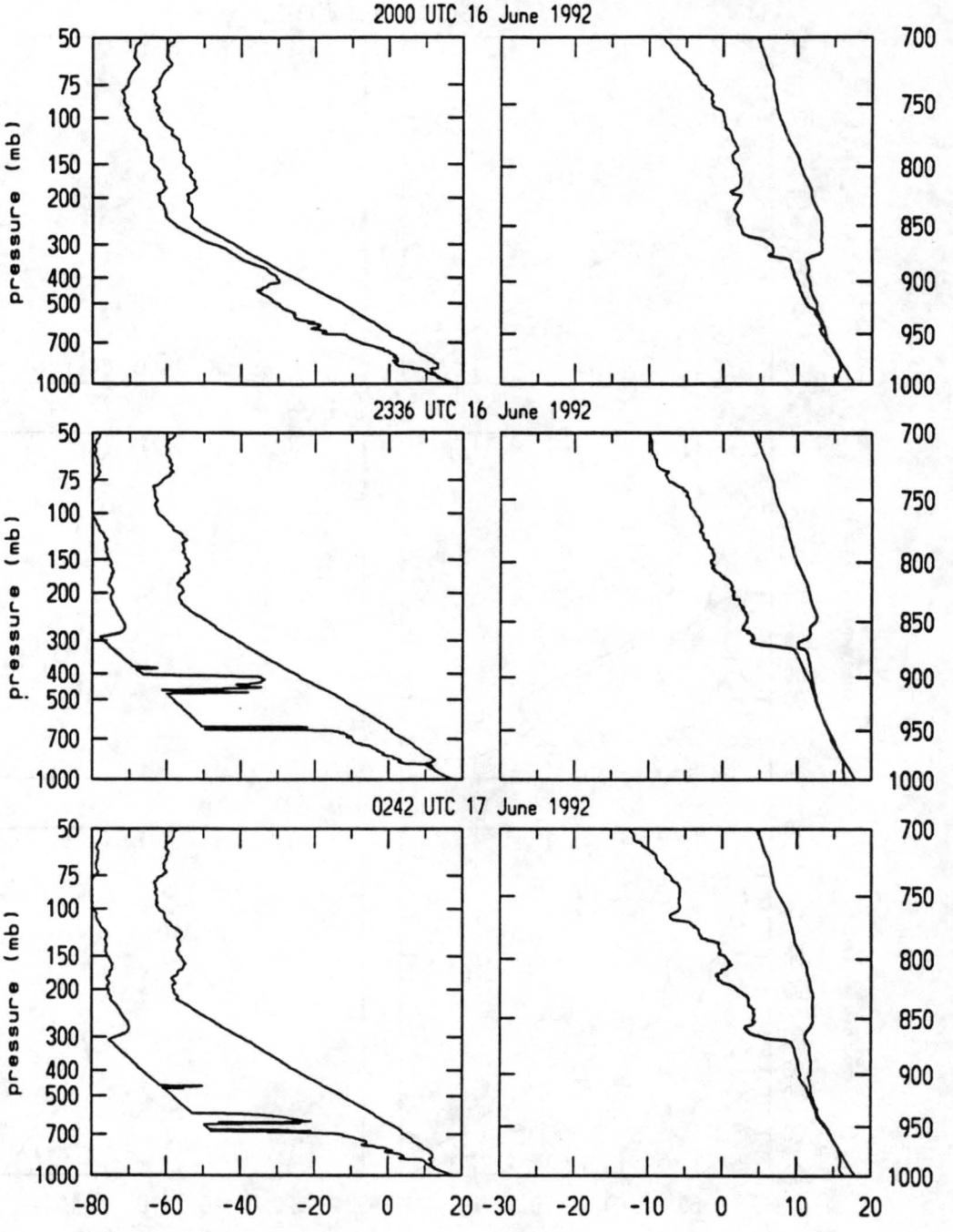
2000 UTC 16 June 1992
2336 UTC 16 June 1992
0242 UTC 17 June 1992
pressure (mb)
50
75
100
150
200
300
400
500
700
1000
700
750
800
850
900
950
1000
-80
-60
-40
-20
0
20
-30
-20
-10
0
10
20

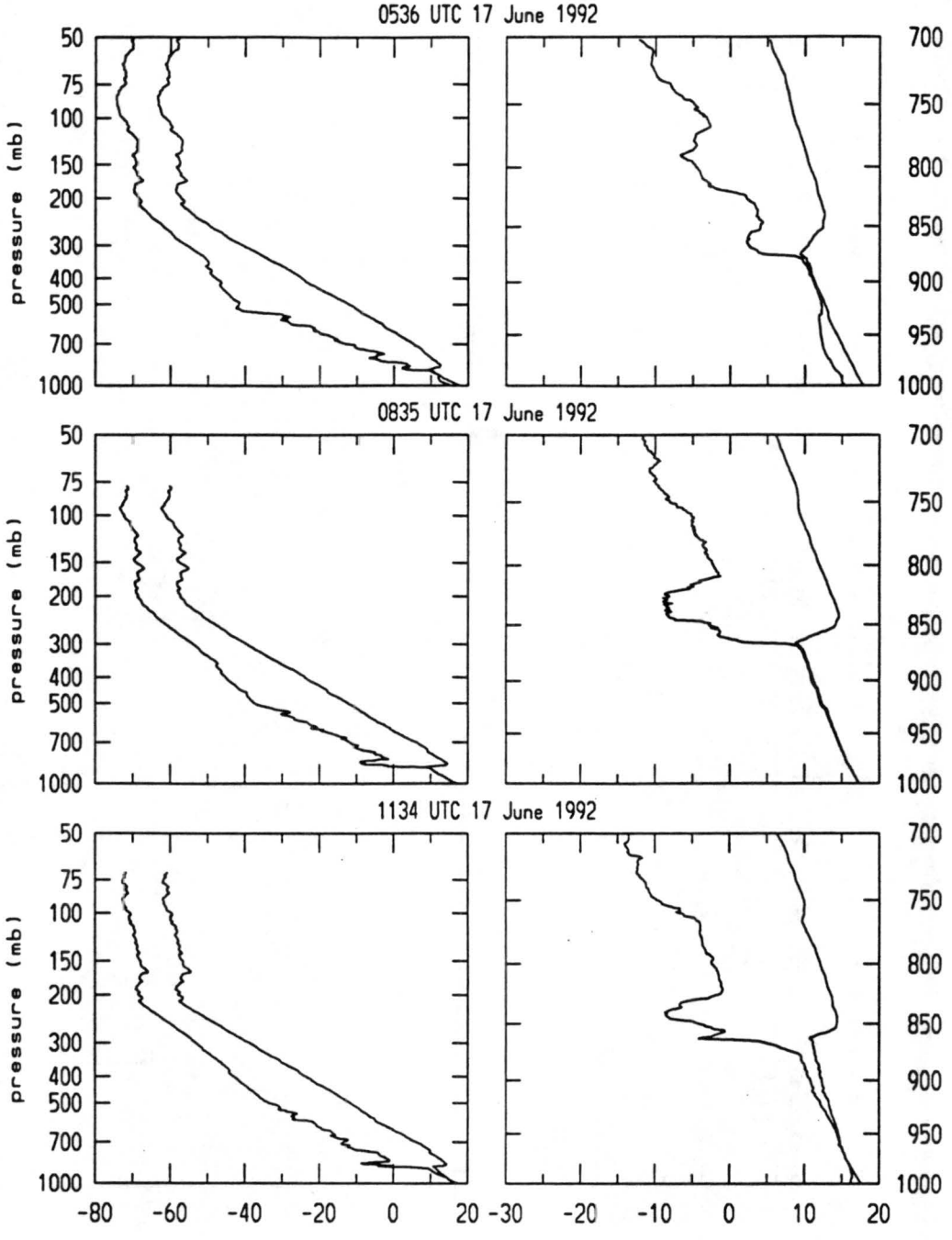
0536 UTC 17 June 1992
0835 UTC 17 June 1992
1134 UTC 17 June 1992
pressure (mb)
50
75
100
150
200
300
400
500
700
1000
700
750
800
850
900
950
1000
-80
-60
-40
-20
0
20
-30
-20
-10
0
10
20

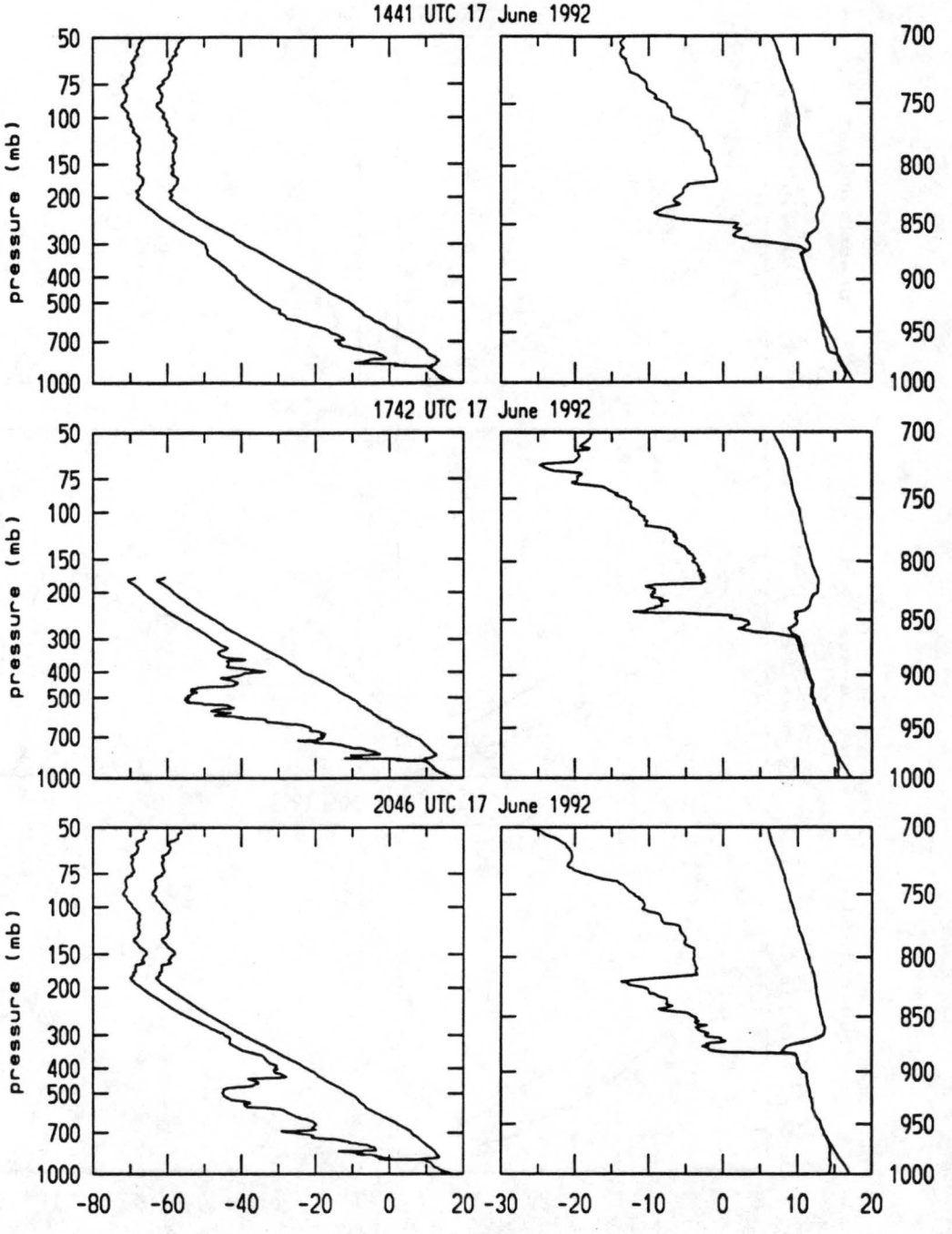
1441 UTC 17 June 1992
1742 UTC 17 June 1992
2046 UTC 17 June 1992
pressure (mb)
50
75
100
150
200
300
400
500
700
1000
700
750
800
850
900
950
1000
-80
-60
-40
-20
0
20
-30
-20
-10
0
10
20

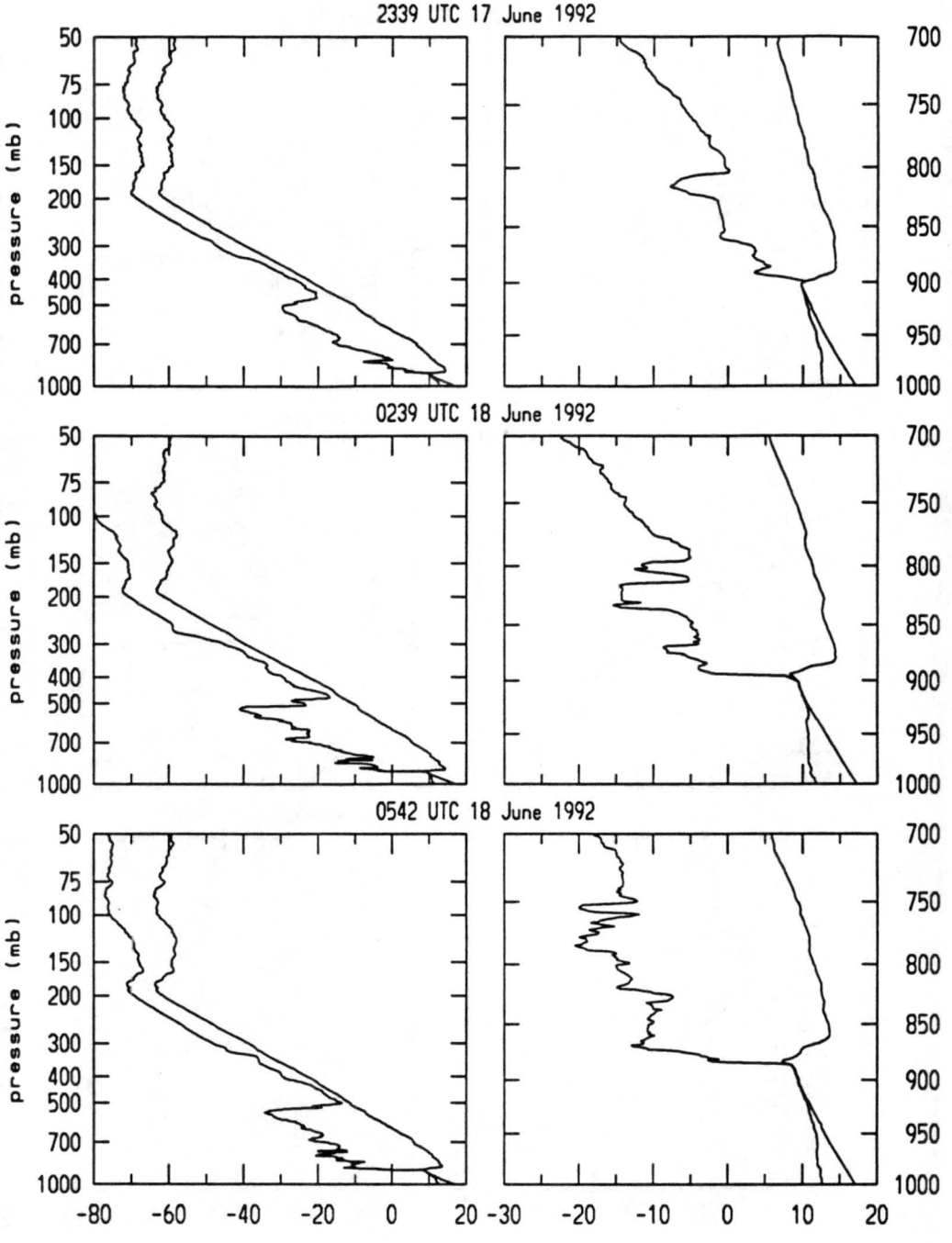
2339 UTC 17 June 1992
0239 UTC 18 June 1992
0542 UTC 18 June 1992
pressure (mb)
50
75
100
150
200
300
400
500
700
1000
700
750
800
850
900
950
1000
-80
-60
-40
-20
0
20
-30
-20
-10
0
10
20

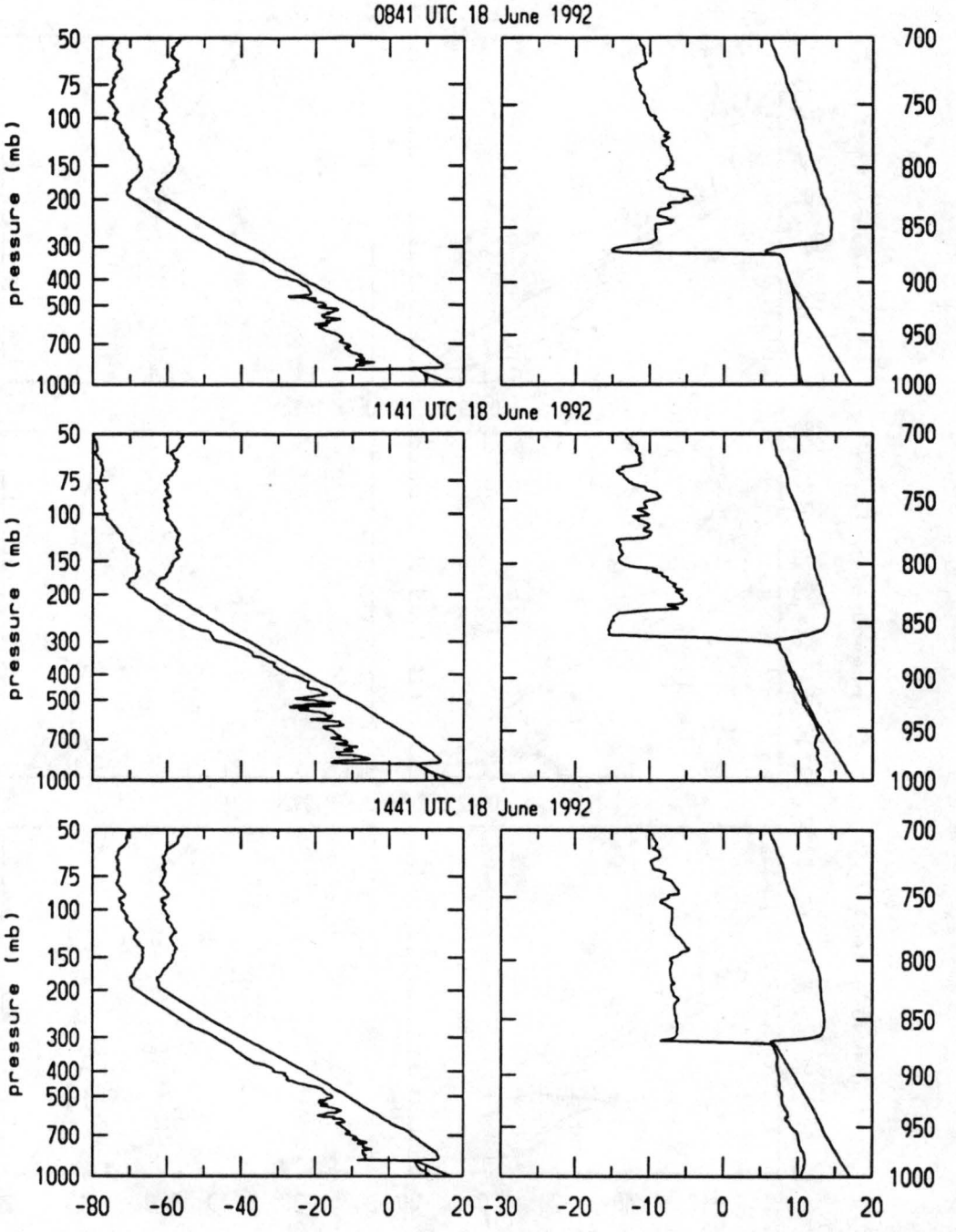
0841 UTC 18 June 1992
1141 UTC 18 June 1992
1441 UTC 18 June 1992
pressure (mb)
50
75
100
150
200
300
400
500
700
1000
700
750
800
850
900
950
1000
-80
-60
-40
-20
0
20
-30
-20
-10
0
10
20

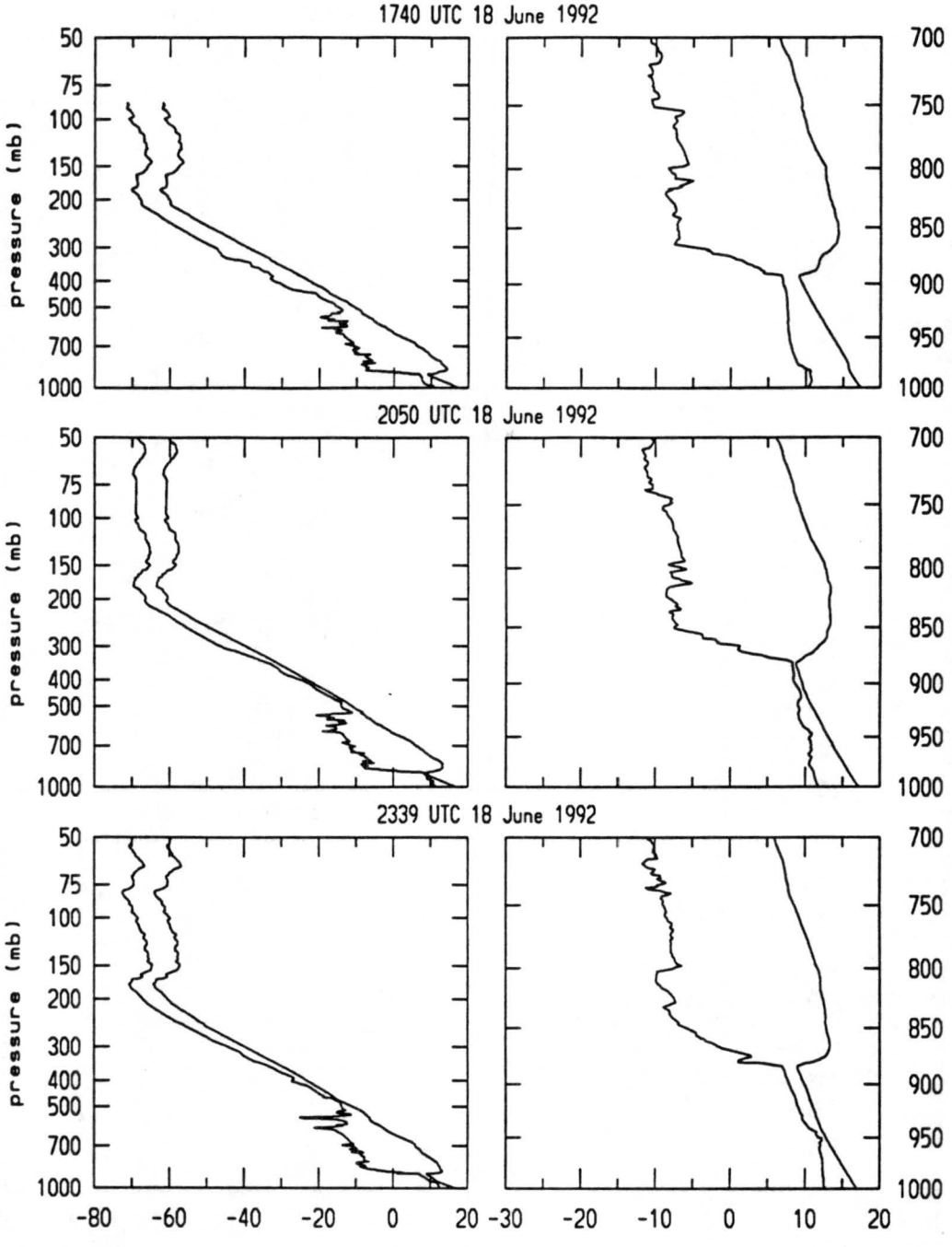
1740 UTC 18 June 1992
2050 UTC 18 June 1992
2339 UTC 18 June 1992
pressure (mb)
50
75
100
150
200
300
400
500
700
1000
700
750
800
850
900
950
1000
-80
-60
-40
-20
0
20
-30
-20
-10
0
10
20

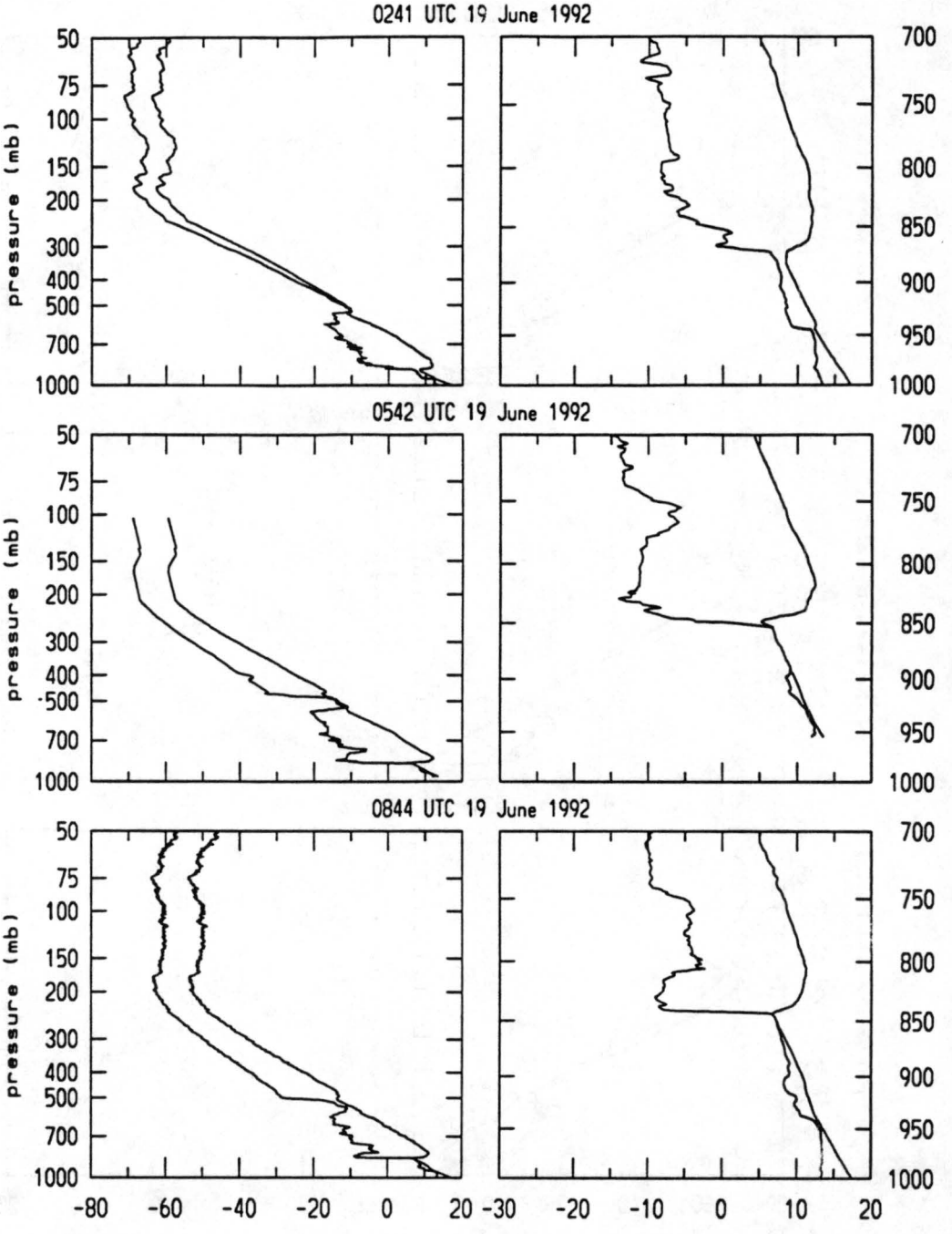
0241 UTC 19 June 1992
0542 UTC 19 June 1992
0844 UTC 19 June 1992
pressure (mb)
50
75
100
150
200
300
400
500
700
1000
700
750
800
850
900
950
1000
-80
-60
-40
-20
0
20
-30
-20
-10
0
10
20

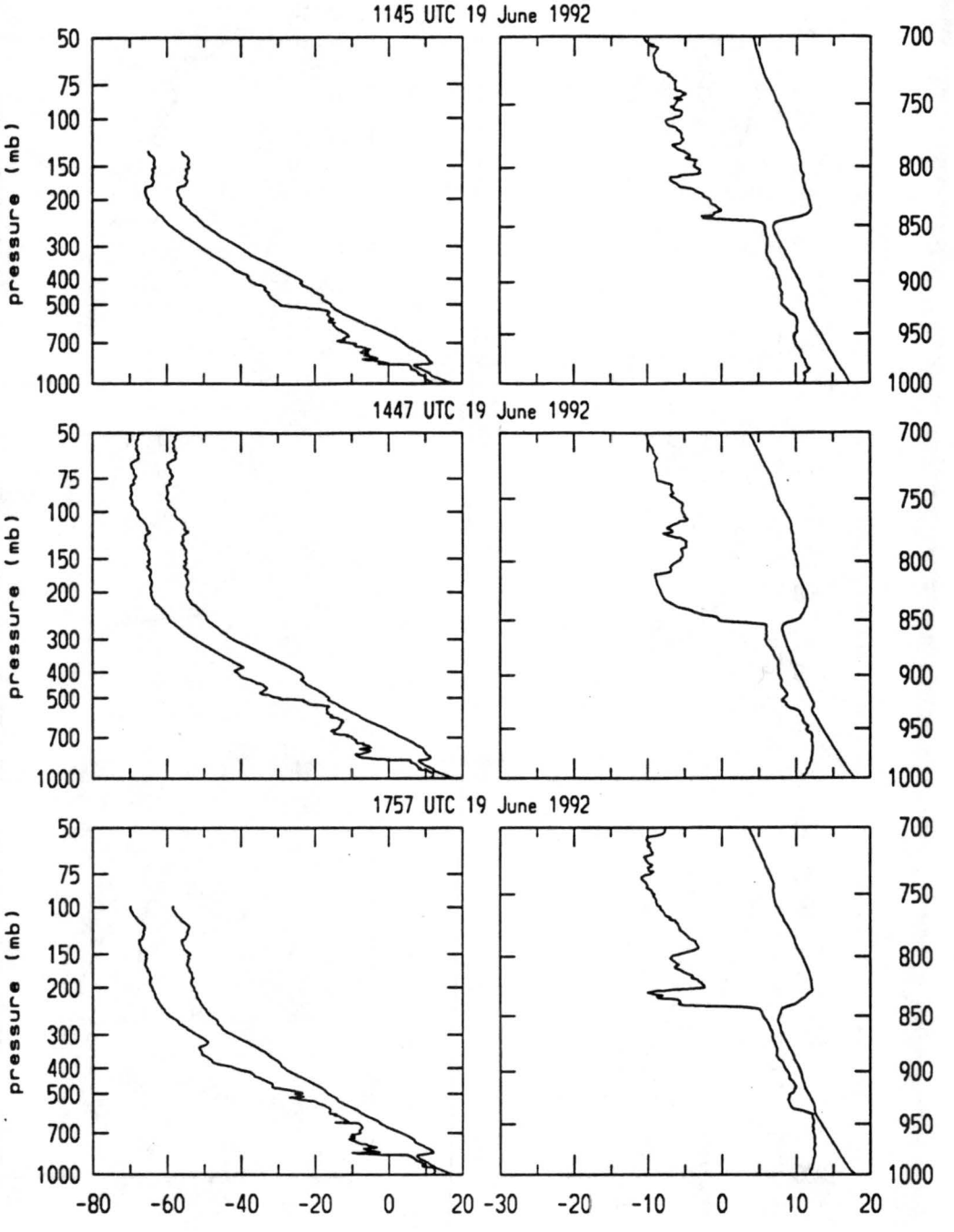
1145 UTC 19 June 1992
1447 UTC 19 June 1992
1757 UTC 19 June 1992
pressure (mb)
50
75
100
150
200
300
400
500
700
1000
700
750
800
850
900
950
1000
-80
-60
-40
-20
0
20
-30
-20
-10
0
10
20

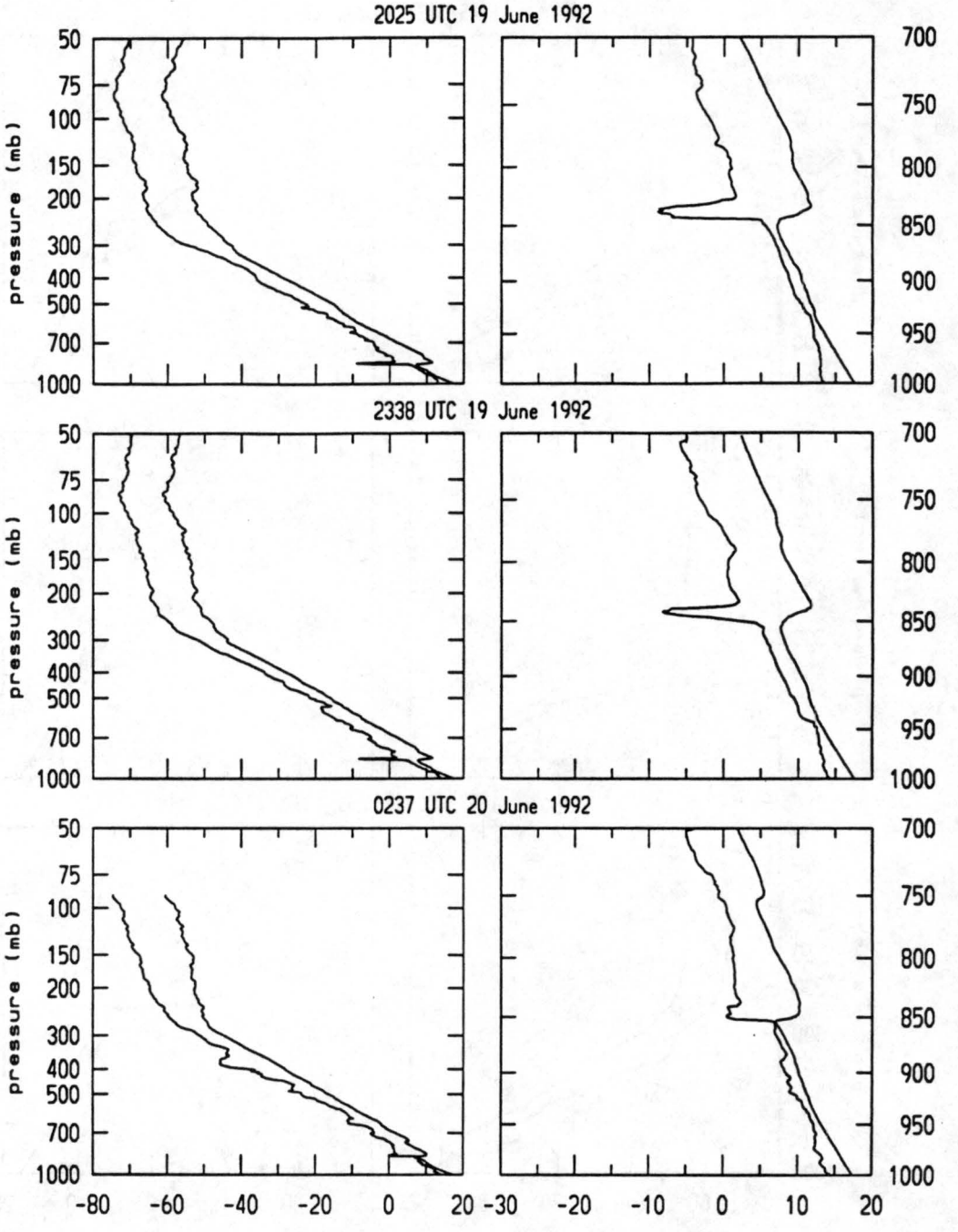
2025 UTC 19 June 1992
2338 UTC 19 June 1992
0237 UTC 20 June 1992
pressure (mb)
50
75
100
150
200
300
400
500
700
1000
700
750
800
850
900
950
1000
-80
-60
-40
-20
0
20
-30
-20
-10
0
10
20

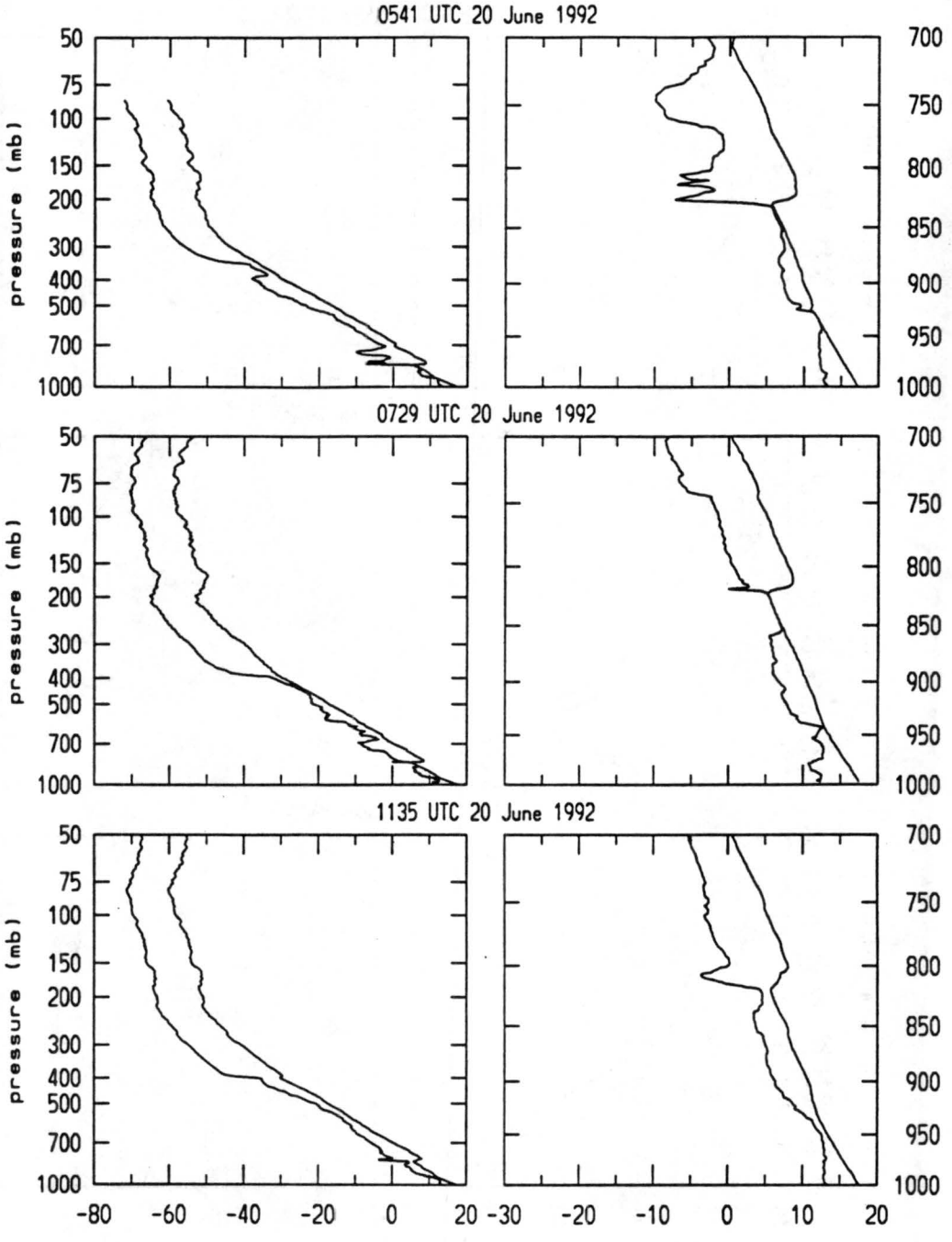
0541 UTC 20 June 1992
0729 UTC 20 June 1992
1135 UTC 20 June 1992
pressure (mb)
50
75
100
150
200
300
400
500
700
1000
700
750
800
850
900
950
1000
-80
-60
-40
-20
0
20
-30
-20
-10
0
10
20

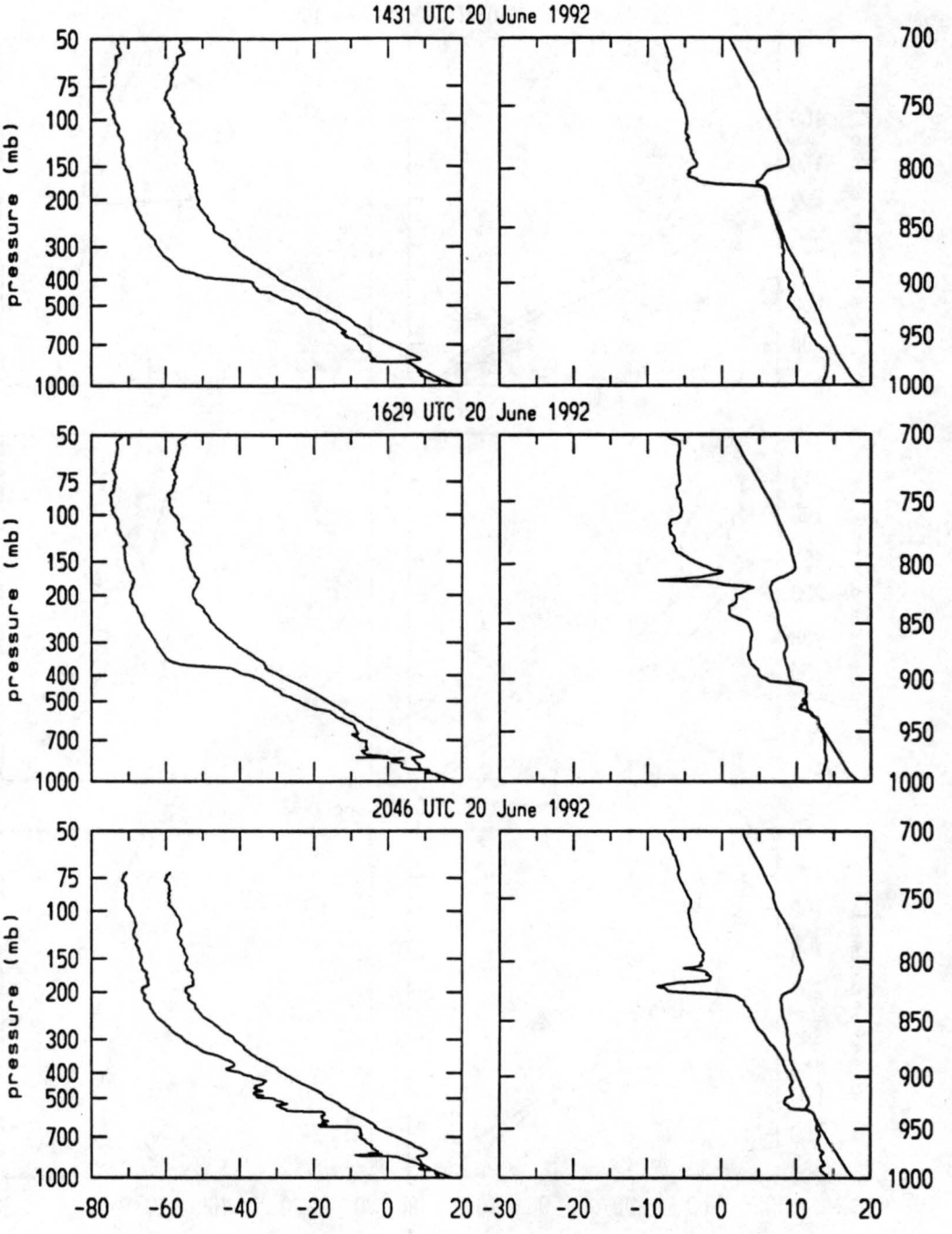
1431 UTC 20 June 1992
1629 UTC 20 June 1992
2046 UTC 20 June 1992
pressure (mb)
50
75
100
150
200
300
400
500
700
1000
700
750
800
850
900
950
1000
-80
-60
-40
-20
0
20
-30
-20
-10
0
10
20

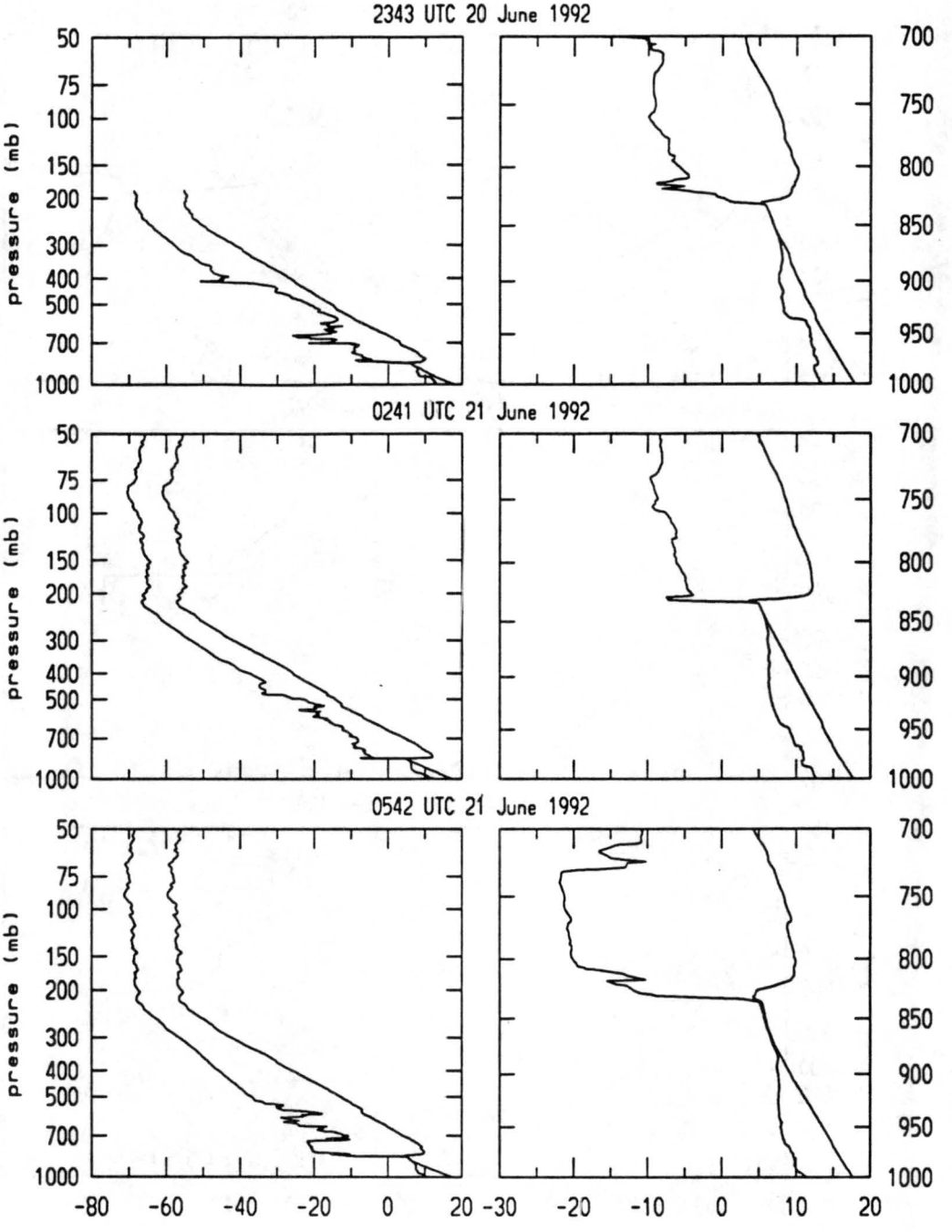
2343 UTC 20 June 1992
0241 UTC 21 June 1992
0542 UTC 21 June 1992
pressure (mb)
50
75
100
150
200
300
400
500
700
1000
700
750
800
850
900
950
1000
-80
-60
-40
-20
0
20
-30
-20
-10
0
10
20

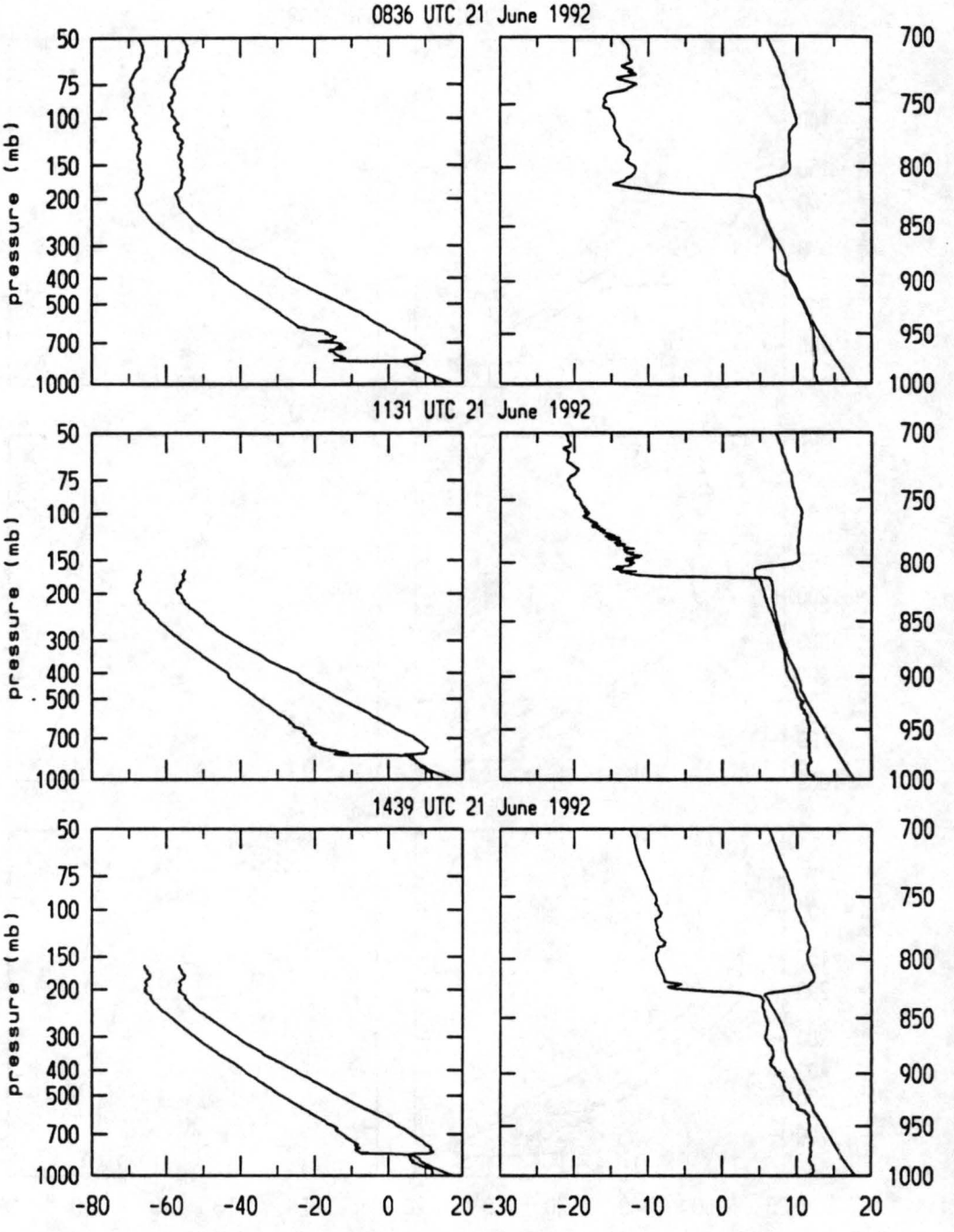
0836 UTC 21 June 1992
1131 UTC 21 June 1992
1439 UTC 21 June 1992
pressure (mb)
50
75
100
150
200
300
400
500
700
1000
700
750
800
850
900
950
1000
-80
-60
-40
-20
0
20
-30
-20
-10
0
10
20

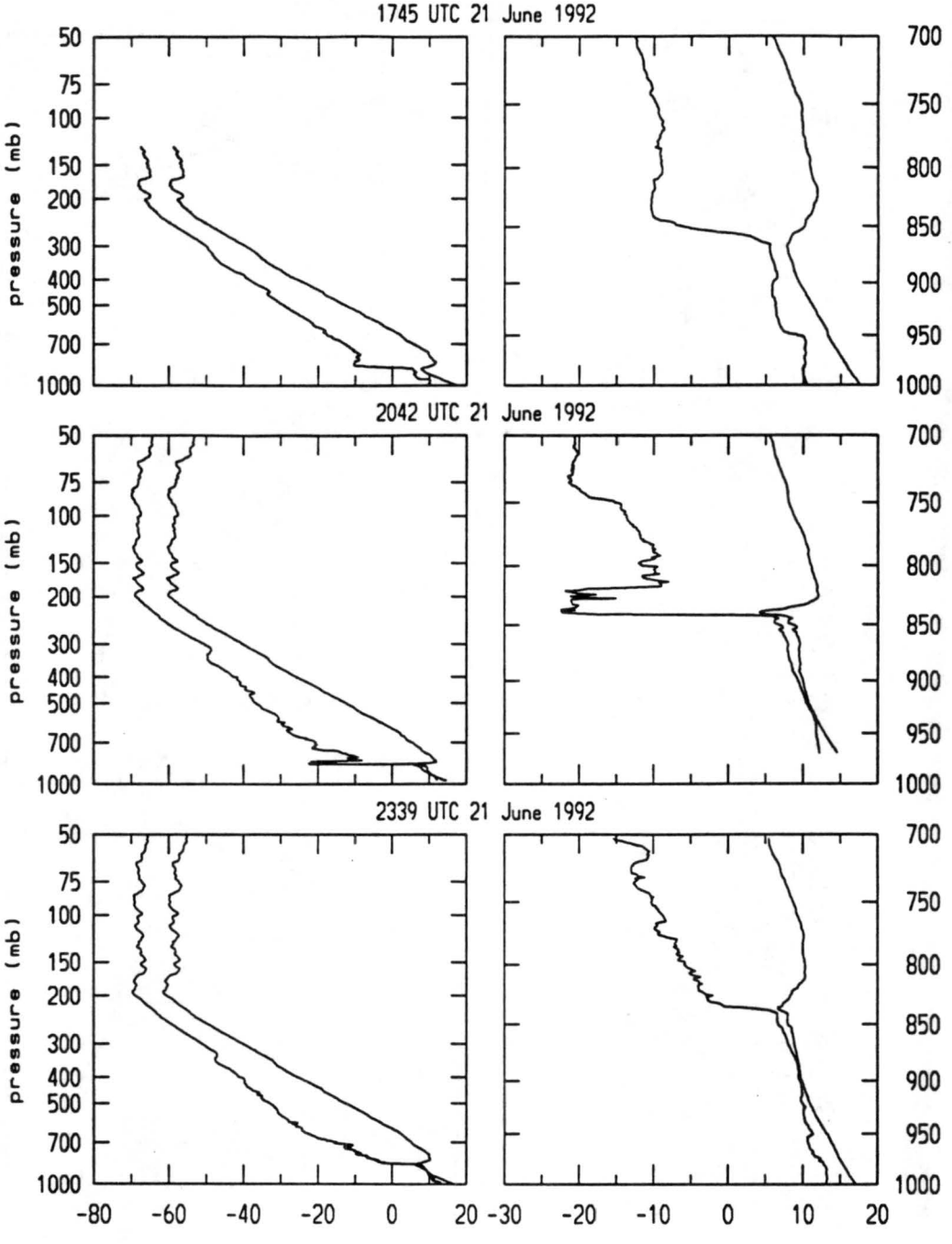
1745 UTC 21 June 1992
2042 UTC 21 June 1992
2339 UTC 21 June 1992
pressure (mb)
50
75
100
150
200
300
400
500
700
1000
700
750
800
850
900
950
1000
-80
-60
-40
-20
0
20
-30
-20
-10
0
10
20

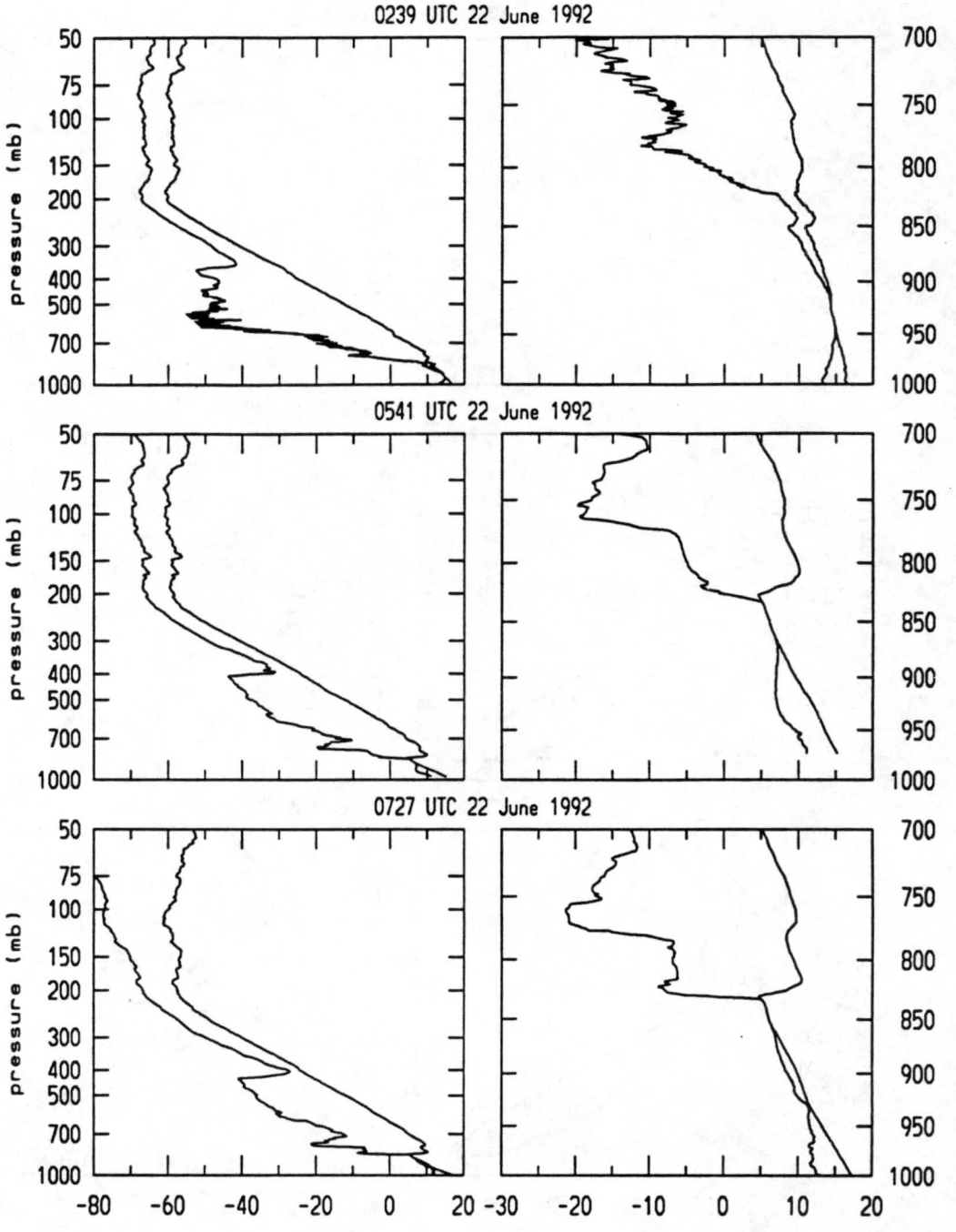
0239 UTC 22 June 1992
0541 UTC 22 June 1992
0727 UTC 22 June 1992
pressure (mb)
50
75
100
150
200
300
400
500
700
1000
700
750
800
850
900
950
1000
-80
-60
-40
-20
0
20
-30
-20
-10
0
10
20

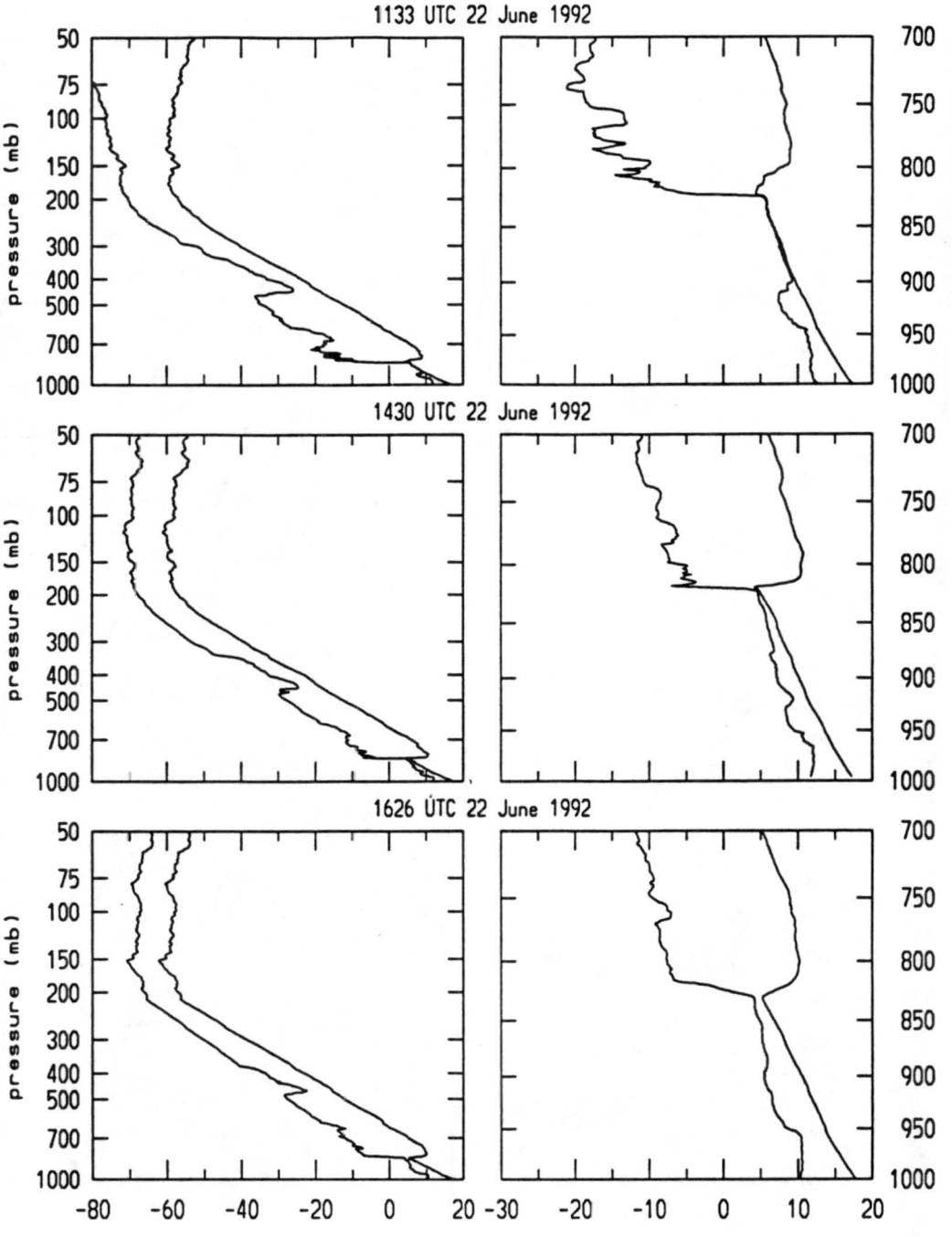
1133 UTC 22 June 1992
1430 UTC 22 June 1992
1626 UTC 22 June 1992
pressure (mb)
50
75
100
150
200
300
400
500
700
1000
700
750
800
850
900
950
1000
-80
-60
-40
-20
0
20
-30
-20
-10
0
10
20

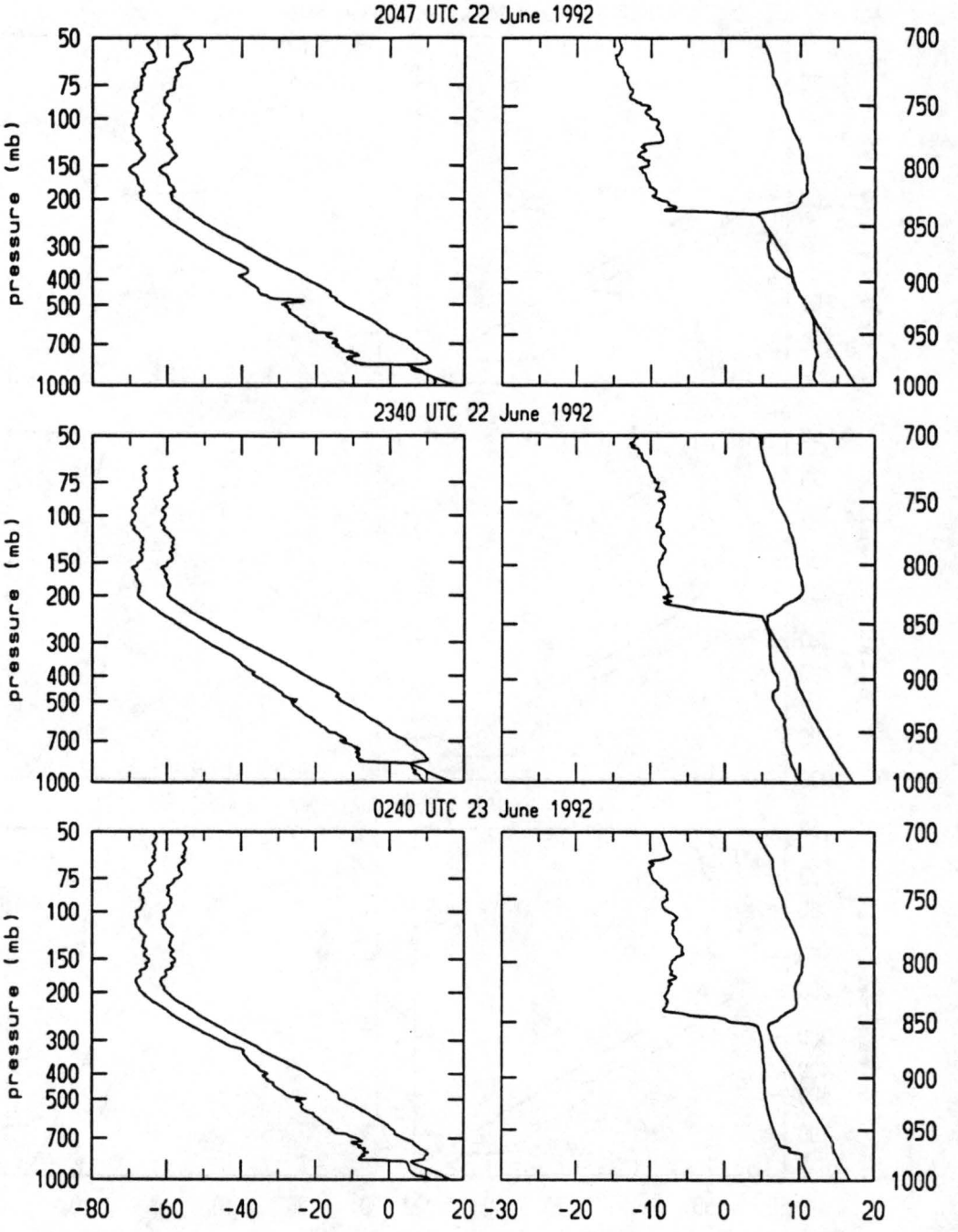
2047 UTC 22 June 1992
2340 UTC 22 June 1992
0240 UTC 23 June 1992
pressure (mb)
50
75
100
150
200
300
400
500
700
1000
700
750
800
850
900
950
1000
-80
-60
-40
-20
0
20
-30
-20
-10
0
10
20

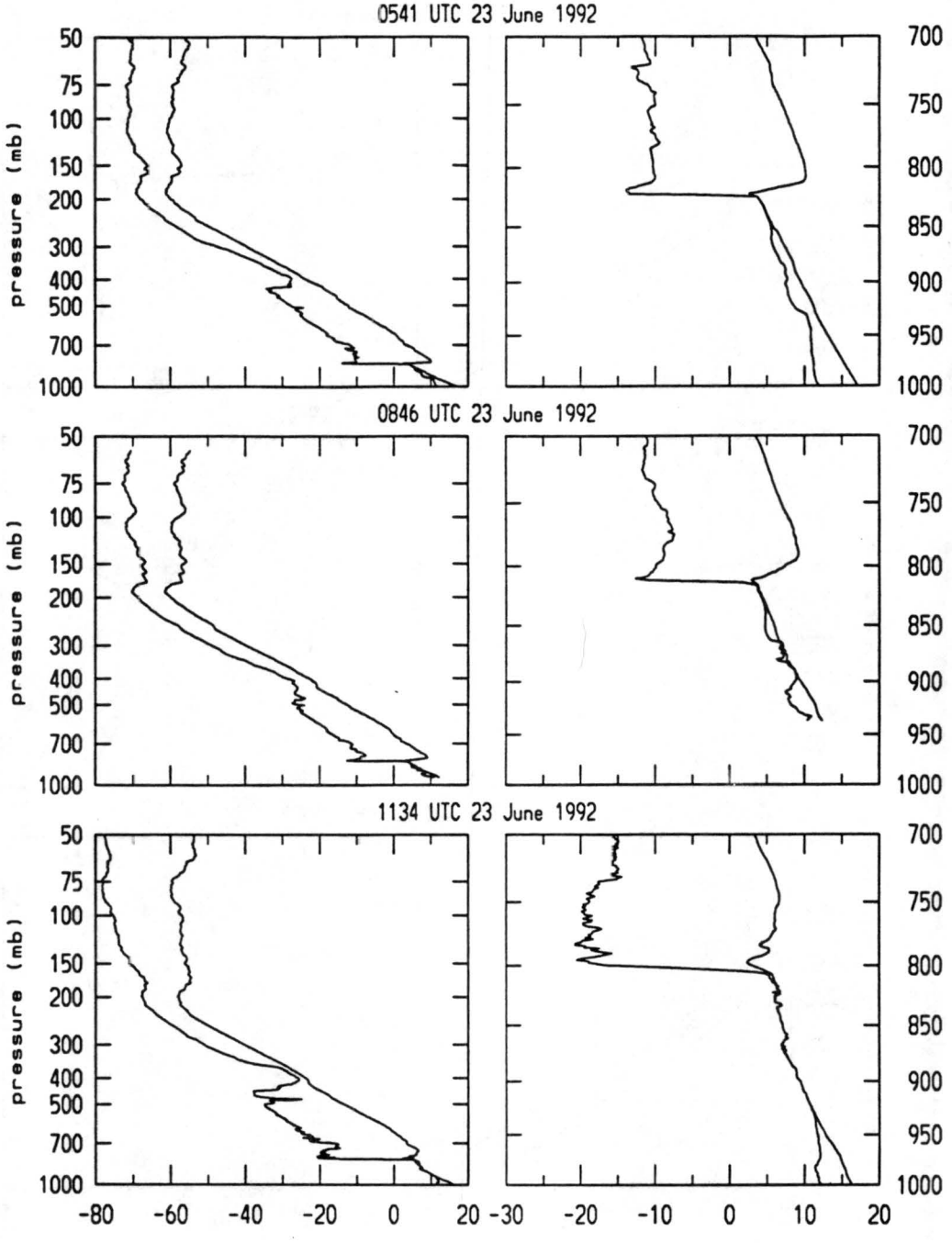
0541 UTC 23 June 1992
0846 UTC 23 June 1992
1134 UTC 23 June 1992
pressure (mb)
50
75
100
150
200
300
400
500
700
1000
700
750
800
850
900
950
1000
-80
-60
-40
-20
0
20
-30
-20
-10
0
10
20

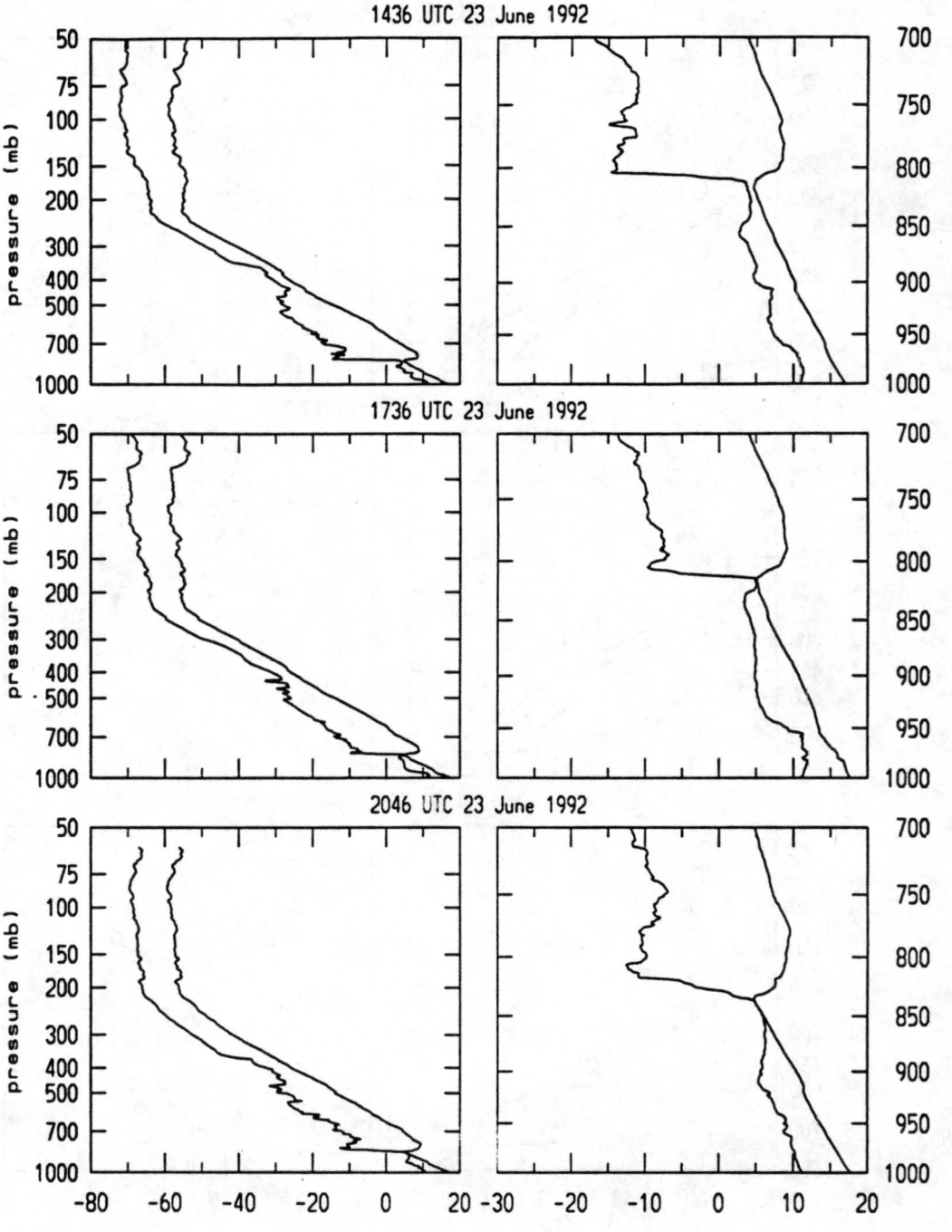
1436 UTC 23 June 1992
1736 UTC 23 June 1992
2046 UTC 23 June 1992
pressure (mb)
50
75
100
150
200
300
400
500
700
1000
700
750
800
850
900
950
1000
-80
-60
-40
-20
0
20
-30
-20
-10
0
10
20

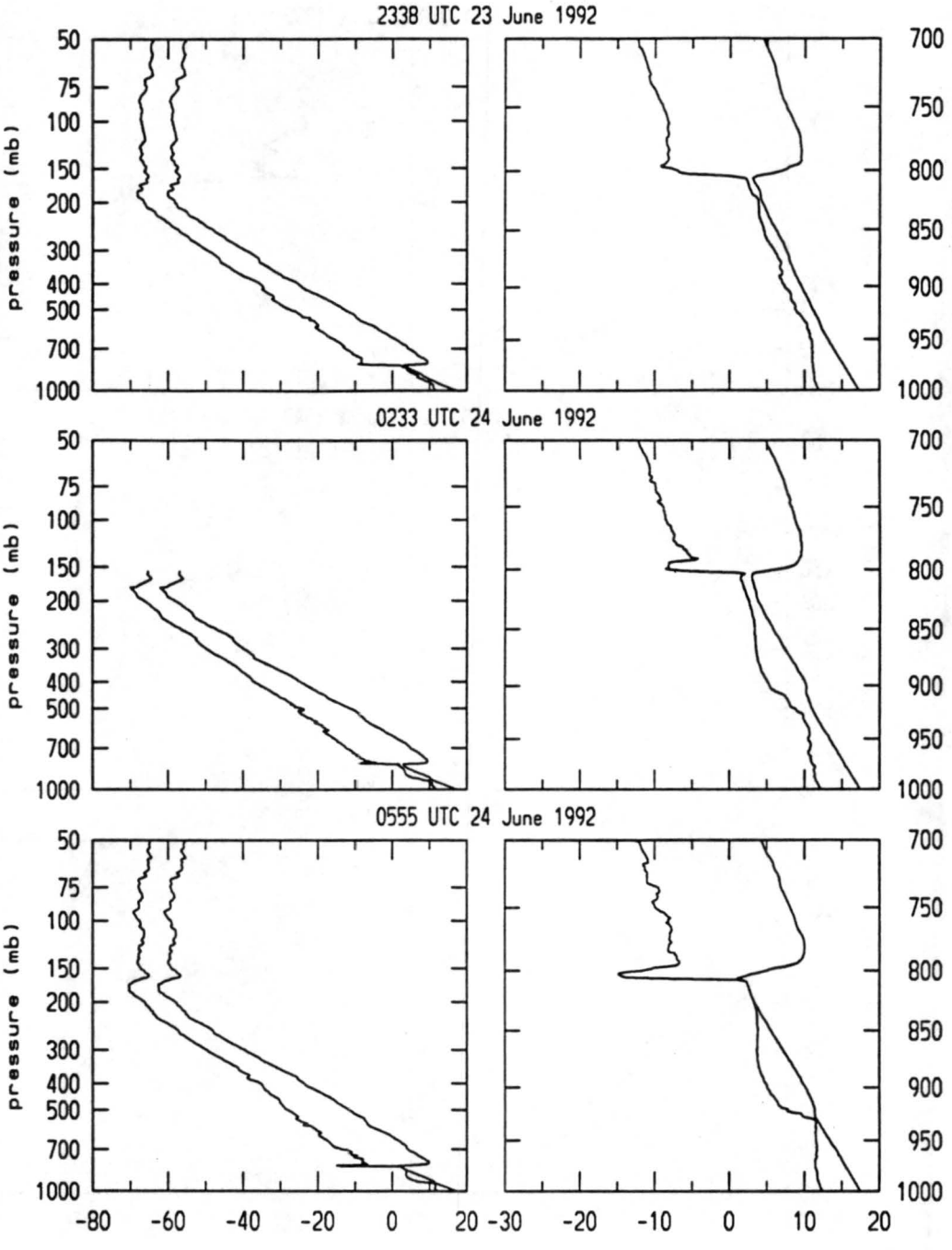
2338 UTC 23 June 1992
0233 UTC 24 June 1992
0555 UTC 24 June 1992
pressure (mb)
50
75
100
150
200
300
400
500
700
1000
700
750
800
850
900
950
1000
-80
-60
-40
-20
0
20
-30
-20
-10
0
10
20

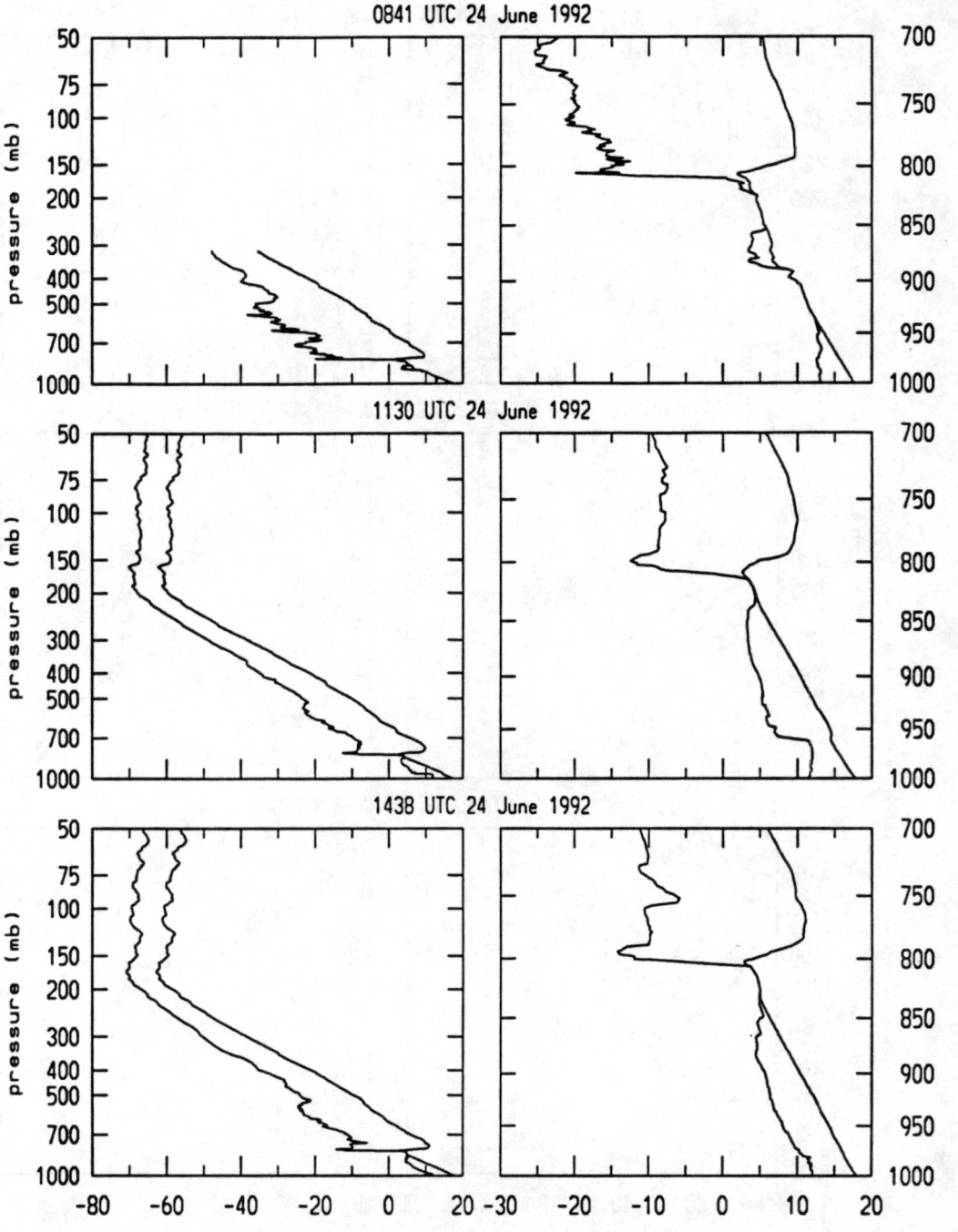
0841 UTC 24 June 1992
1130 UTC 24 June 1992
1438 UTC 24 June 1992
pressure (mb)
50
75
100
150
200
300
400
500
700
1000
700
750
800
850
900
950
1000
-80
-60
-40
-20
0
20
-30
-20
-10
0
10
20

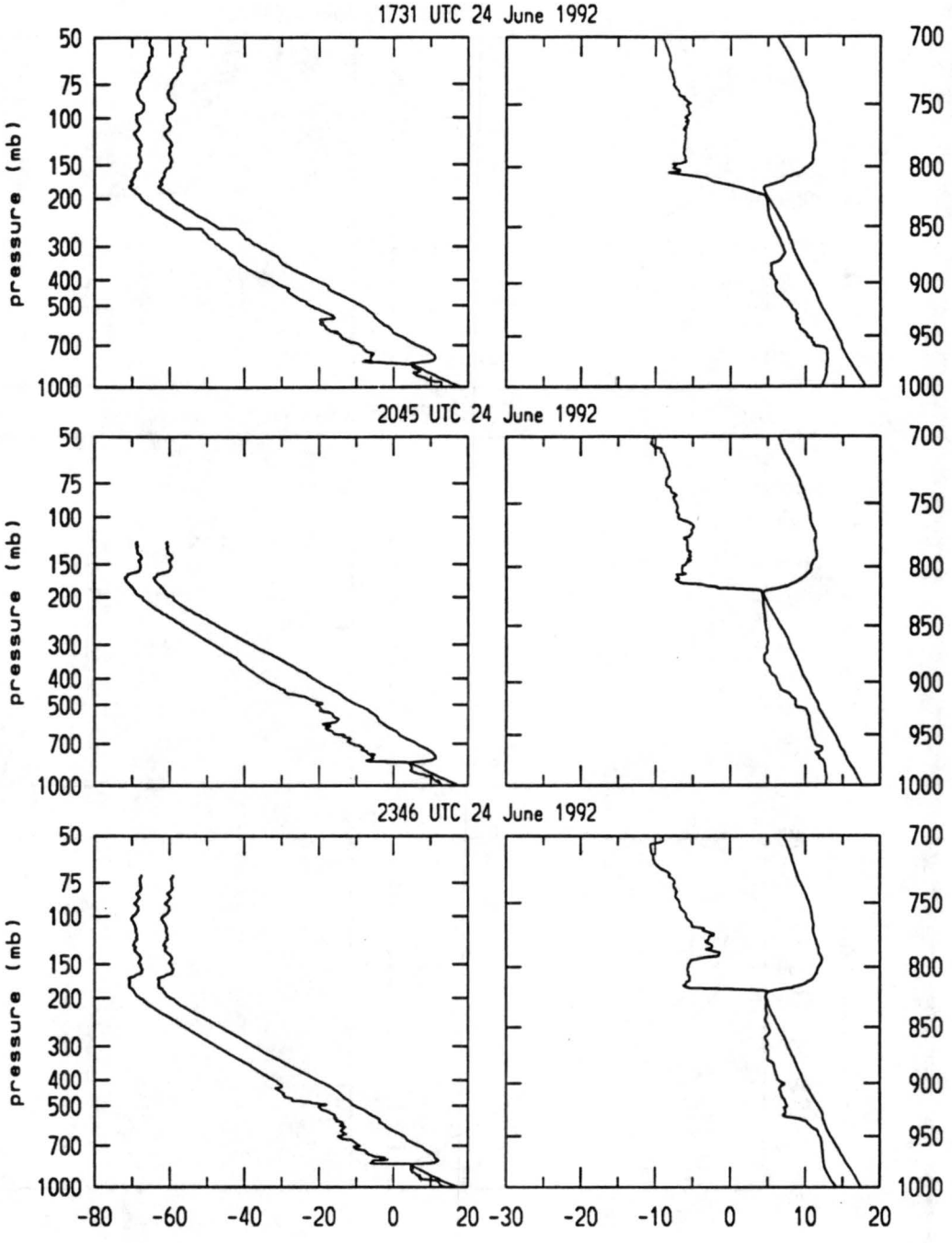
1731 UTC 24 June 1992
2045 UTC 24 June 1992
2346 UTC 24 June 1992
pressure (mb)
50
75
100
150
200
300
400
500
700
1000
700
750
800
850
900
950
1000
-80
-60
-40
-20
0
20
-30
-20
-10
0
10
20

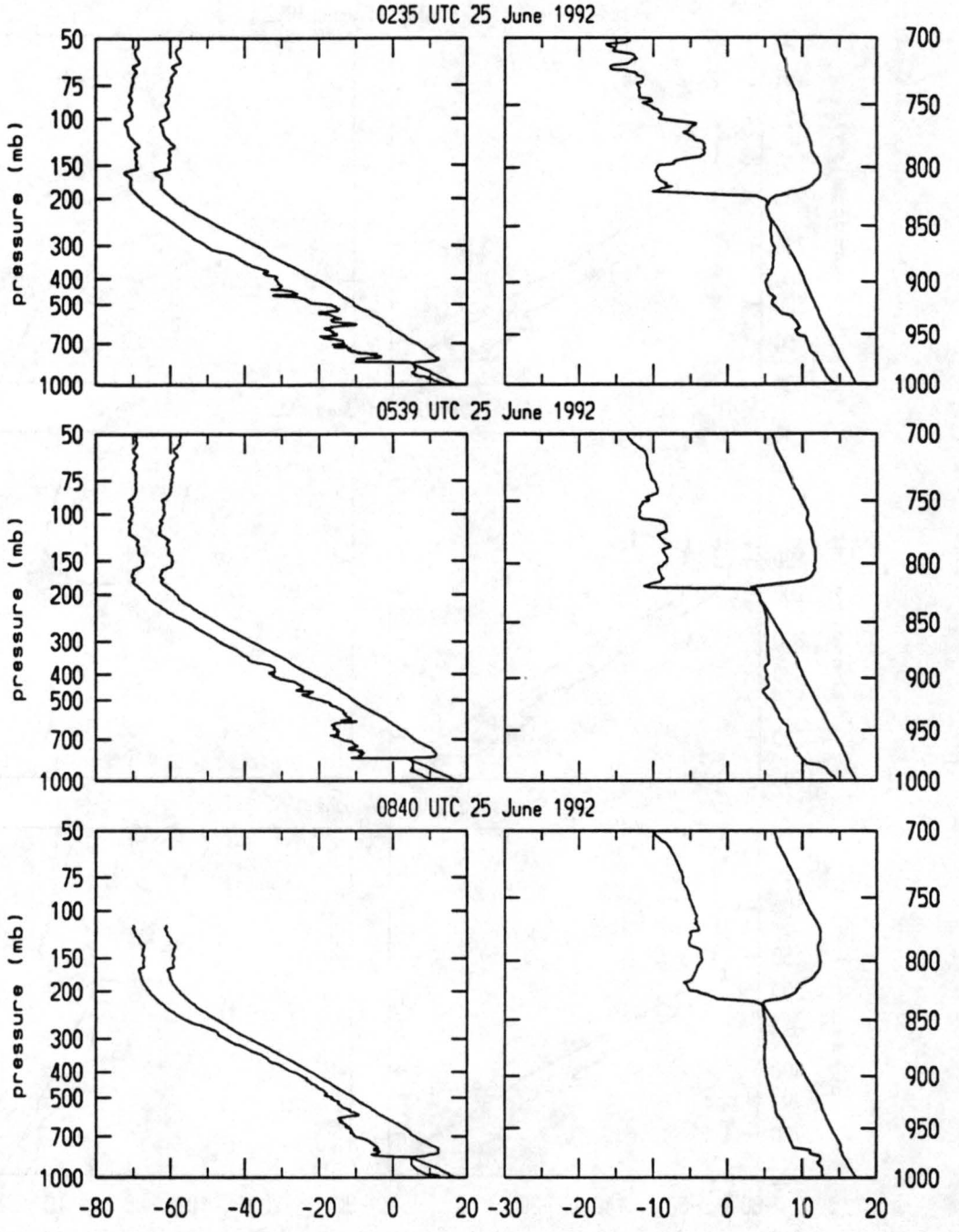
0235 UTC 25 June 1992
0539 UTC 25 June 1992
0840 UTC 25 June 1992
pressure (mb)
50
75
100
150
200
300
400
500
700
1000
700
750
800
850
900
950
1000
-80
-60
-40
-20
0
20
-30
-20
-10
0
10
20

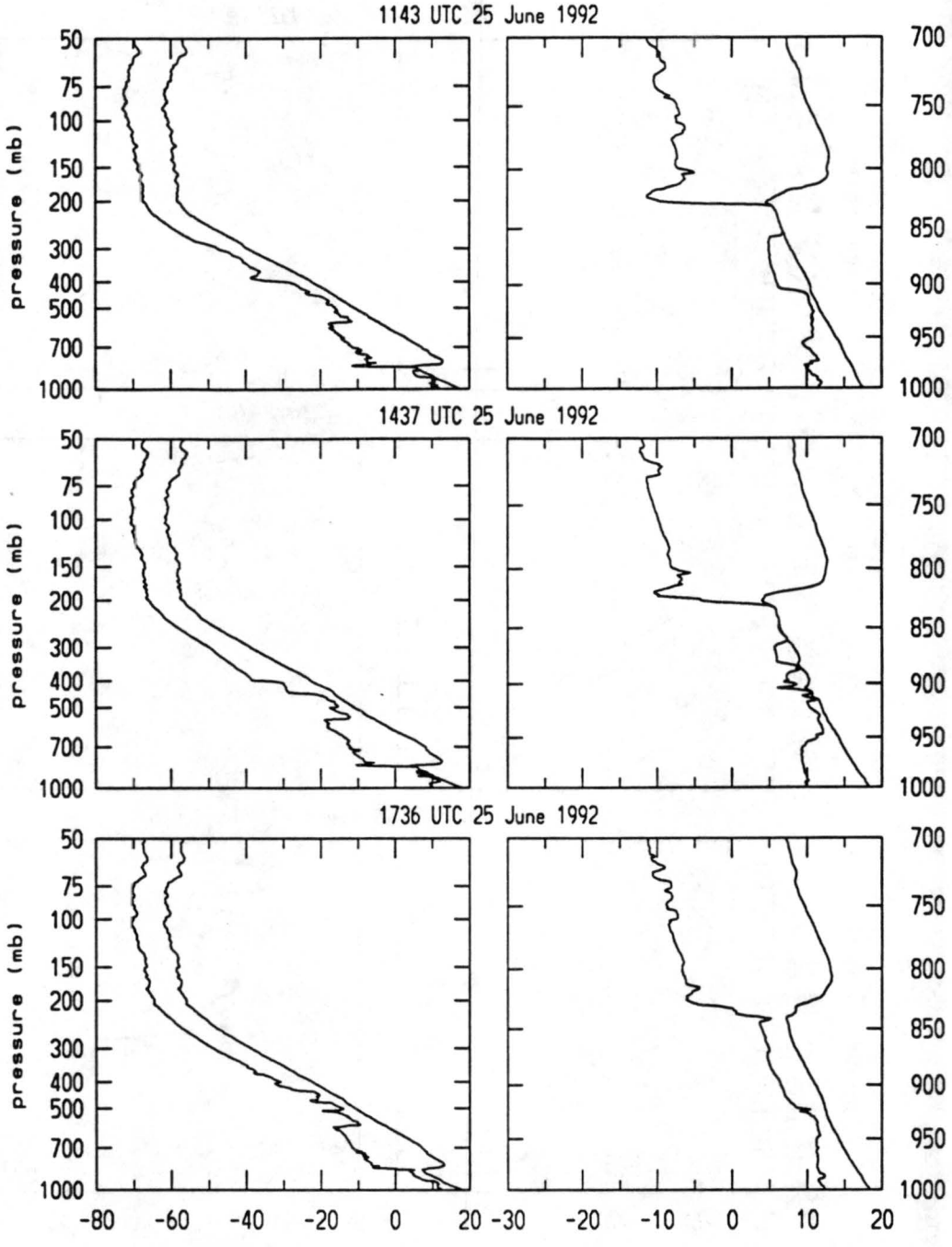
1143 UTC 25 June 1992
1437 UTC 25 June 1992
1736 UTC 25 June 1992
pressure (mb)
50
75
100
150
200
300
400
500
700
1000
700
750
800
850
900
950
1000
-80
-60
-40
-20
0
20
-30
-20
-10
0
10
20

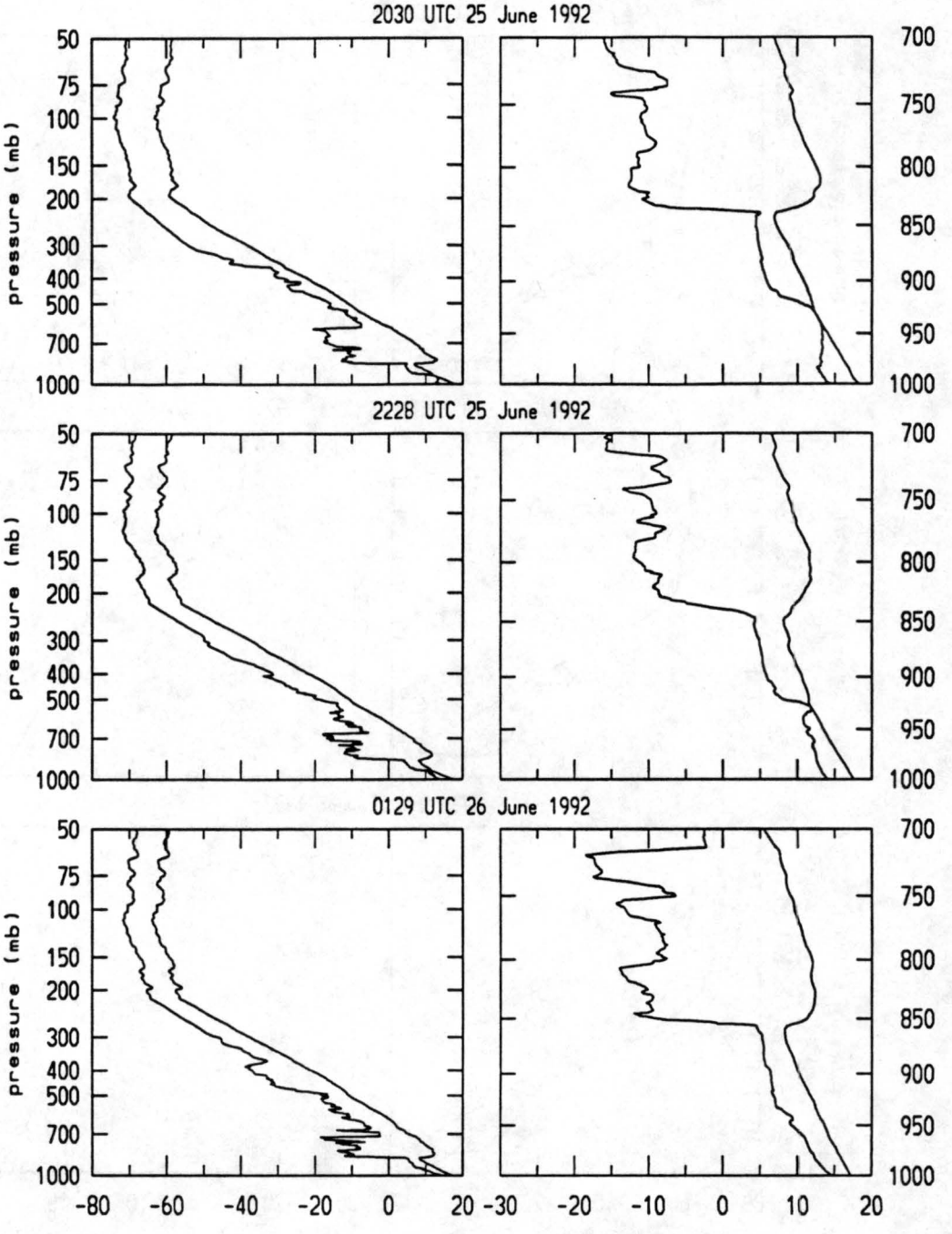
2030 UTC 25 June 1992
2228 UTC 25 June 1992
0129 UTC 26 June 1992
pressure (mb)
50
75
100
150
200
300
400
500
700
1000
700
750
800
850
900
950
1000
-80
-60
-40
-20
0
20
-30
-20
-10
0
10
20

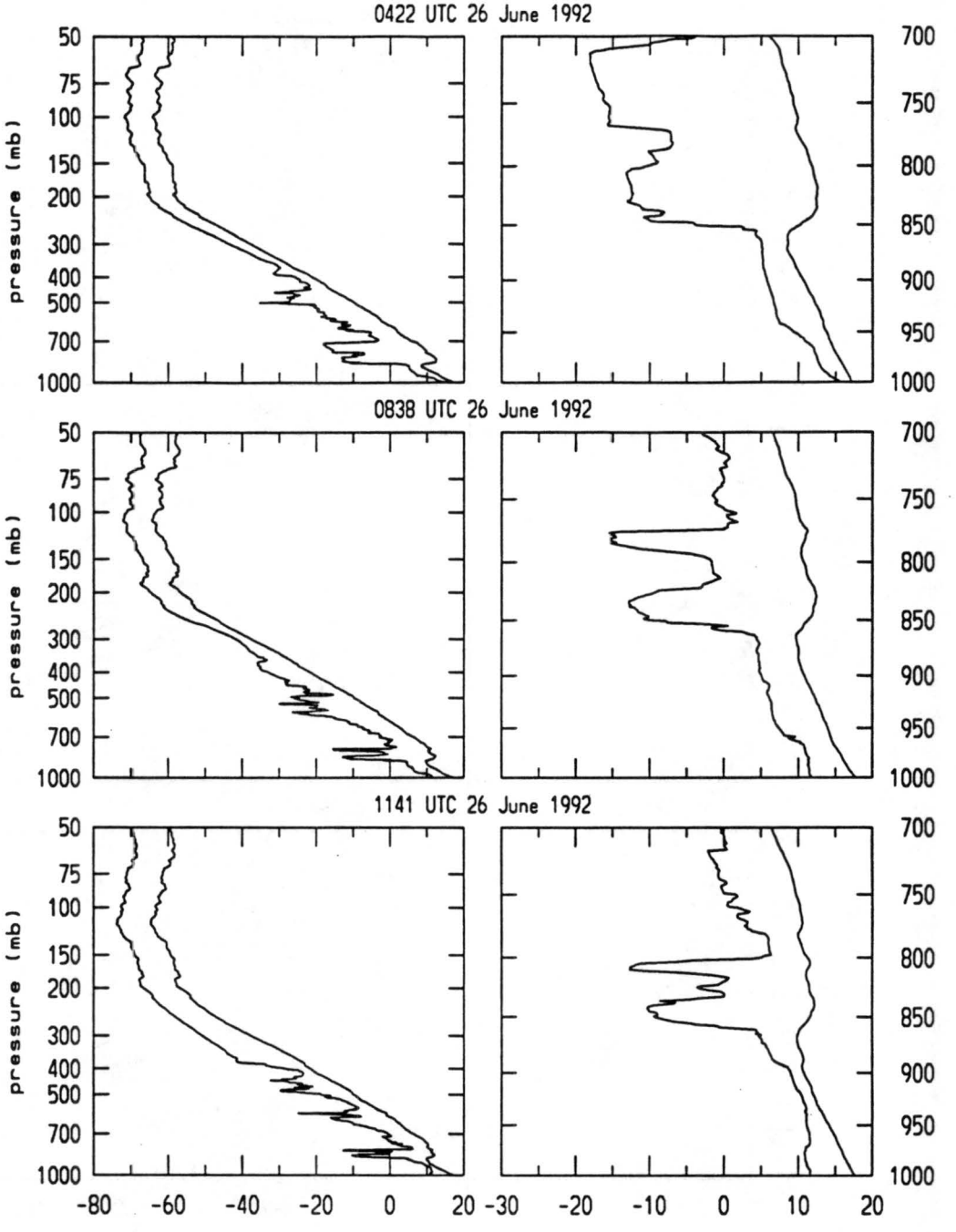
0422 UTC 26 June 1992
0838 UTC 26 June 1992
1141 UTC 26 June 1992
pressure (mb)
50
75
100
150
200
300
400
500
700
1000
700
750
800
850
900
950
1000
-80
-60
-40
-20
0
20
-30
-20
-10
0
10
20

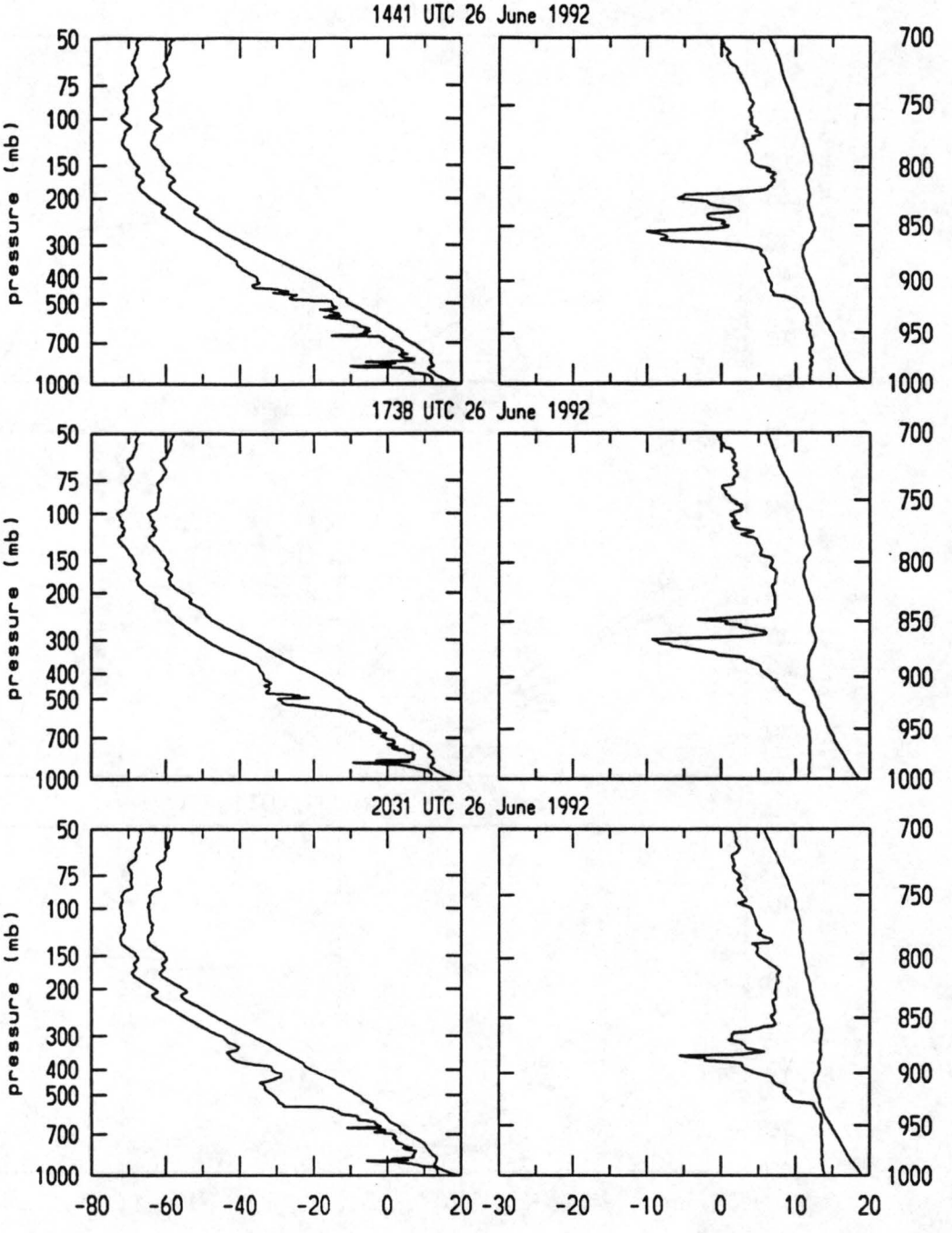
1441 UTC 26 June 1992
1738 UTC 26 June 1992
2031 UTC 26 June 1992
pressure (mb)
50
75
100
150
200
300
400
500
700
1000
700
750
800
850
900
950
1000
-80
-60
-40
-20
0
20
-30
-20
-10
0
10
20

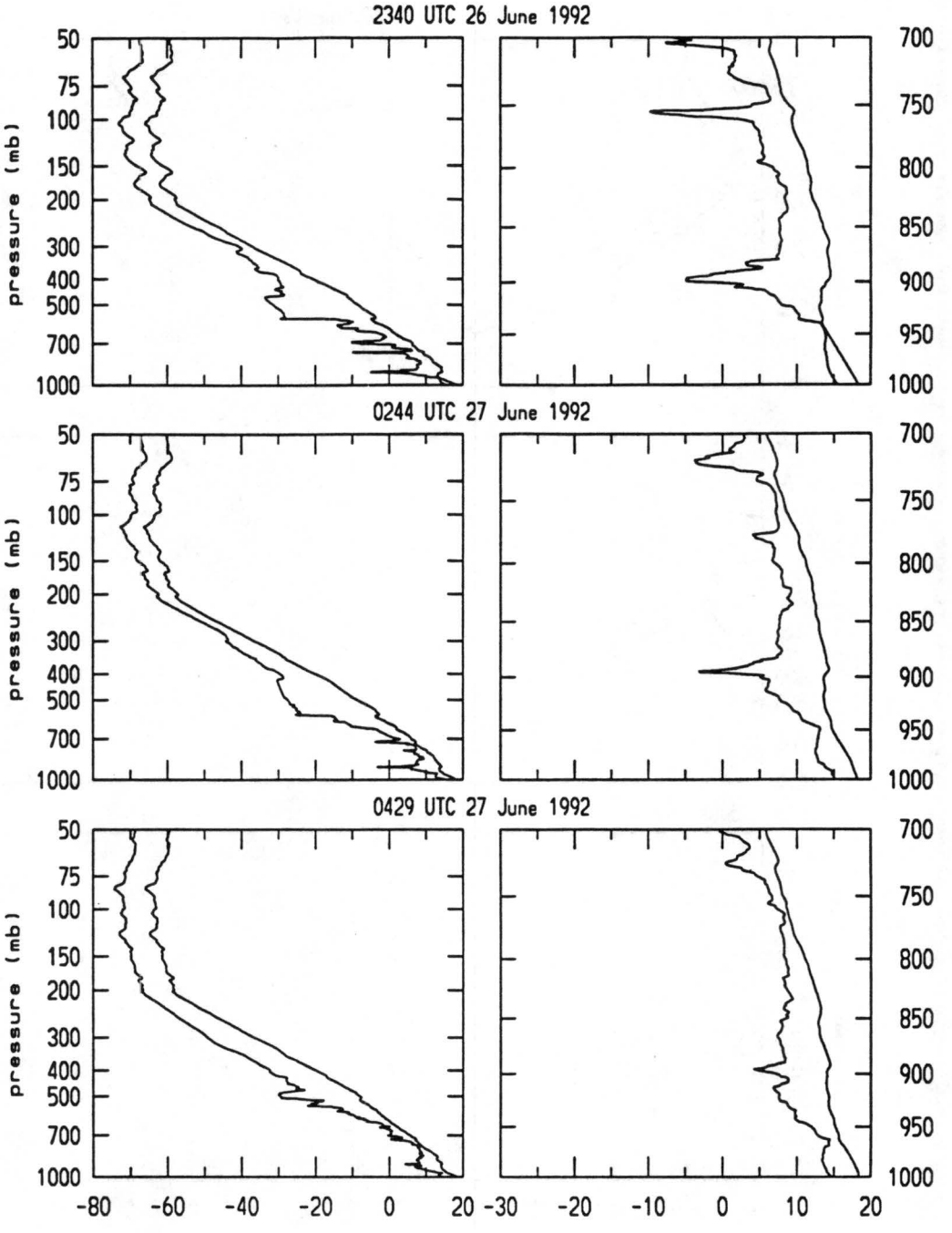
2340 UTC 26 June 1992
0244 UTC 27 June 1992
0429 UTC 27 June 1992
pressure (mb)
50
75
100
150
200
300
400
500
700
1000
700
750
800
850
900
950
1000
-80
-60
-40
-20
0
20
-30
-20
-10
0
10
20

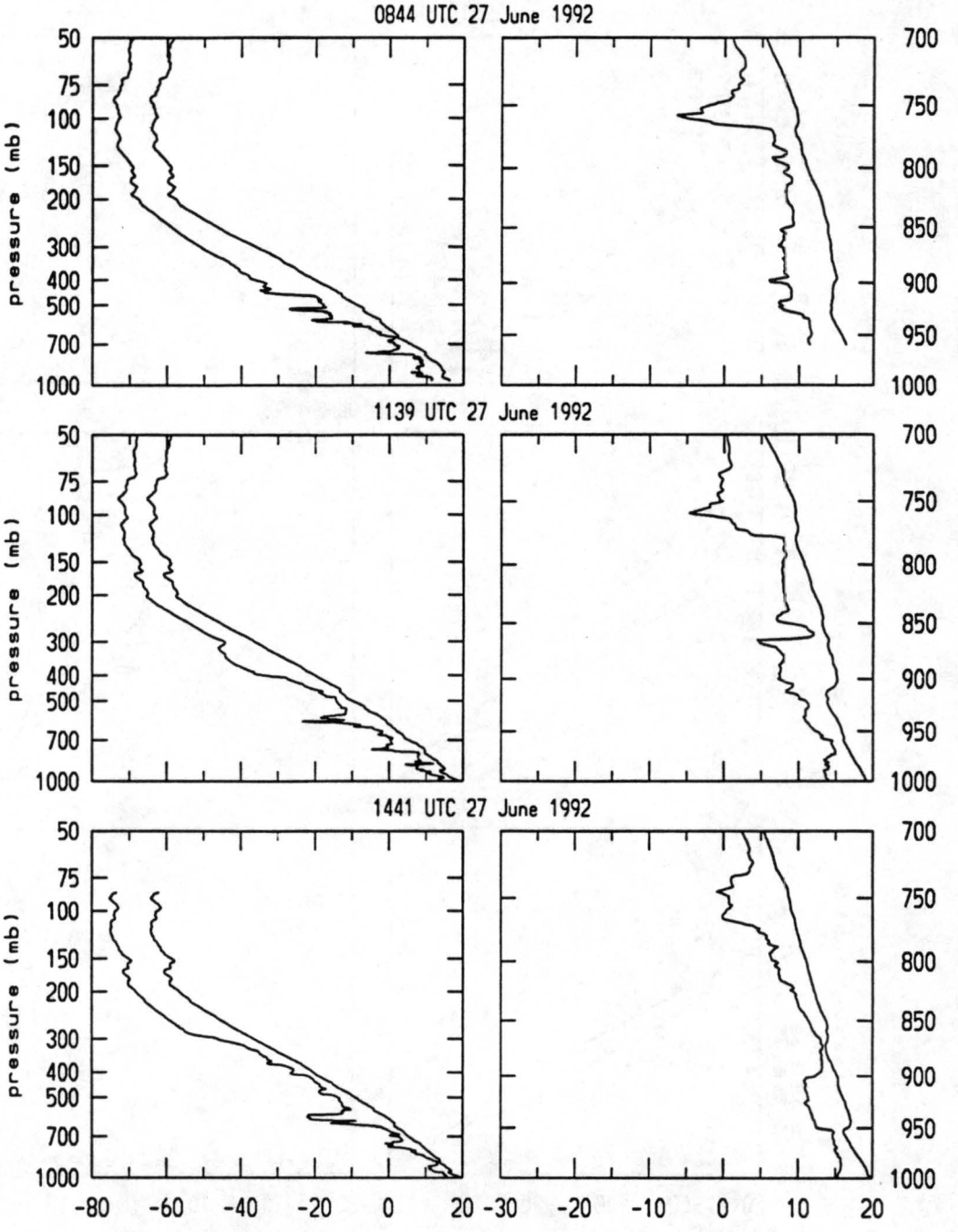
0844 UTC 27 June 1992
1139 UTC 27 June 1992
1441 UTC 27 June 1992
pressure (mb)
50
75
100
150
200
300
400
500
700
1000
700
750
800
850
900
950
1000
-80
-60
-40
-20
0
20
-30
-20
-10
0
10
20

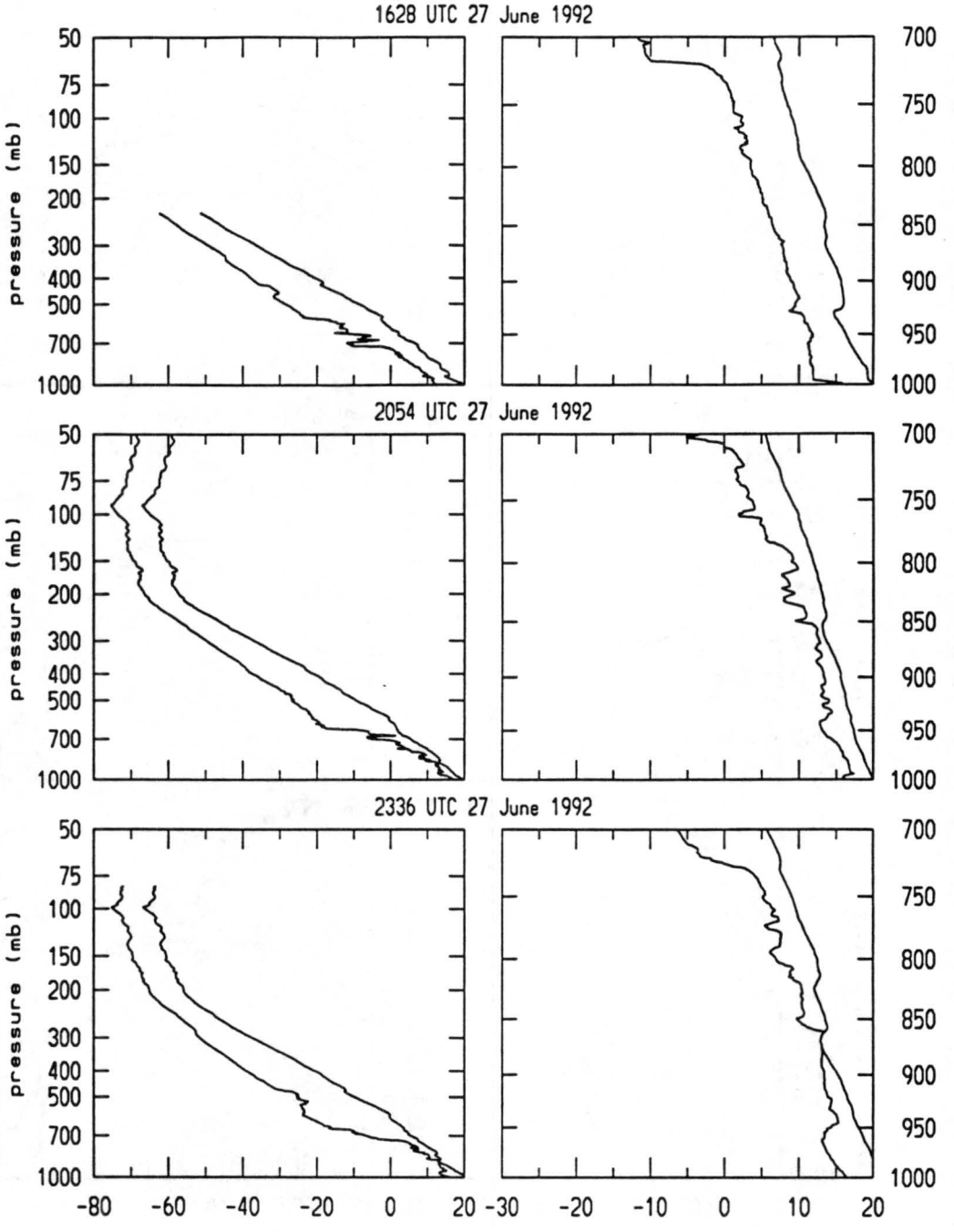
1628 UTC 27 June 1992
2054 UTC 27 June 1992
2336 UTC 27 June 1992
pressure (mb)
50
75
100
150
200
300
400
500
700
1000
700
750
800
850
900
950
1000
-80
-60
-40
-20
0
20
-30
-20
-10
0
10
20

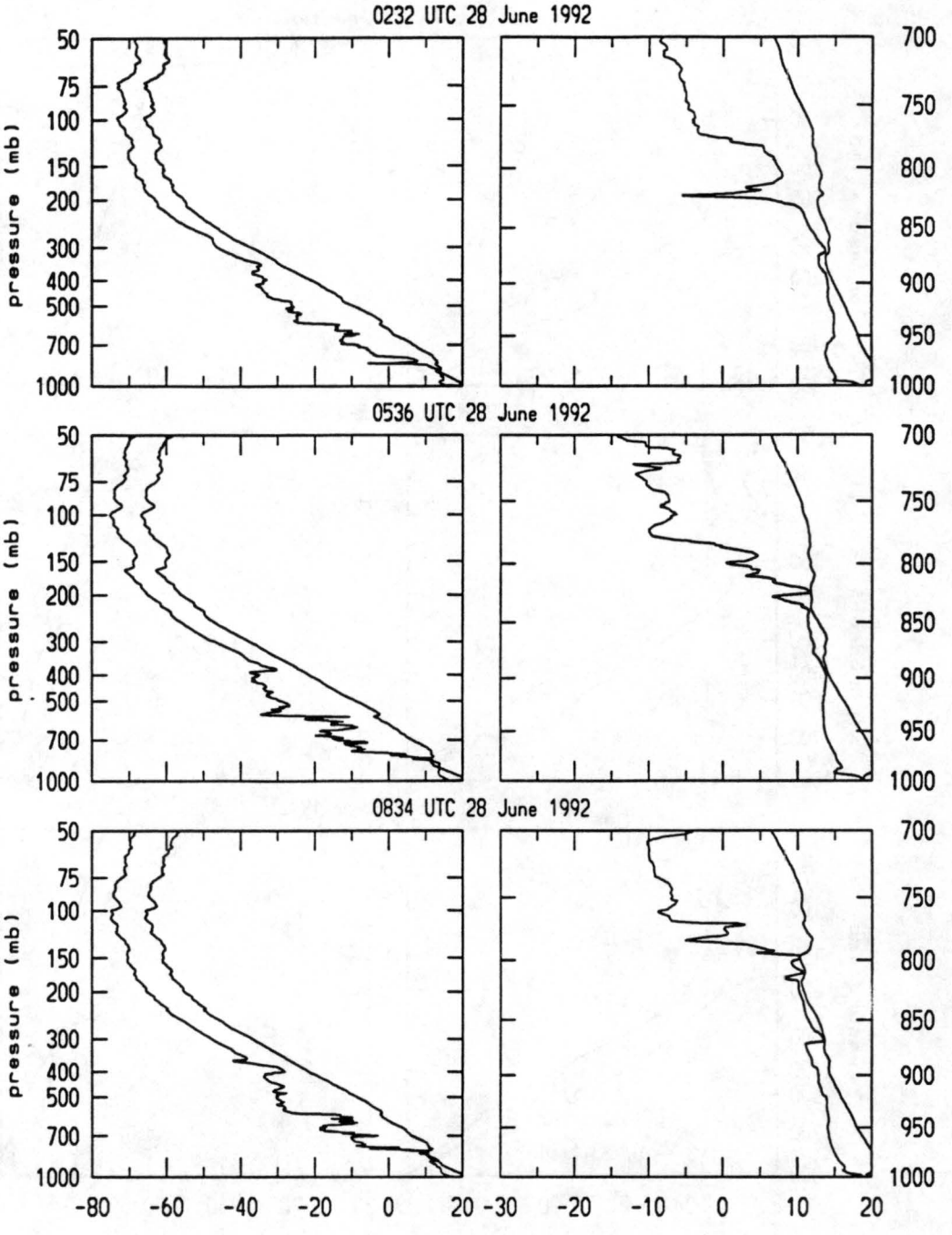
0232 UTC 28 June 1992
0536 UTC 28 June 1992
0834 UTC 28 June 1992
pressure (mb)
50
75
100
150
200
300
400
500
700
1000
700
750
800
850
900
950
1000
-80
-60
-40
-20
0
20
-30
-20
-10
0
10
20

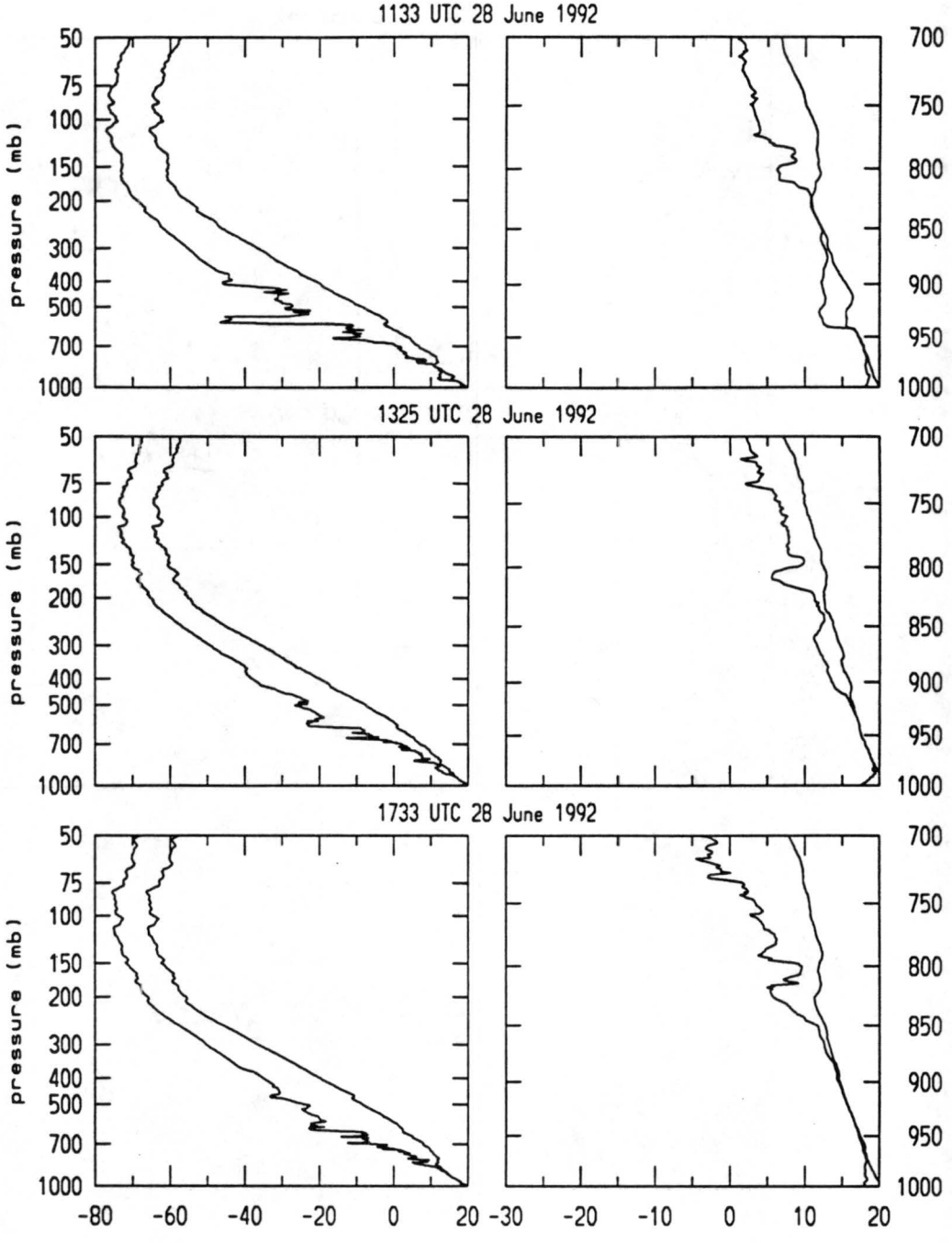
1133 UTC 28 June 1992
1325 UTC 28 June 1992
1733 UTC 28 June 1992
pressure (mb)
50
75
100
150
200
300
400
500
700
1000
700
750
800
850
900
950
1000
-80
-60
-40
-20
0
20
-30
-20
-10
0
10
20

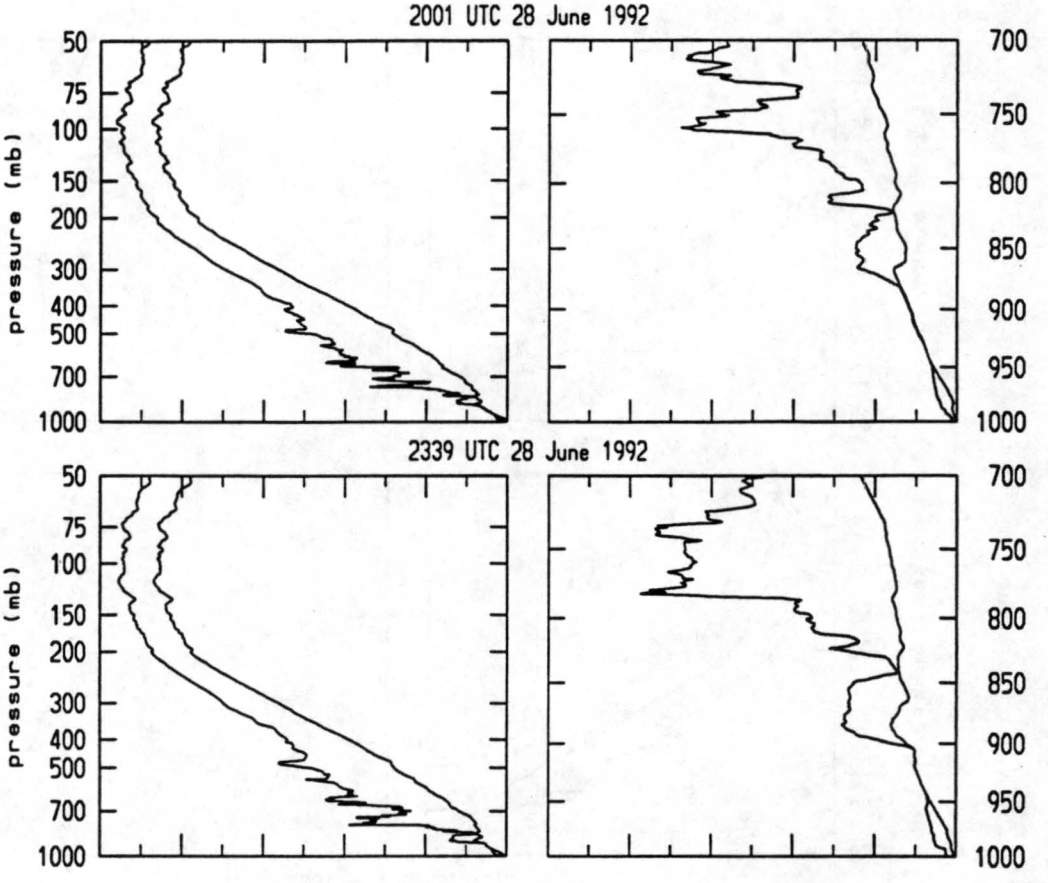
2001 UTC 28 June 1992
2339 UTC 28 June 1992
pressure (mb)
50
75
100
150
200
300
400
500
700
1000
700
750
800
850
900
950
1000